High Efficiency Ultra-precision Grinding of Ceramic Balls

Contents

Abstract

Fine ceramics are expected to have increasing applications in harsh conditions for their high temperature resistance, high corrosion resistance, high wear resistance and low density. However, fine ceramics are also difficult to machine materials. Its high manufacturing cost impedes the spread of the application. Magnetic fluid support grinding of ceramic balls, which is developed by our laboratory, improved the grinding efficiency by over one hundred times against the conventional V-groove grinding method for rough grinding. For super fine grinding, however, the used metal bond super fine diamond grinding wheel suffers from loading and dulling, which results in decrement in material removal rate. A novel grinding system is proposed in this research to improve the efficiency of the superfine grinding of ceramic ball. This grinding system consists of the eccentric grinding machine with magnetic fluid support and the electrolytic in-process dressing system. Both fundamental simulation and grinding experiments were carried out to investigate the grinding performance.

At first, the kinematic analysis of ball grinding is given, showing the dependence of the rotation speed, spin speed and the angle of the spin axis of the ball on the rotation speeds and dimensions of the V-groove components. For traditional concentric V-groove grinding, the spin angle is constant and the grinding tracks on the ball surfaces are fixed circles. Therefore true sphere cannot be obtained unless the spin axis of the ball is changed. This situation can be changed by using spin angle control grinding method or setting the grinding wheel and the V-groove eccentrically. The eccentricity between grinding wheel and V-groove also introduces the skidding between the ball

and the grinding wheel, leading to an increase in material removal rate.

Fundamental simulation experiments of the electrolytic in-process dressing (ELID) were conducted by using a ball-on-disk friction test machine equipped with an electrolyzing system. Copper, which is one of the most widely used metal bond materials of super abrasive wheels, and iron, one of the special bond materials for ELID, were tested in three different types of electrolytes: tap water, electrolyzed water, and CG-7 to tap water. Experimental results showed that there was almost no detectable wear for both copper and iron when electrolysis was not implemented, and also the material removal was little when only electrolysis was applied. Strong synergistic effect between electrolysis and friction was observed for copper in both tap water and electrolyzed water, and for iron in electrolyzed water and CG-7 solution. The friction coefficient of Si_3N_4 ball against iron disk was lower than that of Si_3N_4 ball against copper disk. In addition, it was found that the wear of Si_3N_4 ball was increased by implementing electrolysis for both copper and iron.

The electrolytic in-process dressing grinding of ceramic balls was investigated on a magnetic fluid support grinding machine by grinding Si_3N_4 balls with fine diamond grinding wheels SD16000 of both bronze bond and cast iron bond in two types of grinding fluid: tap water and CG-7 solution. The experimental results showed that increasing the dressing current increased the grinding efficiency. However the ground surface was roughened when the current increased to over 160 mA in the study. The bronze bonded grinding wheel showed a higher dressing effectiveness than the cast iron bonded grinding wheel in both tap water and the CG-7 solution. As an electrolyte, tap water was more effective than CG-7 solution in terms of grinding efficiency improvement.

The difference in the dressing effectiveness between the two bond materials is considered to be due to the difference in chemical equivalent between them. It is found that the equivalent volume of iron is only one-third of that of copper, because the valence of copper is 2, while it is 6 for iron in the anode reaction of this research. This means that, to achieve the same dressing effectiveness, the current for the cast iron bonded grinding wheel may be three times as high as that for the copper bonded grinding wheel.

The dressing current is the sum of the metal oxidation current and the water decomposition current, but only the former contributes to the dressing. Increasing the pH value of electrolyte will accelerate the decomposition of water. Therefore CG-7 solution whose pH value is higher than that of tap water has higher water decomposition rate than tap water. This results in a reduction in the dressing effectiveness under the same dressing current.

Keywords: Wear; Sliding friction; ELID; Copper; Iron; Ceramic ball; Superfine diamond grinding wheel; Metal bond.

Chapter 1
Introduction

1.1 Background

Fine engineering ceramics were quickly developed during recent several decades. Compared to metallic materials, fine ceramic materials are very good in terms of corrosion resistance, abrasion resistance and temperature resistance. Brittleness, which is conventionally a fatal disadvantage for the application of ceramics in engineering, has also been significantly improved. Therefore, fine ceramic materials are becoming more and more promising for biomaterial, cutting tools and tribological applications, especially under severe conditions.

Fine ceramic materials are often used as triboelements due to their following advantage:

1) High temperature resistance: This leads to great interest in using ceramic materials in the construction of both reciprocating and turbine engines for reducing fuel consumption by raising engine operating temperature and thereby increasing thermodynamic efficiency [1].

2) High corrosion resistance or chemical inertness: This leads to great interest in using ceramic materials in corrosive environments such as artificial hip joint and bearings in water pumps.

3) High toughness: Higher Young's modulus leads to lower elastic deformation at the same load. It is necessary for high accuracy control or micro-inaccurate adjustment.

4) Low density: Light moving parts lead to lower kinetic energy. This reduces energy consumption and increases the velocity of movement

especially in reciprocating motions, for example in engines.

On the other hand, fine ceramics are difficult to process. They are so stiff that polishing or lapping is necessary as the finish process. However, two issues restrict the material removal rate in such process. The first one is that the contact area between the grinding wheel/lapping pad and the ball surface is extremely small. Suppose that, a silicon nitride ceramic ball with diameter of 10 mm is ground by cast iron bonded grinding wheel under a load of 1N. And assuming the Young's modulus of the ball and the cast iron bond is 310GPa and 180MPa respectively, while the Poisson's ratio for both is 0.3; we can found that the diameter of the contact area is only about 100 μm. The other one is that balls have to be ground in a rolling state to achieve required sphericity, resulting in low sliding velocity between ball and grinding wheel/lap pad. Consequently, the material removal rate is much lower than that of plane and curved surface finish and the process is greatly time-consuming. Study of the grinding of balls started about 50 years ago by Ido and co-workers [2]. In the past two decade, a lot of new grinding technique was developed and the processing rate in rough grinding increased substantially. However, super fine diamond grinding with metallic bond still suffers from the loading and the dulling issues, which result in a gradual decrement in the grinding efficiency. Dressing of metallic bond in super fine grinding is a very important subject for practical application of ceramics ball.

1.2 Review of literature

In order to understand background and purpose much more clearly, this review of the literature is divided into two parts.

§1.2.1 Finish of balls

§§1.2.1.1 Finish of steel balls

Study of the finish process of steel balls started since 1950s, by Ido et al. and a series of papers were published. In these papers, the effects of various grinding conditions such as the V-groove shape [2-4], the materials of the lapper [5], the grinding fluid [6] and the grinding load [5,7] on the material removal rate and sphericity of balls were investigated.

Today the most popular production method in the world was proposed by Inagaki and Abe in 1976 (Figure 1-1) [8]. They ground the same type steel balls with 14 grinding methods, and found that the apparatus which was consisted of a rotary grinding wheel and a fixed disk can get the best sphericity and surface roughness. The balls were placed into the V-grooves and driven by the rotary disk. When appropriate grinding load and abrasive or lubricant are imposed, the material removal to be obtained at the surface with smaller radius of curvature was greater than that obtained at the position with larger radius of curvature, thus the ball will be ground toward the same radius of curvature, and achieve better sphericity gradually. It is found that, ground by #500 abrasive with the rotating speed of the rotary disk below 100 rpm for 50 hours, the diameter reduction rate, the sphericity and the average surface roughness were of about 0.3 μm/min, 1 μm and 0.1 μm respectively.

In 1993, the Itoigawa et al. [9] analyzed the effect of the geometry of the V-groove on the sphericity. They extrapolated a preferable grinding condition

and ground the balls at a low rotating speed of 60rpm for 4 to 5 hours. A sphericity of 0.05 μm was obtained and the result demonstrated that the sphericity improved with the number of the steel ball to be processed at the same time.

1996 years, Goto et al. [10] simulated the ball formation in the grinding and analyzed the error correction via Fourier series. Based on the simulation results, a three-stage lapping process of steel ball for the ultra-precision bearing was implemented, and a sphericity of 0.018 μm and a surface roughness of 0.002 μm were obtained.

§§1.2.1.2 Finish of ceramic balls

With the development of precision ceramic materials, precision ceramic ball have gradually took place of steel ball in high speed, high temperature, aerospace and other harsh environment. However, most of the precision ceramic ball manufacture is still using the traditional grinding equipment. Since the 1980s, industry and academia started to develop new grinding method and equipment to enhance the processing rate of precision ceramic ball. 1988, Kato et al. [11, 12] developed magnetic fluid grinding method (Figure 1-2), which uses the slurry of magnetic fluid and grits as the abrasive. By virtue of the buoyancy which is produced by the magnetic fluid in the magnetic field, the ball can be ground by the grits in the slurry which is driven by the high speed rotating shaft. After grinding with GC#400 abrasive under 0.7 N for 3 hours, diameter reduction rate of 12 μm/min, sphericity of 0.14 μm and surface roughness of 0.01 μm were obtained.

In 1992, Childs et al. [13] discussed the design of the magnetic fluid grinding cell. Later in 1993, Kato et al. also investigated the grinding

characteristics and did in-depth study to approach a subject of grinding theory [14]. The effect of different grinding conditions, such as the support stiffness of the float and the processing load [15, 16], different groove material, abrasive types, size, slurry viscosity and concentration [17], on the ball grinding were investigated. Child et al. [18] developed a model to predict the motion of balls and float in a magnetic fluid grinding cell, particularly to predict the onset of skidding that results in high grinding rate by the magnetic fluid grinding. In 1996, Umehara et al. [19] reviewed those papers and discussed the improvement on the material removal rate, sphericity and surface roughness.

In 1995, Zhang et al. [20] improved magnetic fluid grinding method by using a taper thrust float, and discussed the effect of eccentricity between the driving shaft and the guide ring. The result showed that the material removal rate increased with the offset. However, the surface roughness is independent of the eccentricity. Later in 1998, Zhang [21] proposed the magnetic fluid support grinding method (Figure 1-3) which can save the cost of expensive magnetic fluid. The magnetic fluid is sealed in the chamber beneath the float with a rubber membrane, and provides a soft support. Thus the ball can be ground by the grinding wheel at a high rotating speed. The diametrical reduction rate was 29 μm/min and the sphericity was improved from 43 μm to 6 μm within a short grinding time of 6 minutes when a SD200 wheel was used. In 2000, Zhang [22] and his research group discussed the spherical surface generation mechanism in the grinding of balls and considered that the eccentric V-groove grinding mechanism may be one solution to distribute the contact trace over the whole ball surface and thus to improve the precision of ground balls. Furthermore, they investigated the relationship between the

vibration of the support system and the error in the surface generation, and discussed the effect of the stiffness and damping [23]. They concluded that ultraprecision grinding requires high damping to increase the magnification factor and minimized the phase difference.

F. Y. Chang et al. [24] also modified the magnetic fluid grinding method in 1998. They used a spring instead of the magnetic fluid. After 1 hour's grinding, the sphericity was improved from 15-16 μm to 3-4 μm. The material removal rate was 5.3 μm/min (SD 64 μm).

In addition, Ichikawa et al. [25] proposed combined lapping tools in 1992. The contact load on the same ball can be independently controlled to investigate the effect of different load ratio on the lapping process. After 40 minutes lapping, the sphericity reached to 2.4 μm.

1996, Kurobe et al. [26, 27] reported spin angle controlled grinding method (Fig. 1-4). They controlled the rotating speed of the three contact points independently to change the rotation axis angle of the ball. The results showed a sphericity of 2.5 μm and a surface roughness of 0.1 μm.

The above review showed that a lot of efforts have concerned on improving grinding method research. However, most of the works based on the rough grinding or lapping. Since lapping process is extremely time consuming and the loose abrasive grains to be used in the lapping will cause the burden on the environment, superfine grinding is expected to take place of lapping process. Unfortunately, the loading and glazing issue still remained on the metallic bond grinding wheel which is popular in the superfine grinding of ceramic balls. Therefore, the dressing process is essential to solve this issue.

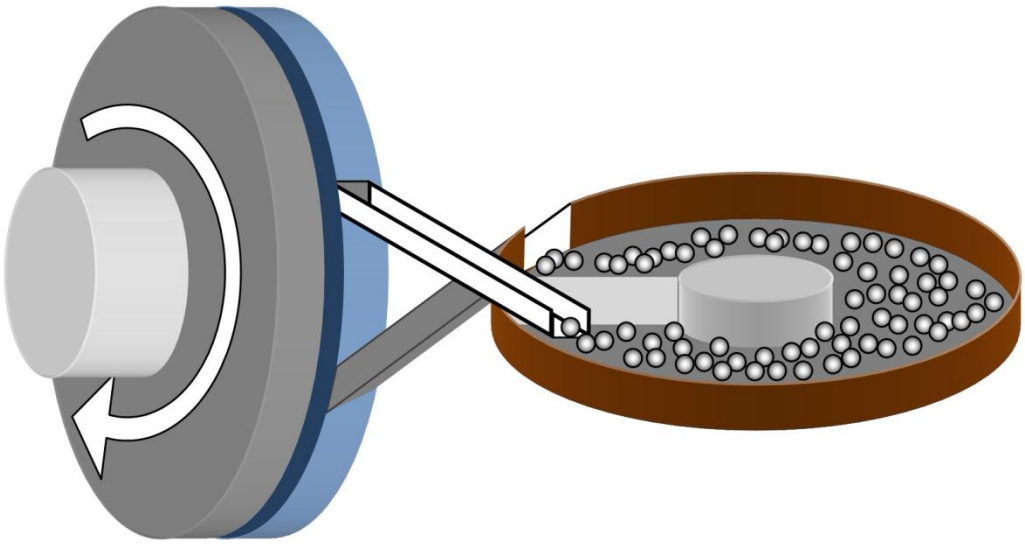

a) Vertical type

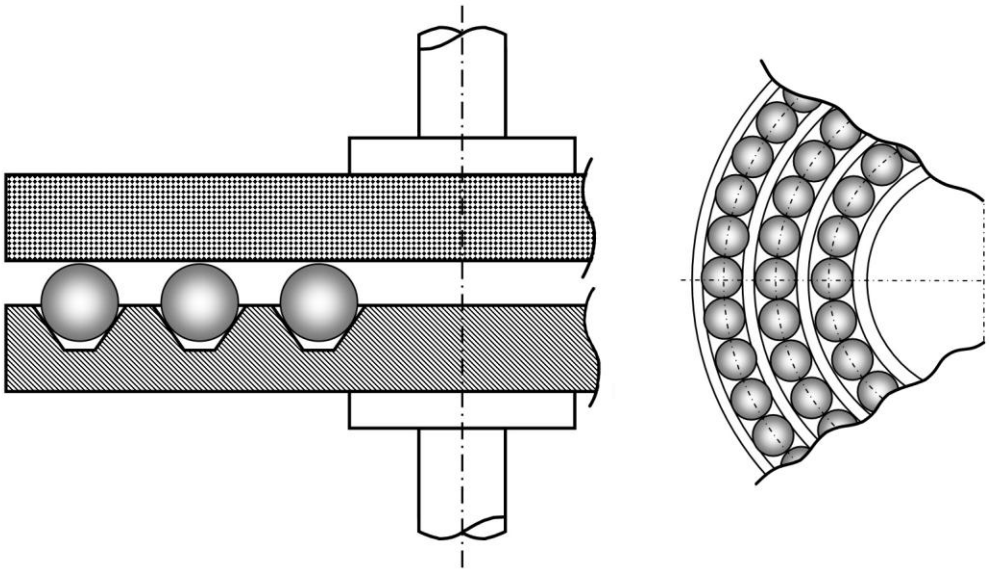

b) Horizontal type

Fig. 1-1 The traditional V-groove grinding method

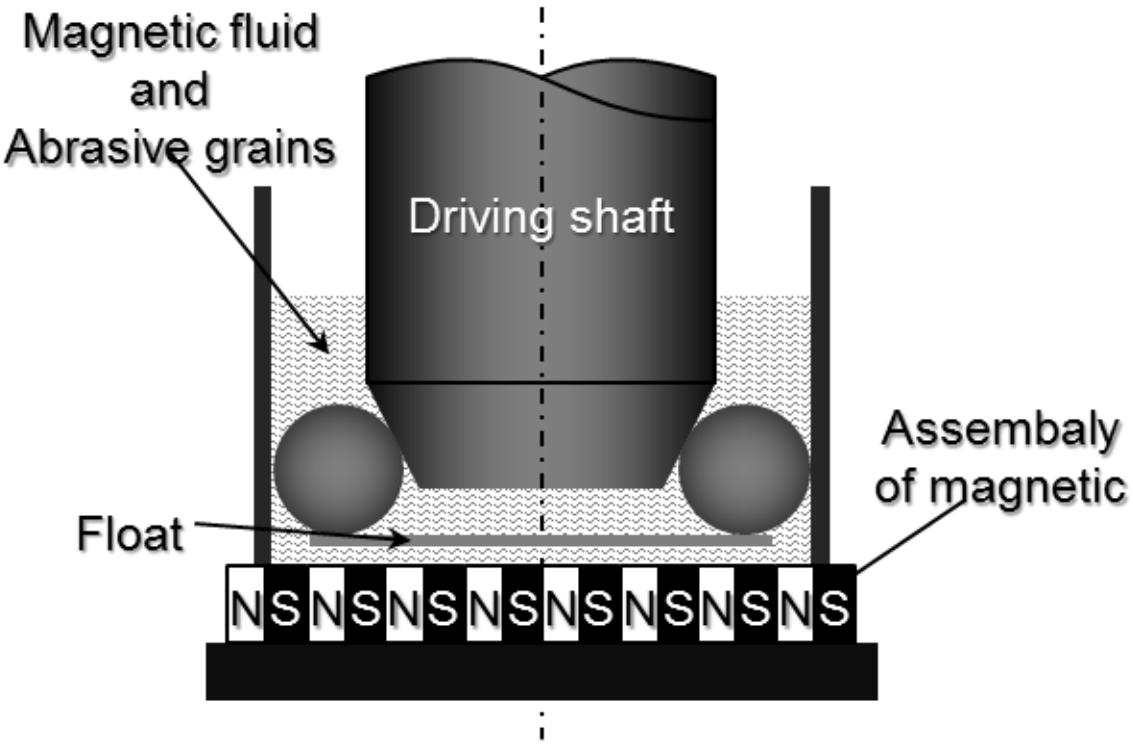

Fig. 1-2 Schematic view of magnetic fluid grinding machine [14]

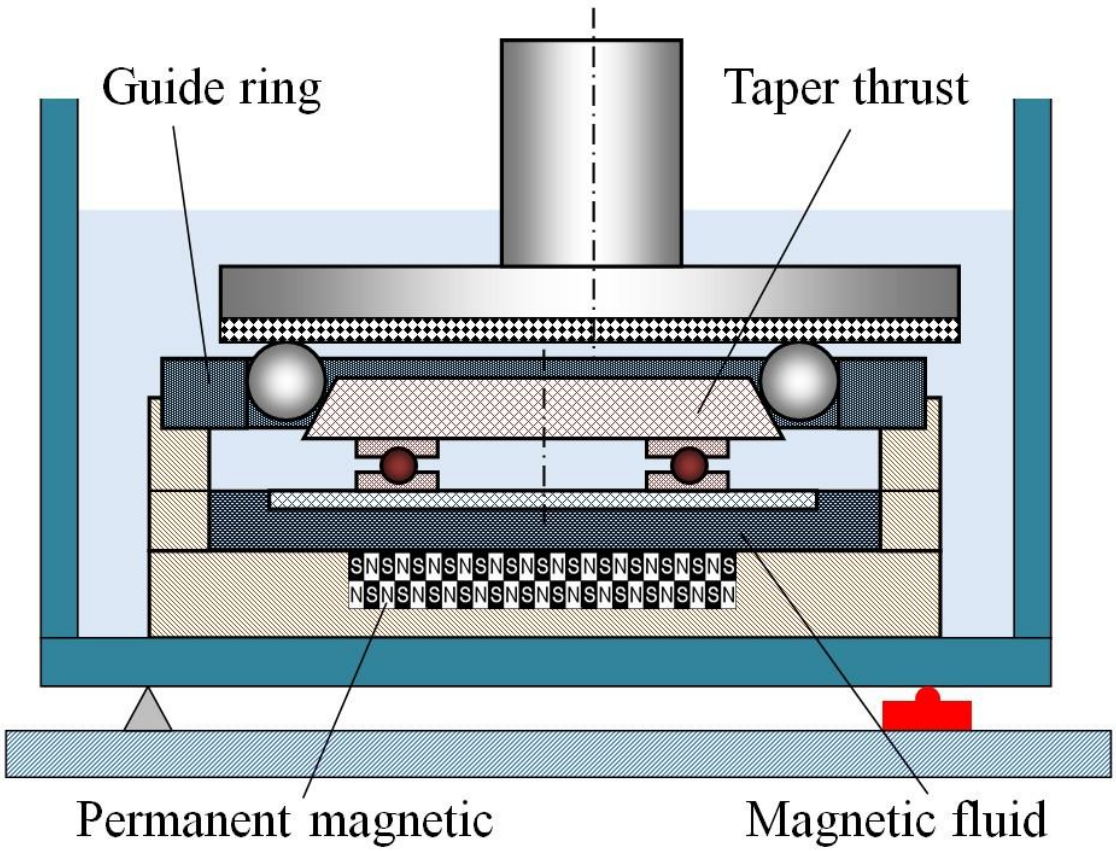

Fig. 1-3 Schematic view of magnetic fluid support grinding machine of ceramic balls [23]

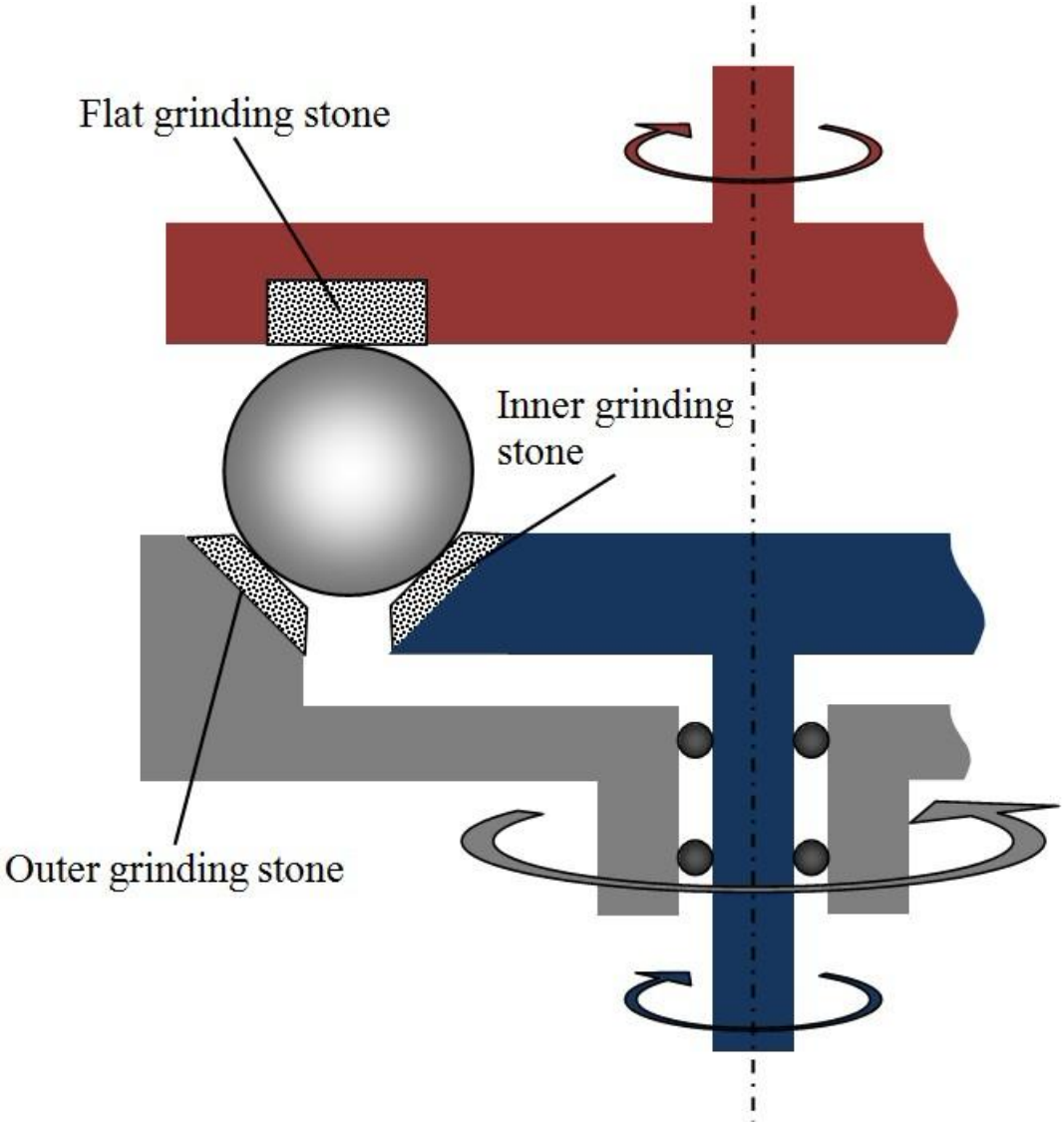

Fig. 1-4 Schematic view of spin angle controlled grinding method [28]

§1.2.2 Dressing of grinding wheels

The state-of-the-art grinding operations are composed of super abrasives (like diamond and CBN) in metal matrix because of their high G-ratio (ratio of material removed to grinding wheel wear). This promotes the difficulty of truing and dressing because the metallic bonds have excellent toughness and wear resistance. So, non-traditional technologies of material removal like electrochemical and thermal processes are introduced to solve the issue.

§§1.2.2.1 Non- traditional dressing technologies

Electro-discharge dressing (EDD) and truing of metal bond grinding wheels was probably first proposed by Suzuki in 1987 (Figure 1-5) [29]. Wang [30] analyzed the process in details and made several important conclusions. It is also an important process for eliminating run-out by truing [31]. A variant of the technology, electro contact discharge dressing (ECDD) uses two electrodes in contact with the grinding wheel [32] to induce thermal erosion. However, the problem of graphitization has also been observed here due to sparking on the diamond particle. Another variant, dry electro-discharge dressing (dry-EDD) has been proposed by Wang [33] with direct contact of dresser with grinding wheel following dry electrical discharge.

Laser technology in assisting grinding was first proposed by Westkamper [34] for dressing and truing of CBN grinding wheels in 1995. Laser dressing poses the risk of thermal damage, bond material resolidification (in case of metal bond), grit damage or graphitization of diamond grits and high initial setup cost, but Hosokawa [35] reported successful elimination of most of these problems. Laser assisted mechanical dressing uses laser irradiation to soften the bond material and the following cutter removes it with ease [36].

Since 1985, several articles on electrolytic and electro-discharge dressing were proposed in Japan. Suzuki [37] proposed a two electrode electrolytic dressing technique with AC supply The technique can be applied to pre-process and in-process dressing of metal bonded grinding wheels (Figure 1-6). The principle of electro chemical discharge machining (ECDM) was also introduced [38] for truing-and dressing. Electrolytic dressing of metal bond super abrasive wheels by the formation of oxide was also reported by other researcher [39, 40]. The most popular of electrolytic dressing is however what is known as ELID (Figure 1-7), which by principle is same as ECM (electro-chemical machining), which was popularized by Ohmori [41].

§§1.2.2.2 Electrolytic In-Process Dressing (ELID)

Ohmori popularized ELID Grinding in 1990 [41] to the international community by efficient grinding of silicon wafers with cast iron bonded diamond (CIB-D) wheel. Different grinding schemes of creep-feed, in-feed and rapid feed grinding were carried out successfully without wheel loading or glazing. There was also a very high increase in surface quality. Stable and reduced grinding forces were reported, demonstrating no wheel loading.

In 1993, Ohmori introduced the concept of ELID cycle (Fig. 1-8) [42]. At the start of the grinding operation, the oxide layer is not valid. Thereby, it is necessary to develop a modest layer of oxide before grinding process. This is called the pre-dressing operation, in which the electrolysis is implemented without the grinding action for duration of 10 minutes [41] to 90 minutes [43]. Then followed by grinding operation, the oxide layer is removed with the dull grits by the collision of the workpiece and exposes sharp ones. Meantime, the resistance decreases with the layer thickness and the current increases to

reform the lost layer.

The electrolytic chemical reactions for the process were reported by Ohmori [44] for CIB (cast iron bond) wheel. Once made anodic, the bond material of iron is electrolyzed into Fe^{2+} firstly. The ionized Fe then forms $Fe(OH)_2$ and/or $Fe(OH)_3$, and further changes into oxides such as Fe_2O_3, which stick to the surface of the grinding wheel.

In 1995, detailed analysis of experimental process for surfaces generating was published [45]. Wheels with different grits size were used to grind mono-crystalline silicon, silicon nitride and BK7 glass. Grinding of glass and silicon, with constant pressure in-feed was reported and found to be effective for ultrafine grits (#120,000 to #3,000,000). Again in 1997, Ohmori [46] explained the variation of the electrolytic behavior and grinding forces for different electrolytes, input voltage wave forms, grinding wheel bond materials and several work piece materials and shapes. The change in current and voltage during pre-dressing was also addressed. The DC power source developed the thickest oxide layer after 30 minutes pre-dressing on CIB-D (cast iron bond diamond) wheel, followed by the pulsed DC and then the AC, but etched layer thickness, i.e. the amount of metal bond corroded was found to be lowest for pulsed DC. Thus, pulsed DC will give lower wheel wear compared to other power sources for electrolysis. In the same year, Bandyopadhyay [47] discussed a modified pre-dressing technique.

The process was further explained in 2002, by Lim [48] who explained its fundamental working principle-in detail. Experiments were conducted with varying feed rates and duty ratio. The result was compared with ordinary grinding results. It proved that the oxide layer built up to a certain thickness until the grinding forces reached high enough to break it, suddenly reducing

its thickness along with grinding forces. It was also found that the oxide layer acts as a damper and in spite of a compromise in machine stiffness, mirror surface generation was possible. Higher duty ratio was reported to decrease surface roughness values but increases the wheel wear. There exists a threshold value of feed rate for grinding, beyond which grinding burn occurs because rate of wheel wear is higher than rate of layer formation.

Bifano et al. [49] published a paper on both fundamental experiment and real grinding with bronze bond wheel in 1999. The experiments used NaCl solution as electrolyte (which is not generally used in modern commercial ELID), and were more intensively done on a cut-off saw than on general grinding. It was found that ELID improved the material removal rate of bronze bond grinding wheel. Based on the results, he suggested a partial model of dressing and an explanation for the thickness of oxide film/layer.

In 2007, Fathima [50] proposed a model for the overall ELID grinding operation. The model was based on the fact that contact between wheel and work piece was not through abrasives in ultra-precision grinding (unlike ordinary grinding), but through asperities on the surface of the wheel and that of the work material. Hertzian contact mechanics was applied to find out the load between the contacting asperities. Several tests and measurement of the grinding wheel were implemented to find parametric values of the model and the final results of the simulation were found to be in good agreement with the experiments.

In the same year, Klocke et al. [51] analyzed the surfaces of iron-bronze, cobalt-bronze and normal bronze materials after electrolysis in CG-7. It was found that an increase in thickness of the oxide layer of iron and cobalt bronze alloy occurred while bronze showed no layer growth. Later in 2009, they

reported that a pure anodic dissolution took place on bronze bond grinding wheel without oxide layer formation [52].

Although an explanation of the mechanism of ELID was proposed by Ohmori, and different kind of models were discussed by other researchers, the real understanding is far from sufficient. The results mentioned above are full of discord, and basically obtained by trial and error.

In addition, to the best of our knowledge, all the researches of ELID was limited to the sliding grinding processes such as the plane and curved surface grinding. The research of ELID of the rolling grinding process such as grinding of balls has not been reported.

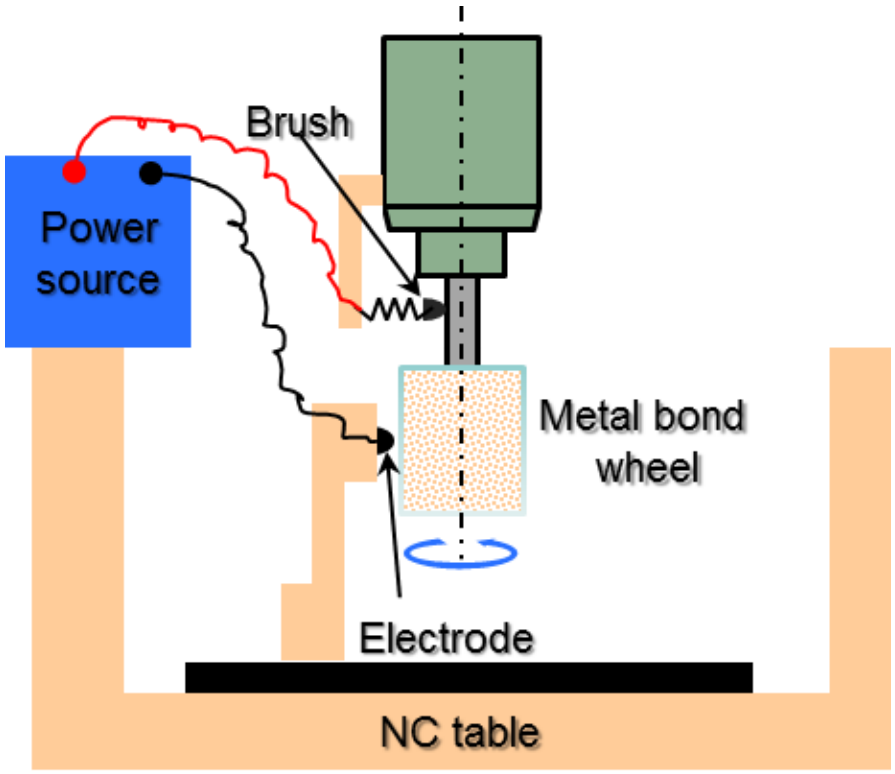

Fig. 1-5 Schematic of on-machine electro-discharge (ED) truing/dressing method [29]

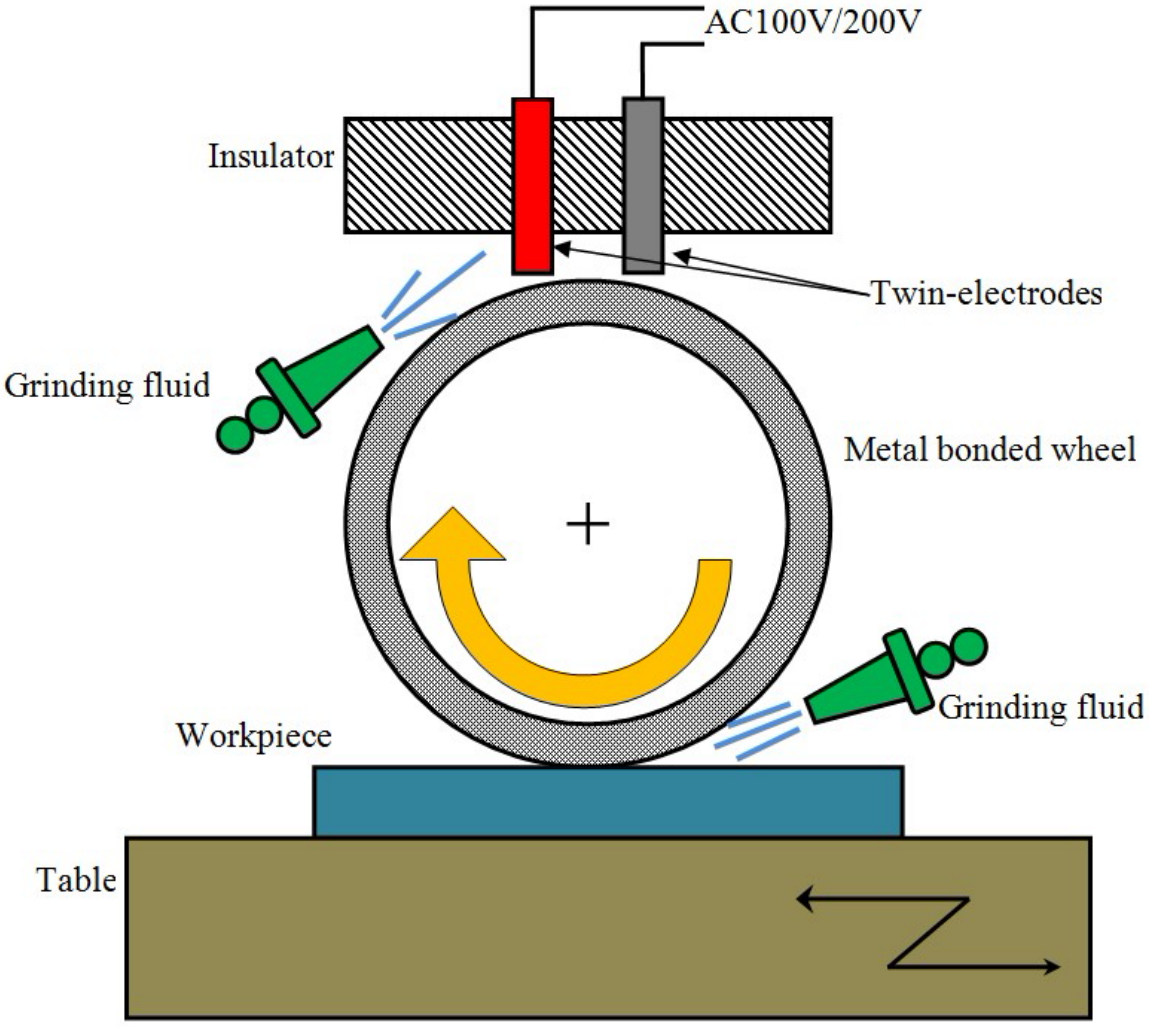

Fig. 1-6 Schematic principle of electrochemical dressing method with twin electrodes (Twin-ECD) [37]

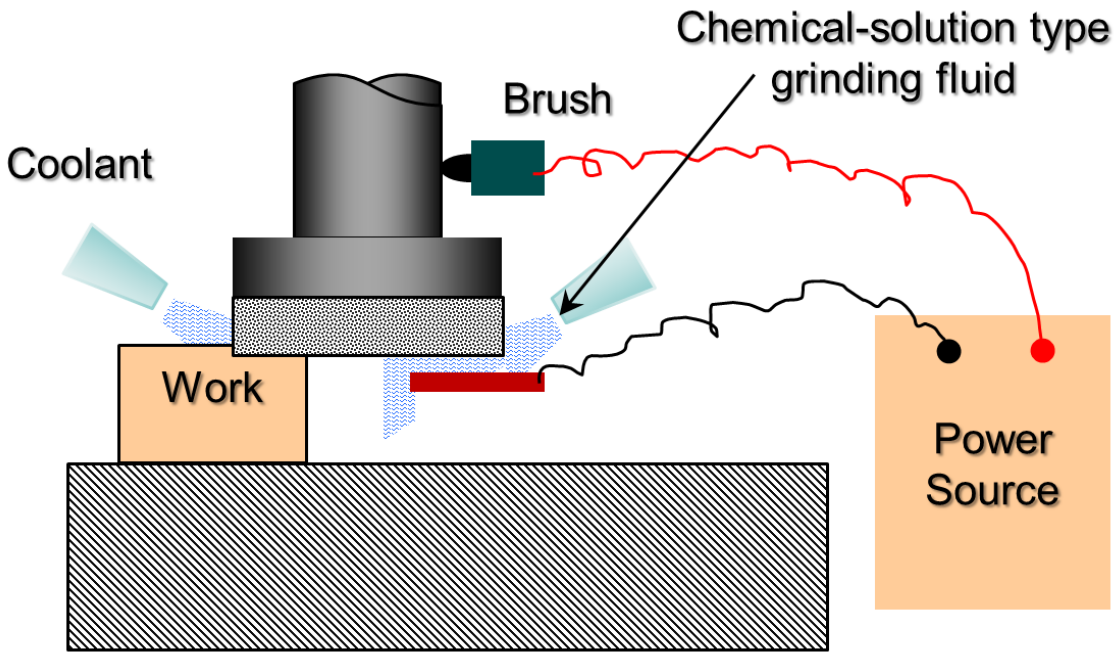

Fig. 1-7 Schematic principle of electrolytic in-process dressing [44]

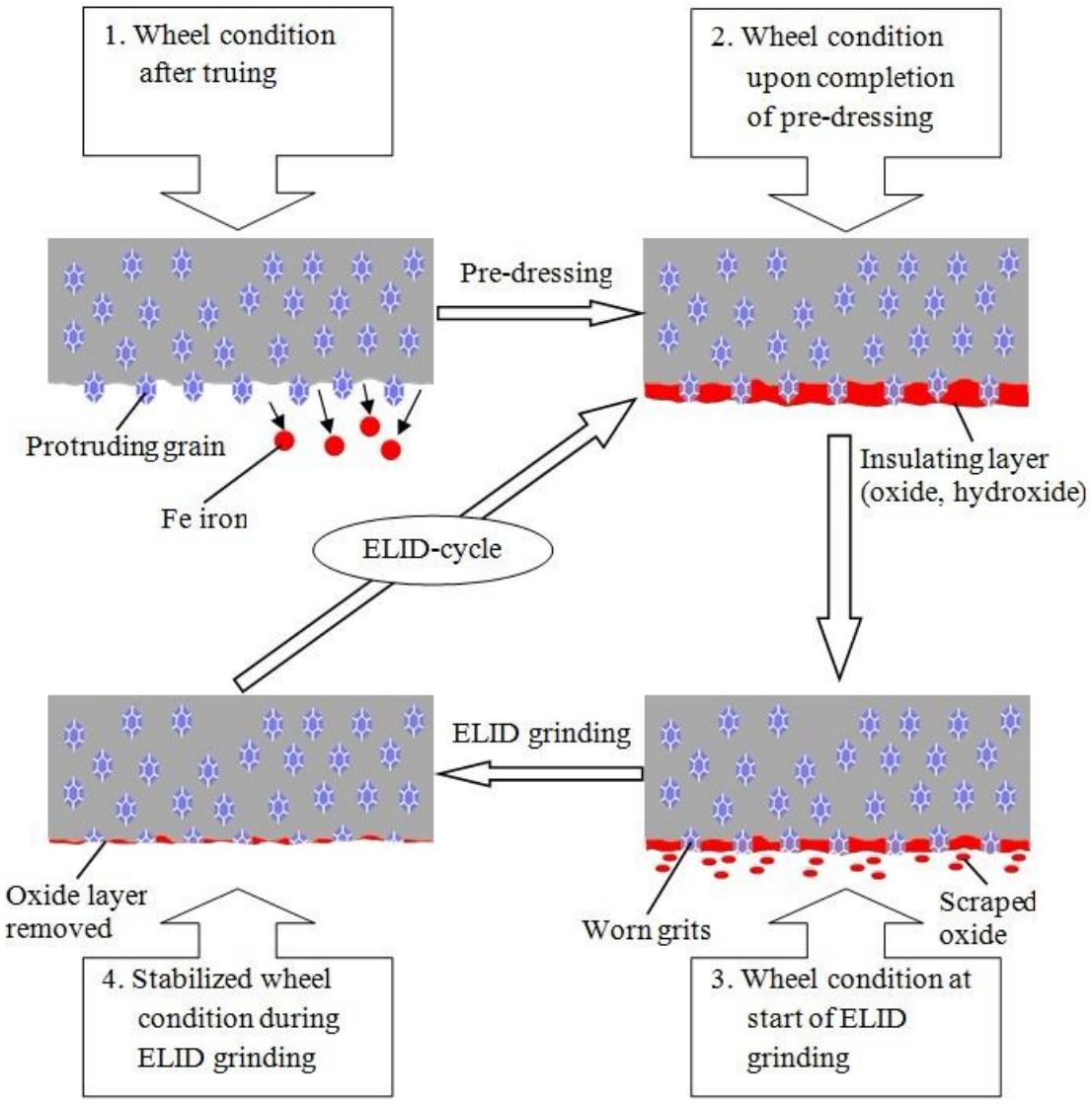

Fig. 1-8 Stages of electrolytic in-process dressing [45]

1.3 Outline of chapters.

Based on the above review and background, the present thesis presents a research on the efficiency superfine grinding of ceramic ball with electrolytic in-process dressing. The paper is composed of the following 4 chapters in detail:

Chapter 1 is the introduction which includes background, review of literature and purpose of the paper.

Chapter 2 presents some basic information about the ball's grinding. The purpose of the chapter is to elucidate the understanding of the kinematics of ball grinding, mechanism of spherical surface generation and material removal.

Chapter 3 presents a basic research on the mechanism of electrolytic dressing by using a ball-on-disk friction test machine in which electrolysis can be implemented simultaneously. The purpose of the chapter is to elucidate how the metal material is removed in the grinding process.

Chapter 4 presents a series of real grinding experiment. The purpose of the chapter is to investigate the effect of electrolytic dressing in different grinding conditions.

Chapter 5 presents the conclusions of the thesis. The main conclusions of the paper are listed in detail. Some outlooks about this research are also given.

1.4 Reference

[1] J. Breznak, E. Breval, N. H. Macmillan. Sliding friction and wear of structural ceramics. J. Mater. Sci. 1985, 20, 5647-4680.

[2] M. Ido. Studies on the method of the manufacture of miniature ball bearings (in Japanese). J. JSPE 1957, 23, 4, 127-131.

[3] M. Ido, T. Hazi, M. Nakazima. On the miniature ball bearings: on the effect of evolutional radius in lapping steel balls (in Japanese). J. JSPE 1960, 26, 8, 470-475.

[4] M. Ido, R. Nagata, T. Hazi. On the miniature ball bearings: on the effect of lap groove angle in lapping steel balls (in Japanese). J. JSPE 1962, 28, 6, 317-213.

[5] M. Ido, T. Hazi. On the miniature ball bearings: on the lapping pressure in lapping steel balls (Part 1) (in Japanese). J. JSPE 1958, 24, 4, 161-168.

[6] M. Ido, M. Nakazima, T. Hazi. On the miniature ball bearings: on the effect of lapping liquid in lapping steel balls (in Japanese). J. JSPE 1961, 27, 5, 261-267.

[7] M. Ido, T. Hazi. On the miniature ball bearings: on the lapping pressure in lapping steel balls (Part 2) (in Japanese). J. JSPE 1958, 24, 5, 254-258.

[8] K. Inagaki, K. Abe. Evaluation of performance of minute sphere grinders prepared for trial (in Japanese), Report of Science and measurement research institute. Tohoku University 1976, 25, 1, 49-65.

[9] F. Itoigawa, T. Nakamura, K. Funabashi. Steel ball lapping by lap with V-shape GROOVE (in Japanese). Trans. JSME 1993, 59, 562, 1906-1912.

[10] K. Goto, H. Mizumoto. A lapping system for ultra-precision bearing balls (in Japanese). J. JSPE 1996, 62, 5, 681-685.

[11] N. Umehara, K. Kato. A study on magnetic fluid grinding: 1st report, the effect of the floating pad on removal rate of Si_3N_4 balls (in Japanese). Trans. JSME 1988, 54, 1599-1604.

[12] N. Umehara, K. Kato. Principles of magnetic fluid grinding of ceramic balls. International Journal of Applied Electromagnetics in Materials 1990, 1, 37-43.

[13] T. H. C. Childs, H. J. Yoon. Magnetic fluid grinding cell design. Annals of the CIRP 1992, 41, 1, 343-346.

[14] K. Kato, B. Zhang, N. Umehara, T. H. C. Childs, D. A. Jones, S. Mahmood. Kinematics of balls in magnetic fluid grinding: predictions of the onset of skidding motion between balls and driving shaft (in Japanese). Trans. JSME, C, 1994, 60, 572, 1433-1439.

[15] N. Umehara. Magnetic fluid grinding – a new technique for finishing advanced ceramics. Annals of the CIRP 1994, 43, 1, 185-188.

[16] N. Umehara, K. Kata, M. Takegoshi. Effects of supporting stiffness of a float and grinding load on fundamental grinding characteristics of ceramic balls in magnetic fluid grinding (in Japanese). Trans. JSME, C 1995, 61, 584, 1709-1714.

[17] T. H. C. Childs, S. Mahmood, H. J. Yoon. Magnetic fluid grinding of ceramic balls. Tribology international 1995, 28, 6, 341-348.

[18] T. H. C. Childs, D. A. Jones, S. Mahmood, B. Zhang, K. Kato, N. Umehara. Magnetic fluid grinding mechanics. Wear 1994,175, 189-198

[19] N. Umehara, K. Kato. Magnetic fluid grinding of advanced ceramic balls. Wear 1996, 200,148-153.

[20] B. Zhang, N Umehara, K. Kato. Effect of the eccentricity between the driving shaft and the guide ring on the behavior of magnetic fluid

grinding of ceramic balls (in Japanese). J. JSPE 1995, 61, 4, 585-590.

[21] B. Zhang, T. Uematsu and Akira Nakajima. High efficiency and precision grinding of Si_3N_4 ceramic balls aided by magnetic fluid support using diamond wheels. JSME International Journal C 1998, 41, 3 499-505.

[22] B. Zhang, A. Nakajima. Spherical surface generation mechanism in the grinding of balls for ultraprecision ball bearing. Proc, Instn Mech Engrs, Part J 2000, 214, 351-357.

[23] B. Zhang, A. Nakajima. Dynamics of magnetic fluid support grinding of Si_3N_4 ceramic balls for ultraprecision bearings and its importance in spherical surface generation. Precision Engineering 2003, 27, 1-8.

[24] F. Y. Chang, T. H. C. Childs. Non-magnetic fluid grinding. Wear 1998, 233, 7-12.

[25] S. Ichikawa, H. Ona, I. Yoshimoto. A proposal new lapping method for ceramic balls (in Japanese). J. JSPE 1992, 58, 9, 1557-1562.

[26] T. Kurobe, H. Kakuta, M. Onoda. Spin angle control lapping of balls (1st Report) -Theoretical analysis of lapping mechanism- (in Japanese). J. JSPE 1996, 62, 12, 1773-1777.

[27] T. Kurobe, H. Kakuta, M. Onoda. Spin angle control lapping of balls (2nd Report) -Lapping of silicon nitride ball- (in Japanese). J. JSPE 1997, 63, 5, 726-730.

[28] T. Kurobe, T. Morita, N. Tsuchihashi. Super fine finishing ceramic ball using spin angle controlled machining method (in Japanese). J. JSPE 2004, 70, 11, 1392-1396.

[29] K. Suzuki, T. Uematsu, T. Nakagawa. On-machine trueing/dressing of metal bond grinding wheels by electro-discharge machining. Annals of

the CIRP 1987, 36, 115-118.

[30] X. Wang, B, Ying, W. Liu. EDM dressing of fine grain super abrasive grinding wheel. International Journal of Materials Processing Technology 1996, 62, 299-302.

[31] N. Ortega, J. A. Sanchez, J. Aranceta, J. A. Maranon, X. Maidagan. Optimisation of grit protrusion in the electro-discharge dressing process of large grit size CBN grinding wheels. Journal of Materials Processing Technology 2004, 149, 524-529.

[32] H. K. Tonshoff, T. Friemuth. In-process dressing of fine diamond wheels for tool grinding. Precision Engineering 2000, 24, 58-61.

[33] Y. Wang, X. J. Zhou, D. J. Hu. An experimental investigation of dry-electrical discharge assisted truing and dressing of metal bonded diamond wheel. International Journal of Machine Tools and Manufacture 2006, 46, 333-342.

[34] E. Westkämper. Grinding assisted by Nd:YAG lasers. Annals of the CIRP 1995, 44, 317-320.

[35] A. Hosokawa, T. Ueda, T. Yunoki. Laser dressing of metal bonded diamond wheel. Annals of the CIRP 2006, 55, 329-332.

[36] C. Zhang, Y. C. Shin. A novel laser-assisted truing and dressing technique for vitrified CBN wheels. International Journal of Machine Tools and Manufacture 2002, 42, 825-835.

[37] K. Suzuki, T. Uematsu, T. Yanase, M. Honma, S. Asano. Development of a simplified electrochemical dressing method with twin electrodes. Annals of the CIRP 1991, 40, 363-342.

[38] M. Schopf, I. Beltrami, M. Boccadoro, D. Kramer. ECDM (Electro Chemical Discharge Machining), a new method for trueing and dressing

of metal bonded diamond grinding tools. Annals of the CIRP 2001, 50, 125-128.

[39] D. Kramer, E. Rehsteiner. ECD (Electrochemical In-Process Controlled Dressing), a new method for grinding of modern high-performance cutting materials to highest quality. Annals of the CIRP 1999, 48, 265-268.

[40] E. S. Lee, J. D. Kim. A study on the analysis of grinding mechanism and development of dressing system by using optimum in-process electrolytic dressing. International Journal of Machine Tools and Manufacture 1997, 37, 1673-1689.

[41] H. Ohmori, T. Nakagawa. Mirror surface grinding of silicon wafers with electrolytic in-process dressing. Annals of the CIRP 1990, 39, 329-332.

[42] H. Ohmori. Electrolytic In-Process Dressing grinding technique for ultraprecision mirror surface machining. J. JSPE 1993, 59, 9, 1451-1457.

[43] N. Itoh, H. Ohmori. Grinding characteristics of hard and brittle materials by fine grain lapping wheels with ELID. Journal of Materials Processing Technology 1996, 62, 315-320.

[44] H. Ohmori, I. Takahashi, B. P. Bandyopadhyay. Ultra-precision grinding of structural ceramics by Electrolytic In-Process Dressing (ELID) grinding. Journal of Materials Processing Technology 1996, 57, 272-277.

[45] H. Ohmori, T. Nakagawa. Analysis of mirror surface generation of hard and brittle materials by ELID (Electrolytic In-Process Dressing) grinding with superfine grain metallic bond wheels. Annals of the CIRP 1995, 44, 287-290.

[46] H. Ohmori, T. Nakagawa. Utilization of nonlinear conditions in precision grinding with ELID (Electrolytic In-Process Dressing) for fabrication of

hard material components. Annals of the CIRP 1997, 46, 261-264.

[47] B. P. Bandyopadhyay, H. Ohmori, I. Takahashi. Efficient and stable grinding of ceramics by Electrolytic In-Process Dressing (ELID). Journal of Materials Processing Technology 1997, 66, 18-24.

[48] H. S. Lim, K. Fathima, A. S. Kumar, M. Rahman. A fundamental study on the mechanism of Electrolytic In-Process Dressing (ELID) grinding. International Journal of Machine Tools and Manufacture 2002, 43, 935, 943.

[49] T. Bifano, R. Krishnamoorthy, H. Fawcett, E. welch. Fixed-load electrolytic dressing with bronze bonded grinding wheels, Journal of Manufacturing Science and Engineering. Transactions of the ASME 1999, 21, 20-27.

[50] K. Fathima, M. Rahman, A. S. Kumar, H. S. Lim. Modeling of ultra-precision ELID grinding. SAME Journal of Manufacturing Science and Engineering, 2007, 129, 296-302.

[51] F. Klocke, A. Klink, U. Schneider. Electrochemical oxidation analysis for dressing bronze-bonded diamond grinding wheels. Production Engineering 2007, 1, 141-148.

[52] F. Klocke, A. Klink, M. Henerichs. ELID dressing behavior of fine grained bronze bonded diamond grinding wheels. International Journal of Abrasive Technology 2009, 2, 4, 358-367.

Chapter 2

Basics of Ball Grinding

2.1 Kinematics of ball grinding

NOTATION	
r	Radius of the ball
R_b	Circulation radius of the balls
Ω_b	Revolution speed of balls
V_b	Velocity of the ball
ω	Spinning speed of the ball
θ	Direction of the spinning axis of the ball
R_g, R_o, R_i	The distance between the V-groove center and the contact point at the grinding wheel, the outer wall and the inner wall of the V-groove
Ω_g , Ω_o , Ω_i	Angle speed of the grinding wheel, the outer wall and the inner wall of the V-groove
V_g, V_o, V_i	Velocities of the grinding wheel, the outer wall and the inner wall of the V-groove at the contact points
α, β	V-groove angles
δ	Eccentricity between the upper lapper and the lower lapper

To grinding balls efficiently, it is necessary to understand the motion of the balls during the grinding process. In 2000, Zhang [1] analyzed the kinematics of the ball for kinds of grinding system, but the analysis ignored the effect of the distance difference caused by the radius difference between the inner wall and the outer wall. With circumference difference being taken into account, Kurobe et al. [2, 3] analyzed the ball motion when using spin angle controlled machining method in 1996.

Overall, there are many types of ball grinding mechanism and they can be generally classified as the following five types: (Fig. 2-1):

1) Concentric V-groove grinding mechanism;

2) Eccentric V-groove grinding mechanism;

3) Twin V-groove grinding mechanism;

4) Cross twin V-groove grinding mechanism;

5) Tri-block grinding mechanism.

Among these mechanisms, the twin V-groove grinding mechanism, which may have multi-concentric V-grooves, is most widely used in industry.

The balls to be ground are placed in a V-groove of a lower lapper and are pressed on by an upper lapper which may be flat or with another V-groove. During grinding process, the balls are driven by the upper lapper to circulate around the V-grooves, and material removal occurs at the contact area. For the case of the tri-block grinding mechanism, the lower lapper also rotates, but in the opposite direction of rotation to the upper lapper.

Except for the eccentric grinding mechanism (Fig. 2-1(b)) and cross twin V-groove grinding mechanism (Fig. 2-1(d)), the other concentric grinding mechanisms can be simplified in geometry as shown in Fig. 2-2. Suppose that, the inner block and the outer block are separated as shown in Fig. 2-3, and

they rotate at an angle speed of Ω_i and Ω_o while the grinding wheel rotates at an angle speed of Ω_g. The distance between the contact point and the center of the V-groove, also the rotating shaft of the grinding wheel, are R_g, R_o, R_i respectively, then the velocity of the each block at the contact point are as follow:

$$V_g = R_g \Omega_g \tag{2-1a}$$

$$V_o = R_o \Omega_o = (R_b + r\sin\alpha)\Omega_o \tag{2-1b}$$

$$V_i = R_i \Omega_i = (R_b - r\sin\beta)\Omega i \tag{2-1c}$$

where R_b is the circulation radius of the balls, r is the radius of the ball, and α, β are the angle of the outer wall and inner wall respectively.

Since the motion of the mechanism is symmetric about the central axis, there is no speed in the radial direction. Under the assumption of that gyroscopic effect can be ignored, the spinning axis of balls must be in a plane determined by the circulation central line O-O and the central point of the ball as shown in Fig. 2-2. The speeds v_g, v_o, v_i at contact points on the ball surface are then given as:

$$v_g = \omega r_g = \omega r \sin(\theta + \frac{\pi}{2}) = \omega r \cos\theta \tag{2-2a}$$

$$v_o = \omega r_o = \omega r \sin(\theta - \alpha - \frac{\pi}{2}) = -\omega r \cos(\theta - \alpha) \tag{2-2b}$$

$$v_i = \omega r_i = \omega r \sin(\theta + \beta - \frac{\pi}{2}) = -\omega r \cos(\theta + \beta) \tag{2-2c}$$

where θ is the direction of the spin axis. All the velocities are perpendicular to the paper plane and the velocities pointing to the paper is negative while that pointing to the outside of the paper point is positive. If there is no skidding at the contact points, then the motion of the ball are given as:

$$\Omega_b R_g + \omega r \cos\theta = V_g \tag{2-3a}$$

$$\Omega_b R_o - \omega r \cos(\theta - \alpha) = V_o \tag{2-3b}$$

$$\Omega_b R_i - \omega r \cos(\theta + \beta) = V_i \tag{2-3c}$$

Equations (2-3) give expressions for the spinning axis direction θ, the spinning speed ω of balls and the revolution speed of balls center Ω_b as follow:

$$\theta = \tan^{-1}\left[\frac{R_o R_g \cos\beta(\Omega_o - \Omega_g) - R_i R_g \cos\alpha(\Omega_i - \Omega_g) + R_o R_i(\Omega_o - \Omega_i)}{R_o R_g \sin\beta(\Omega_o - \Omega_g) + R_i R_g \sin\alpha(\Omega_i - \Omega_g)}\right] \tag{2-4}$$

$$\omega = \frac{V_g R_o - V_o R_g}{r_g R_o - r_o R_g} \tag{2-5}$$

$$\Omega_b = \frac{V_g r_o - V_o r_g}{R_g r_o - R_o r_g} \tag{2-6}$$

Equations (2-4) to (2-6) indicate that the circulation speed and the spinning speed of balls are fully determined by the contact geometry and the speeds of each wall of the V-groove. This suggests that, under stable grinding conditions, both the circulation speed and the spinning speed are constant and do not change during grinding. Equations (2-4) to (2-6) comprise the basic kinematic equation for ball grinding.

For the normal concentric grinding system (Fig. 2-1(a)), the inner block and the outer block of the V-groove are integrated and fixed, thus $\Omega_i = \Omega_o = 0$. Then Eq. (2-4) can be simplified into:

$$\tan\theta = \frac{R_o \cos\beta - R_i \cos\alpha}{R_o \sin\beta + R_i \sin\alpha} \tag{2-8}$$

For the case when the V-groove is symmetric, that is $\alpha = \beta$, Eq. 2-8 can be further simplified into:

$$\tan\theta = \cot\alpha \frac{R_o - R_i}{R_o + R_i} = \cos\alpha \frac{r}{R_b} \tag{2-9}$$

And

$$\Omega_b = \Omega_g \frac{\cos\alpha}{1+\cos\alpha} \tag{2-10}$$

$$\omega = \Omega_g \frac{\cos\alpha}{(1+\cos\alpha)\sin\theta} \tag{2-11}$$

Equations (2-9) to (2-11) show that in such case the direction of the spin axis and the spin speed is only determined by the angle of the V-groove and the ratio r/R_b. It is clear that the contact trace is a fixed circle on the ball surface. This is an unexpected result because it is impossible to generate a spherical surface during grinding when the contact trace is a fixed circle.

Several experiments were conducted to confirm the above analysis. A fix contact trace was obtained and the direction of the relative spinning speed of balls was measured in terms of the diameter of the contact trace circle of contact point C on the ball surface, and it agrees well with the theoretical predictions.

The analytical and experimental results appear to be contrary to common knowledge and experience to date. The study shows that the contact trace on the ball surface is a fixed circle and it is impossible to grind a real spherical surface by using the concentric V-groove grinding mechanism. However, in industry, ball grinding using the V-groove grinding mechanism seems to be a successful method to some extent. The contradiction between the study and conventional industry experience is expected to disappear in the ultraprecision grinding of balls, because, in the analysis, it is assumed that the contact status is stable but this assumption is not true in the conventional grinding of balls. The contact status of balls may be disturbed by the vibrations caused by, for example, the shape error in the balls being ground and the grinding machine itself. However, in ultraprecision grinding of balls, the shape error in the balls will be so small that the vibration will be very weak. At the same time it is

also necessary for ultraprecision grinding to use high-precision grinding machines, and therefore the vibration of the grinding machine itself will also be very small.

For the twin V-groove grinding mechanism, the contact trace can also be obtained in the same way (Fig. 2-4). Basically, if the contact deformation of both the balls and the lappers is neglected, one ball cannot come into contact simultaneously at more than three points. Consequently, for the case of the twin V-groove grinding mechanism, points A, B, C and D will act alternately, and there is always one point losing contact. This means that the contact condition for the twin V-groove grinding mechanism is not stable even if the speed of the lapper is constant. In Fig. 2-4, ω_1 is the spinning axis of a ball when point C comes into contact, and ω_2 is the spinning axis of a ball when point D comes into contact. In the same way, it can be concluded that the contact traces are also fixed circles for the cross twin V-groove grinding.

Thus, the only method that positively changes the contact trace is thought to be the eccentric V-groove grinding mechanism (Fig. 2-1b). The kinematic of the ball in the eccentric V-groove grinding mechanism is much more complex. Zhang et al. [4] discussed the effect of eccentricity on the contact track; however, the analysis does not take the skidding caused by the constant revolution speed of the ball into account.

The top view of this grinding mechanism is shown in Fig. 2-5. From Fig. 2-5, it is known that the tangential velocity at the contact point on the grinding wheel will change from far end to proximal end during half circle of the ball. The velocity is determined by the position of the ball and, except the far end and the proximal end, the direction of the velocity is different from the direction of the ball's revolution. However since the balls are neatly arranged

in the V-groove, if the gap between the ball and the ball can be ignored, the revolution speed of the ball should be the same in any place in a stable grinding, and it is determined by the minimum resistance torque. Because the revolution speed of the inner block and outer block of V-groove, revolution speed of the balls and the geometry of the V-groove are constant while the driven speed of the grinding wheel is a variable, the ball cannot spin without skidding at the contact point. Assuming the balls rotate in the V-groove in a revolution speed of Ω_b, after a time t, the ball turned an angle of ζ, that is:

$$\zeta = \Omega_b t \tag{2-12}$$

Then

$$L_{OX} = R_b \cos\zeta \tag{2-13a}$$

$$L_{XB} = R_b \sin\zeta \tag{2-13b}$$

$$L_{OO'} = \delta \tag{2-13c}$$

$$L_{O'X} = R_b \cos\zeta + \delta \tag{2-13d}$$

where δ is the eccentricity. Then the distance between the ball center and the rotating axis of the grinding wheel is:

$$L_{O'B} = \sqrt{\left(R_b \cos\zeta + \delta\right)^2 + \left(R_b \sin\zeta\right)^2} = \sqrt{R_b^2 + \delta^2 + 2\cos\zeta R_b \delta} \tag{2-14}$$

$$\sin\gamma = \frac{\delta}{\sqrt{R_b^2 + \delta^2 + 2\cos\zeta R_b \delta}} \sin\zeta \tag{2-15a}$$

$$\cos\gamma = \frac{R + \delta\cos\zeta}{\sqrt{R_b^2 + \delta^2 + 2\cos\zeta R_b \delta}} \tag{2-15b}$$

$$V_g = \sqrt{R_b^2 + \delta^2 + 2\cos\zeta R_b \delta} \cdot \Omega_g \tag{2-16}$$

The velocity component of V_g in the rotation direction of the ball is:

$$V_{gt} = V_g \cos\gamma = \Omega_g R_b + \Omega_g \delta\cos\zeta \tag{2-17}$$

Thus the motion of the ball in eccentric grinding mechanism is given by:

$$\Omega_b R_b + v_g + v'_g = V_{gt} \quad (2\text{-}18a)$$

$$\Omega_b R_b + v_g + v'_g = V_{gt} \quad (2\text{-}18b)$$

$$\Omega_b R_i + v_i + v'_i = V_i \quad (2\text{-}18c)$$

where v'_g, v'_o, v'_i are the skidding speeds at each contact point and define skidding ratio as:

$$S = \frac{v_j'}{V_j - \Omega_b R_j}$$

where $j = gt, o, i$ for grinding wheel, outer wall and inner wall of V-groove. The most straightforward case is shown in Fig. 2-1b, in which the V-groove is integrated and fixed, that is $V_o = V_i = 0$

$$\omega r \cos\theta = (V_{gt} - \Omega_b R_b)(1 - S_g) \quad (2\text{-}19a)$$

$$\omega r \cos(\theta - \alpha) = \Omega_b R_o (1 - S_o) \quad (2\text{-}19b)$$

$$\omega r \cos(\theta + \beta) = \Omega_b R_i (1 - S_i) \quad (2\text{-}19c)$$

To facilitate explanation, suppose the extreme case of $S_o = S_i = 0$, that is no skidding occurs at contact point of V-groove, then the direction of the ball's spin axis θ is determined only by the geometry of the V-groove, as same as concentric grinding system. The contact trace will be a fixed circle, but the velocity difference at the contact of ball and grinding wheel will cause much more linear skidding, leading to more material removal.

For the case of $S_g = 0$, S_o or $S_i = 0$, then the direction of the ball's spin axis θ will change from

$$\tan^{-1}\left(\frac{\Omega_b R_o}{\Omega_g R_b - \Omega_g \delta - \Omega_b R_b} - \cos\alpha\right) \Big/ \sin\alpha$$

to

$$\tan^{-1}\left(\frac{\Omega_b R_o}{\Omega_g R_b + \Omega_g \delta - \Omega_b R_b} - \cos\alpha\right) \Big/ \sin\alpha$$

or from

$$\tan^{-1}\left(\cos\beta - \frac{\Omega_b R_i}{\Omega_g R_b - \Omega_g \delta - \Omega_b R_b}\right) \Big/ \sin\beta$$

to

$$\tan^{-1}\left(\cos\beta - \frac{\Omega_b R_i}{\Omega_g R_b - \Omega_g \delta - \Omega_b R_b}\right) \Big/ \sin\beta$$

as shown in Fig. 2-5.

The analysis shows that, if appropriate conditions are selected, the eccentric V-grove grinding mechanism can avoid the centralization of the contact trace and skidding between ball surface and the grinding wheel.

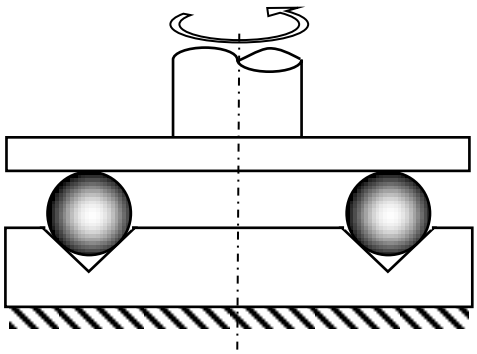

(a) concentric V-groove grinding mechanism

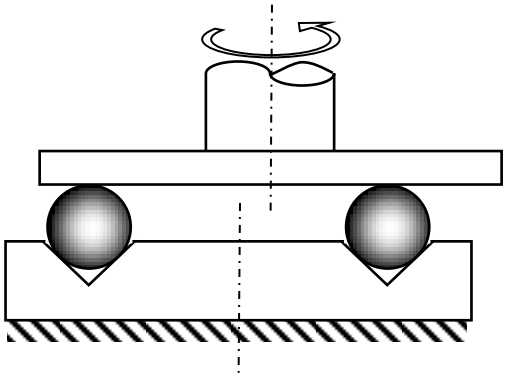

(b) eccentric V-groove grinding mechanism

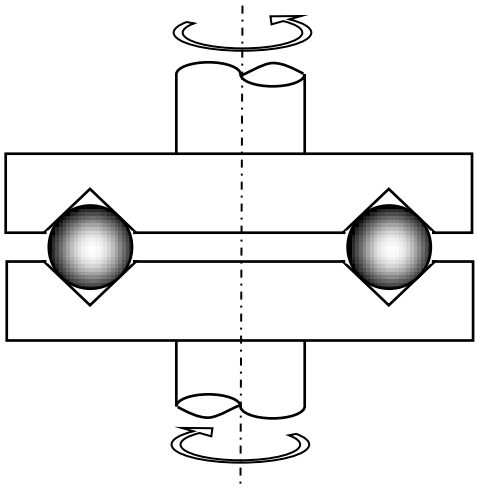

(c) twin V-groove grinding mechanism

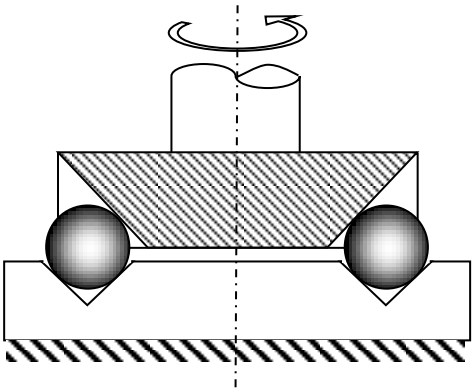

(d) cross twin V-groove grinding mechanism

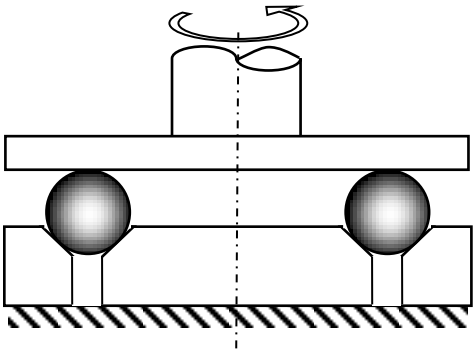

(d) tri-block grinding mechanism

Fig. 2-1 Schematic diagrams of various grinding mechanisms of balls

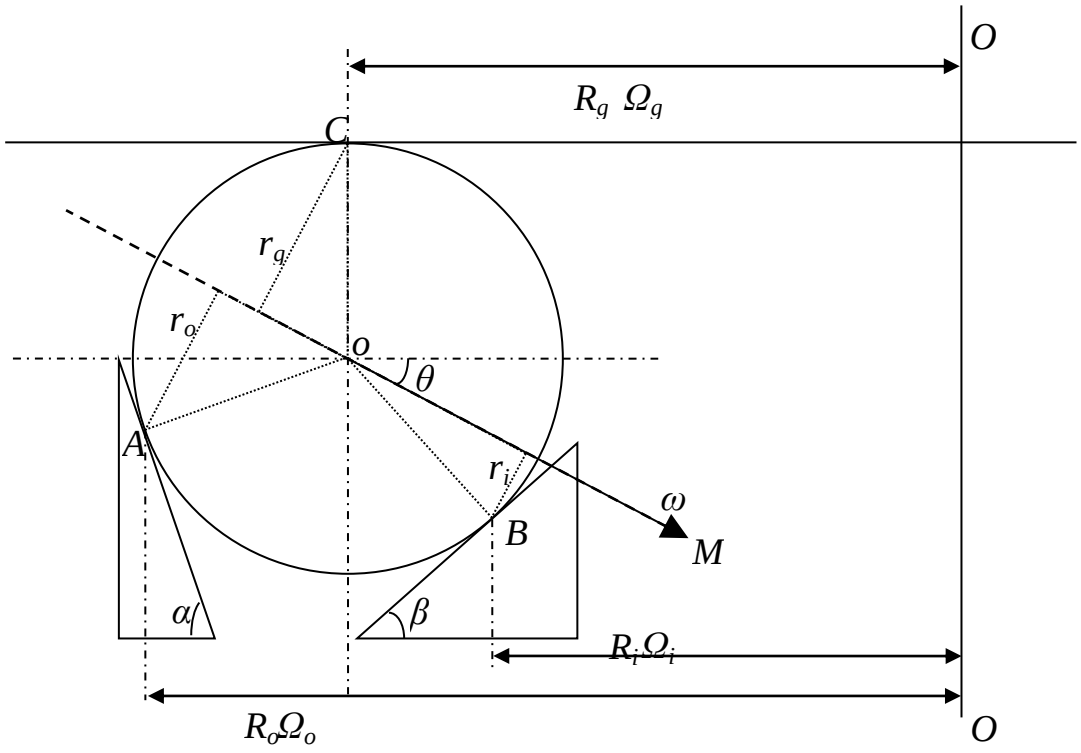

Fig. 2-2 Contact geometry and kinematics of ball grinding

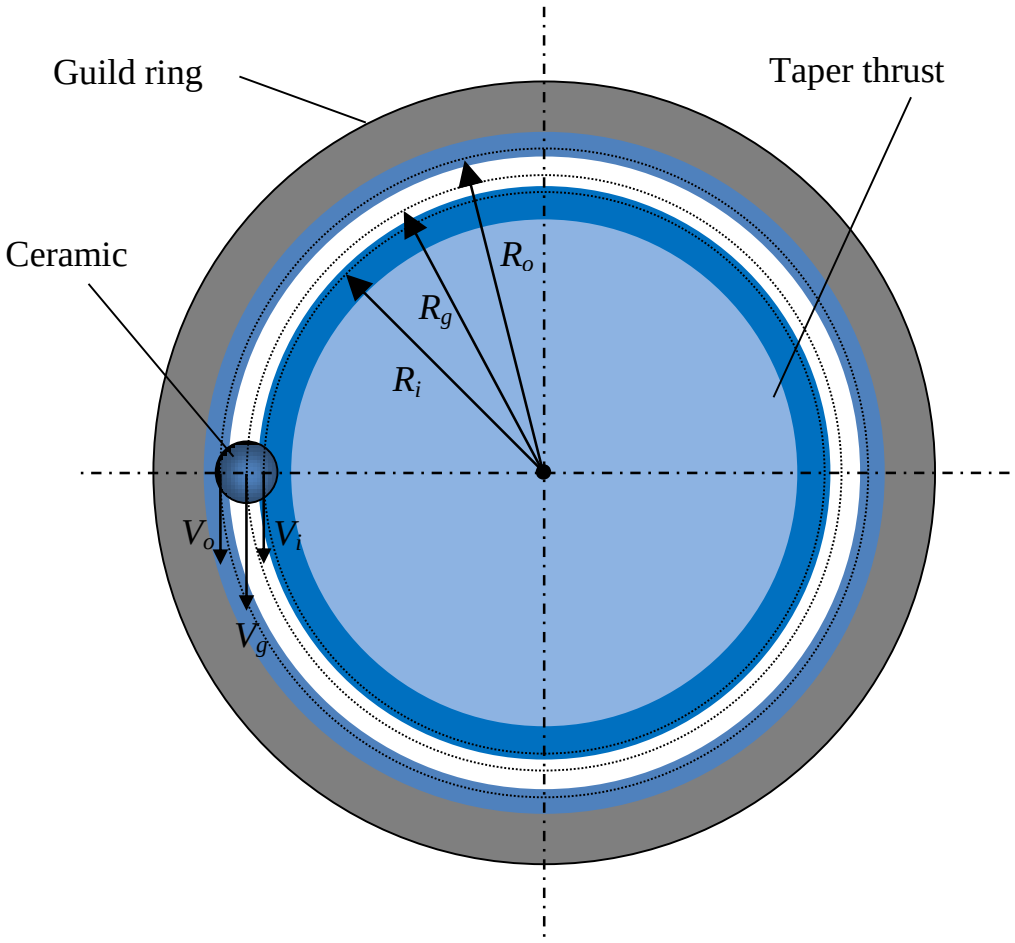

Fig. 2-3 Top view of the concentric V-groove grinding mechanism

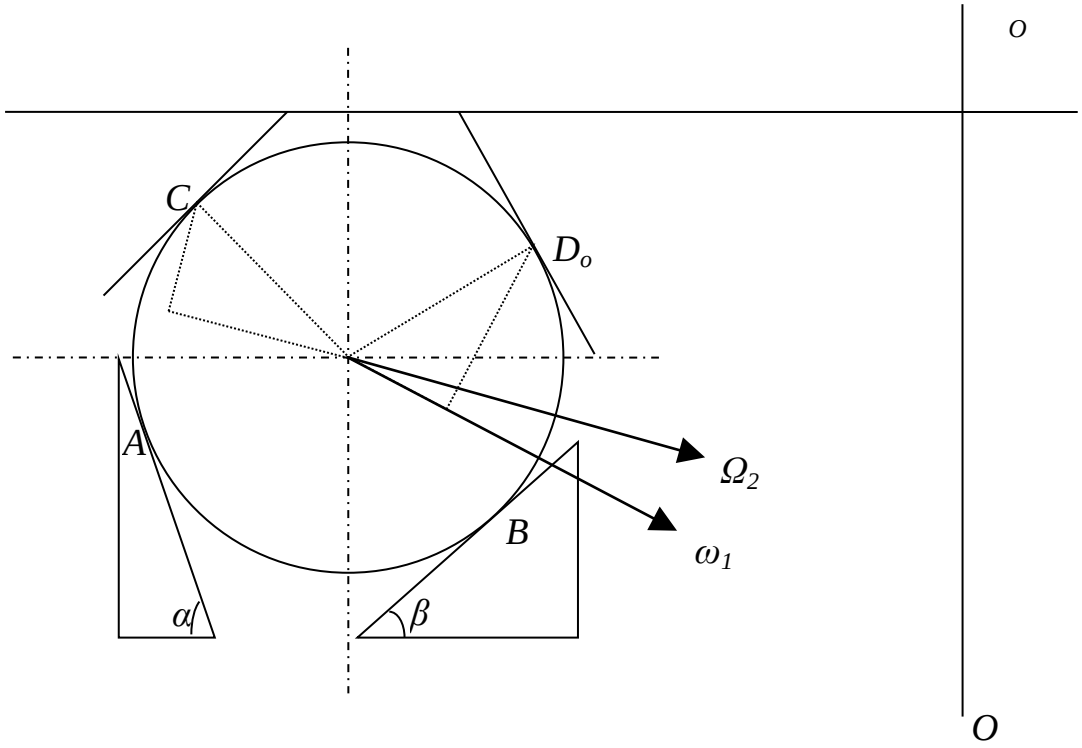

Fig. 2-4 Contact traces for the twin V-groove grinding mechanism at contact points C and D

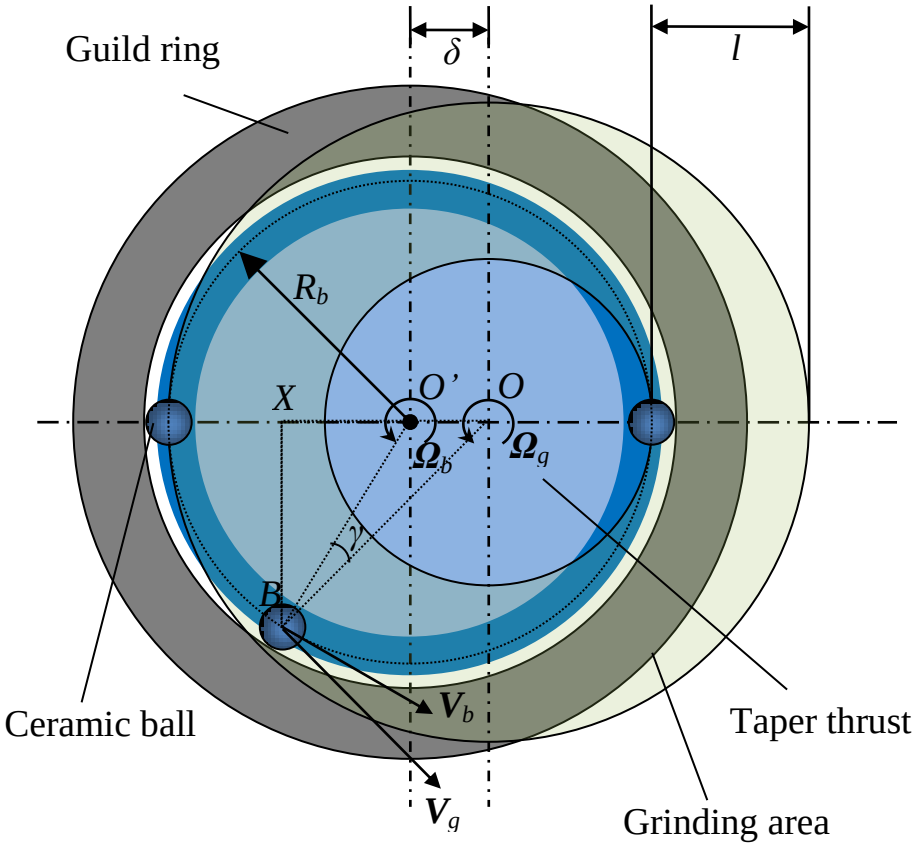

Fig. 2-5 Top view of the eccentric V-groove grinding mechanism

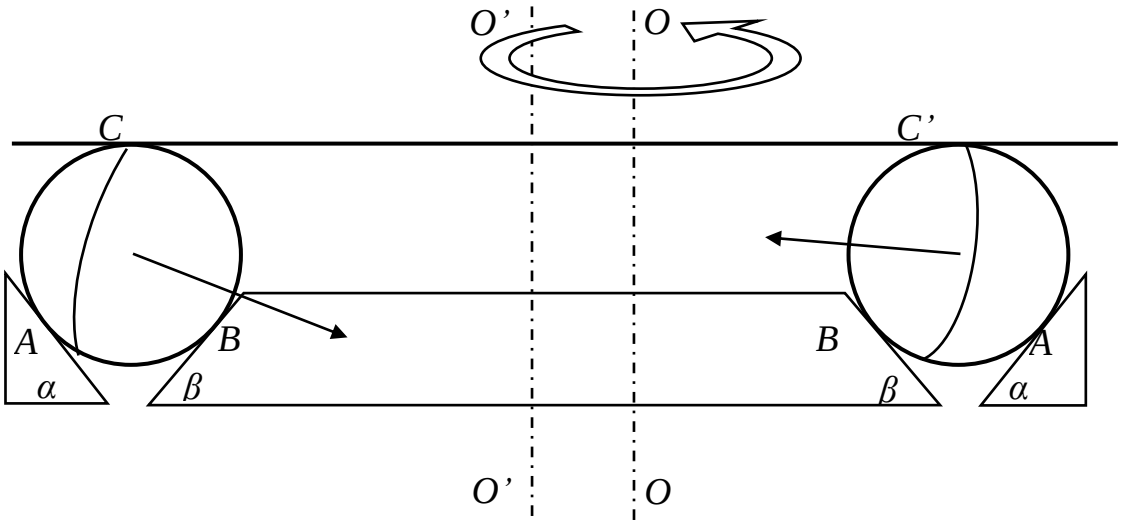

Fig. 2-6 The contact trace shifting at point C of the eccentric V-groove grinding mechanism

2.2 Mechanism of spherical surface generation

Notation

c	damping of the support system
c_{cr}	critical damping
F	variation in force due to shape error of balls
k	static stiffness of one ball
L	actual grinding load
L_0	preset grinding load
m	equivalent mass of support system
N	peak number of the shape error of balls
p	natural frequency of support system
R_g	the inner radius of the guide ring
R_b	radius of the ball

Greek letters

α	taper angle of taper thrust
γ	damping ratio
δ	shape error of balls
ζ	angular frequency
Δ	amplitude of the shape error
λ	magnification factor
ϕ	phase difference between the displacement of support and force
ω	ball spinning speed
Ω	grinding wheel speed

In a previous section, the mechanism of spherical surface generation in grinding is analyzed in terms of kinematics. It is found that the contact trace between the balls and the grinding tool surfaces would concentrate within a fixed circle trace on ball surface if no special measure is taken, which would worsen the sphericity of ground balls, instead of improving it. In other words, ensuring the uniform distribution of contact trace over the whole ball surface is a key point of ultraprecision grinding of balls.

Later in 2003 Zhang and Nakajima [5] also analyzed the spherical surface generation mechanism of ball grinding in terms of dynamic. Theoretical analysis of the magnetic fluid support grinding system was conducted and grinding experiments on the dependence of grinding performance on supports were carried out using four different types of supports.

In the grinding process, any deviation in shape of ceramic balls from ideal spherical surface will cause the support component to move up and down, leading to a variation in the grinding load. This variation in grinding load is considered to play a decisive role in rectification of the shape error of balls. However, the actual situation is different because the support system may have a damping characteristic, which results in a phase difference in the displacement of the support component.

For a straightforward analysis, suppose that a representative ball is supported by a support system composed of a mass m, a spring with stiffness k and a damping with damping coefficient c, as shown in Fig. 2-7. It is reasonable to assume that the ball has shape error given by equation 2-20 without losing any generality, because any form of shape error can always be decomposed into a series of sinusoidal waveforms in terms of Fourier analysis.

$$\delta = \Delta \sin\left(\frac{\zeta}{2\pi}\theta\right) \tag{2-20}$$

where Δ is the amplitude of the shape error and ζ the angular frequency. This shape error will result in a vibration of the support when the ball rolls on the surface of the grinding wheel, which is related to rolling angular speed ω of the ball by the following equation:

$$z = \Delta \sin\left(\frac{\zeta}{2\pi}\omega t + \pi\right) \tag{2-21}$$

where π is the phase difference between shape error and the displacement of the support since when the point of larger diameter comes into contact the support will be put downward in the coordinates shown in Fig. 2-7. It is easy to show that $\zeta/2\pi$ is equal to the peak number in the shape error curve. Therefore, Eq. (2-21) can be rewritten as

$$z = \Delta \sin(N\omega t + \pi) \tag{2-21}$$

where N is the peak number.

According to the vibration theory [4], the force variation is given by

$$F = m\frac{\mathrm{d}^2 z}{\mathrm{d}t^2} + c\frac{\mathrm{d}z}{\mathrm{d}t} + kz \tag{2-22}$$

Putting Eq. (2-21) into Eq. (2-22) and rearranging it give

$$F = \Delta k \lambda \sin(N\omega t + \pi + \phi) \tag{2-23}$$

where

$$\lambda = \sqrt{\left(1 - \left(\frac{N\omega}{p}\right)^2\right)^2 + \left(\frac{N\omega c}{k}\right)^2} \tag{2-24}$$

And

$$\phi = a\tan\left(\frac{N\omega c/k}{1 - (N\omega/p)^2}\right) \tag{2-25}$$

where p is the natural frequency of the support system, and is defined by

$$p = \sqrt{\frac{k}{m}} \tag{2-26}$$

The actual grinding load is then obtained by the following equation:

$$L = L_0 - F = L_0 - \Delta k\lambda \sin(N\omega t + \pi + \phi) \tag{2-27}$$

where λ is generally called magnification factor and ϕ the phase difference. In order to rectify the shape error it is desirable that the grinding force is higher for the place where the diameter is larger. Eq. (2-27) demonstrates that the maximum grinding force is reached when Eq. (2-23) gives the minimum value, which is desirably correspondent to the place on ball surface of maximum diameter. This means that when Eq. (2-23) gives the minimum value, Eq. (2-20) should reach its maximum value. This can be realized only when the phase difference ϕ in Eq. (2-23) is 0. Although it has been thought that the largest grinding load will always occur at the largest diameter part of a ball and therefore the shape error would be rectified during grinding, it is true only if the phase difference of Eq. (2-25) is 0, which means that the damping of support is 0. This is impossible for a practical grinding system.

The magnification factor λ is also very important since, if the magnification factor A is 0, the grinding system will lose its ability to rectify the shape error of balls. Figs. 2-8 and 2-9 give the numerical results of the dependence both of magnification factor and of phase difference on the frequency ratio at different damping ratio, which are defined as follows:

$$\gamma = c/c_{\text{cr}}\ ,\ c_{\text{cr}} = 2\sqrt{km} \tag{2-28}$$

From Fig. 2-8 it is known that, for a grinding system of low damping ratio, the magnification factor decreases steeply near the natural frequency. This suggests that, for such a grinding system, there may exist unrectifiable shape

error of special frequency. This is not desirable for a practical grinding system. To eliminate such danger, the damping ratio of the grinding system should be larger than 0.7.

As to the phase difference, Fig. 2-9 shows that the 0 phase difference is possible only when the damping ratio is 0 and the vibration frequency is less than the natural frequency. It is specially worth noting the fact shown in Fig. 2-9 that the phase difference has a reverse dependence on the damping ratio when the frequency ratio is larger than unity. If the frequency ratio is less than unity, the phase difference increases with the damping ratio. However when the frequency ratio is larger than unity, the phase difference decreases with the damping ratio. Therefore, to minimize the phase difference it is necessary to know whether the grinding system is working at a frequency ratio larger than unity or not. For a system working under a frequency higher than its natural frequency, the damping ratio should be increased to decrease the phase difference. Otherwise, the damping ratio should be decreased.

Fig. 2-10 shows the relationship of the phase among the shape error, the displacement of the support, dynamic force and the actual grinding force. Since the phase difference between grinding force and the shape error, the maximum grinding force is not always coinstantaneous with the maximum diameter. This means that the shape rectification in ball grinding process does not proceed as expected. To reduce the shape error and to obtain a real sphere, it is expected that the part with greater diameter is removed greater. However, it is not the case in ball grinding process because of the phase difference between the grinding force and the shape error due to the damping of the support system.

Grinding experiments of the dependence of grinding performance on

supports were conducted using four different types of supports by Zhang et al. The results show that the grinding performance of ceramic balls is dependent on the dynamic behavior of the support system. It seems that lower stiffness and higher damping is a desirable combination of the dynamic characteristics for idea support systems, in perspective of both the quick improvements of the sphericity and the low available sphericity.

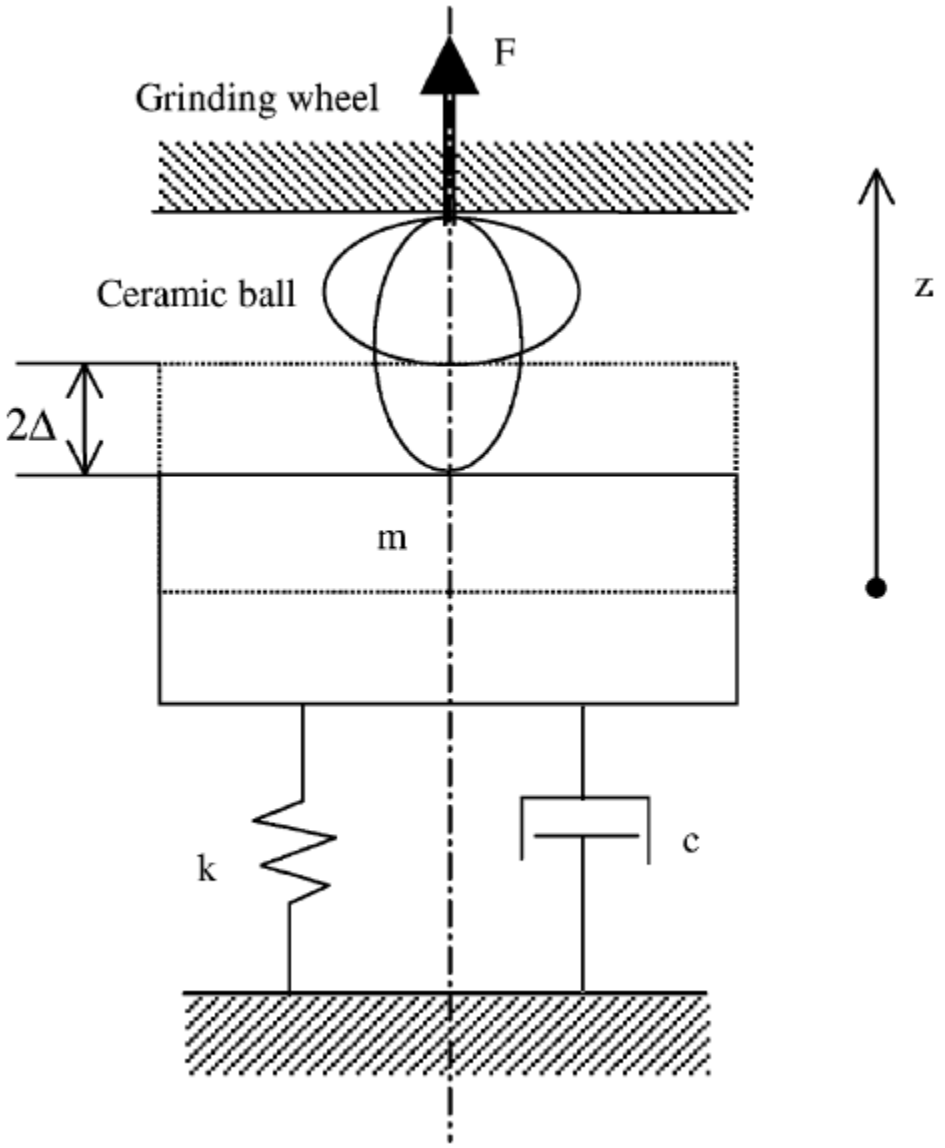

Fig. 2-7 Dynamic model of magnetic fluid support grinding system of ceramic balls

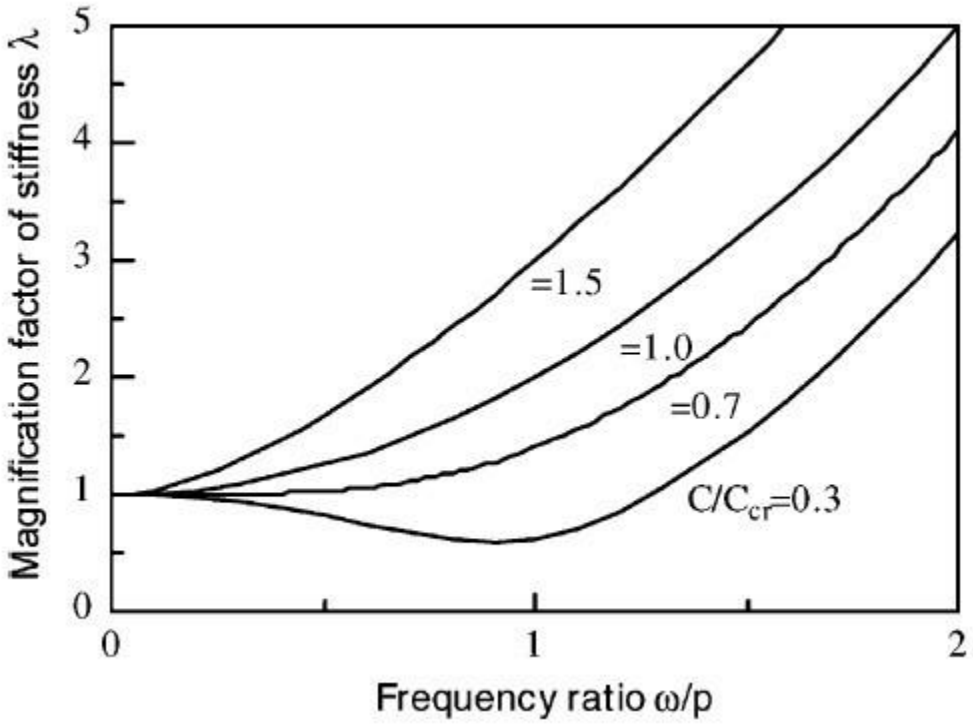

Fig. 2-8 Dependence of magnification factor on the frequency ratio at different damping ratio

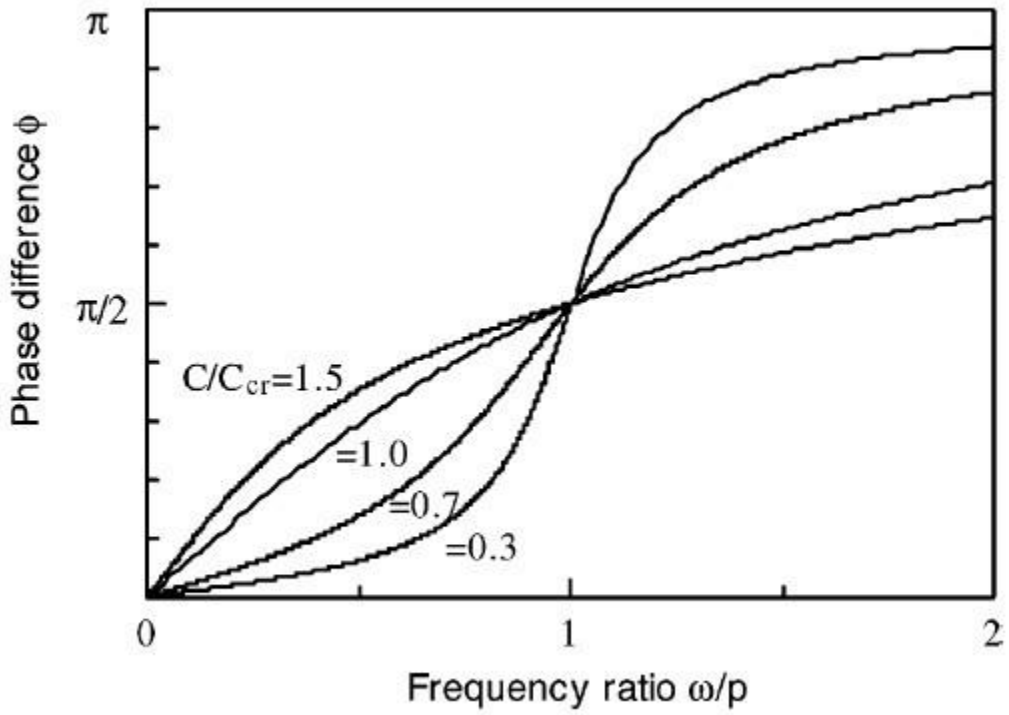

Fig. 2-9 Dependence of phase difference on the frequency ratio at different damping ratio

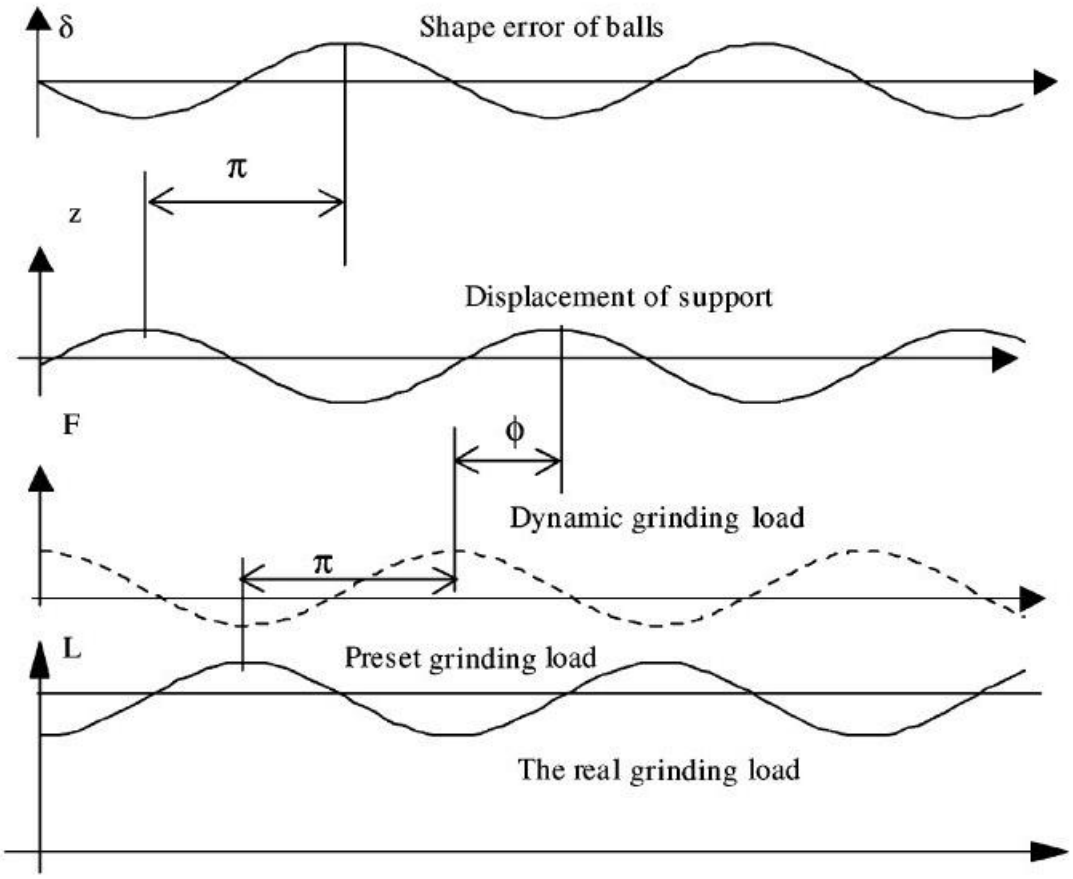

Fig. 2-10 The phase relationship among the shape error, displacement, dynamic force and the actual grinding force.

2.3 Material removal mechanisms

In ball grinding process, the material is removed by means of the relative sliding of the grits on the ball surface at the contact point to the grinding wheel. The relative sliding can be divided into two types: One is the linear slide and the other is the rotary slide, as shown in Fig. 2-11.

It is said that in ball grinding, the effect of the linear slide is significantly less than that of cyclotron slip [2]. This may be true in the concentric V-groove grinding mechanism (Fig. 2-1a). For in this case, the contact trace is a fixed circle. Zhang's research gave the direct evidence [1]. Thus in industrial processing, after each circulation, the balls must be removed from the processing and put back into the V-groove, to replace the spin direction as shown in Fig 1.1.

However, this mechanism seemingly does not handle the magnetic fluid grinding, although its structure also belong to the concentric V-groove system. As a representative of non-traditional grinding method, magnetic fluid grinding method is developed for ceramic ball by Umehara and Kato [6] and a 40-fold increase in material removal rate was obtained. The high material removal rate was observed when skidding occurred between the balls and the drive shaft. The relationship between the volumetric removal rate and the product of the load and sliding speed between the ball and the driving shaft was studied [7]. It was shown that the volumetric removal rate was proportional to the skidding speed between the ball and the driving shaft. The wear coefficient of Si_3N_4 balls was calculated as 0.07 ± 0.02. From these results, the dominant action of the abrasives was found to be two-body abrasion by the abrasives fixed on the surface of the driving shaft. After determining the importance of the sliding speed between the balls and the driving shaft, the

mechanics of the balls during the process was investigated in order to predict the removal rate followed by prediction of the sliding speed [8].

On the other hand, to magnify the effect of the rotary slide, Kurobe et al. [2] developed the spin angle control lapping system (Fig. 1-4). The theoretical analysis showed that, by adjusting the rotate speed of the separate V-groove block and the lapping plate, the direction of the ball's spin axis can be adjusted freely. Furthermore, the relative skidding distance in the contact area increases with the angle of the spin axis, hence the material removal rate increase. This analysis was proved by the later experiment [3].

The material removal mechanism for the eccentric grinding system is opposite to that of the spin angle control lapping. It is obvious that the balls in the V-groove circulated in identical speed while the tangential velocity of the wheel at the contact point is determined by the ball’s position. Thereby, the direction of the tangential velocity is not as same as the revolution direction of the ball except those in the axis line of the two rotation center. Consequently, the linear skidding is expected to occur at the contact point and it dominates the material removal mechanism. Moreover, if the skidding occurs at the contact point of the balls and the V-groove, the direction of the spin axis will change with the driven speed of the wheel, leading to the entire spherical grinding. Fig. 2-12 is an observation of the ball surface ground by the eccentric grinding machine. It is clear that the surface is full of linear scratch with random direction.

Based on the above explanation, it is clear that the eccentricity between the grinding wheel and the guide ring, the property of the support system, the depth of cut and the skidding speed are very important to the grinding of ceramic ball. The next chapter introduces the magnetic fluid support grinding

coupled with the electrolytic in-process dressing which is used to resolve the dulling and loading issue of metal bond grinding wheel.

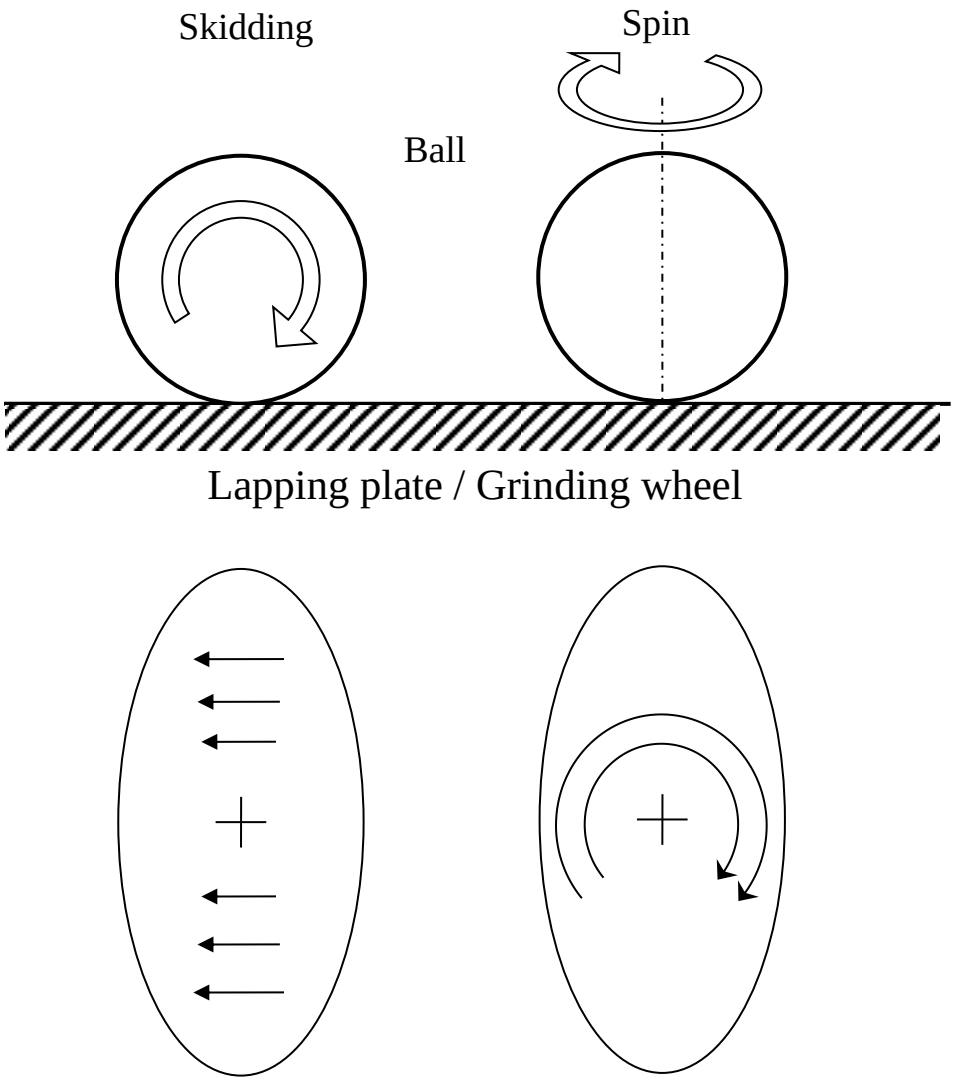

Fig. 2-11 Linear slide and rotary slide of a ball

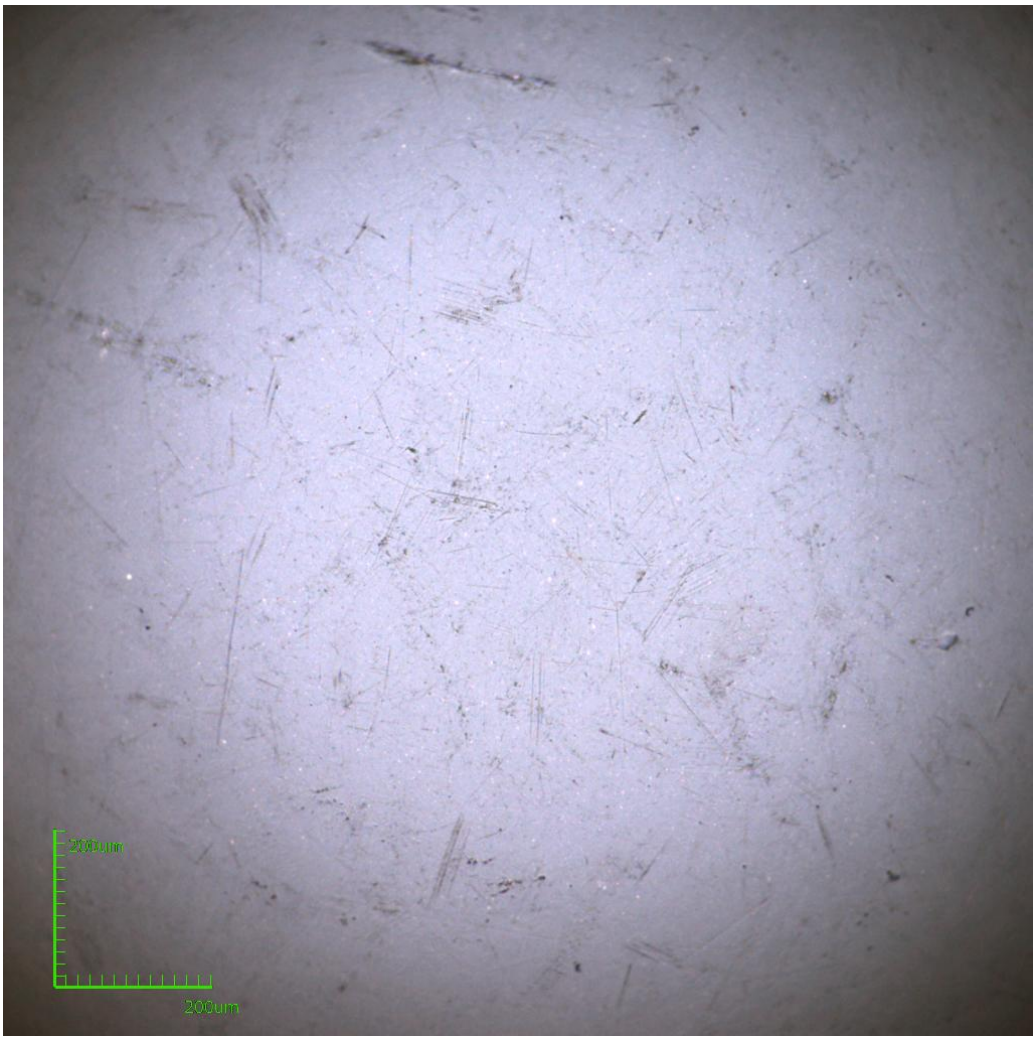

Fig. 2-12 Ball surface ground by the eccentric grinding machine

2.4 Reference

[1] B. Zhang, A. Nakajima. Spherical surface generation mechanism in the grinding of balls for ultraprecision ball bearing. Proc, Instn Mech Engrs, Part J 2000, 214, 351-357.

[2] T. Kurobe, H. Kakuta, M. Onoda. Spin angle control lapping of balls (1st Report) -Theoretical analysis of lapping mechanism- (in Japanese). J. JSPE 1996, 62, 12, 1773-1777.

[3] T. Kurobe, H. Kakuta, M. Onoda. Spin angle control lapping of balls (2nd Report) -Lapping of silicon nitride ball- (in Japanese). J. JSPE 1997, 63, 5, 726-730.

[4] B. Zhang, N. Umehara, K. Kato. Effect of the eccentricity between the driving shaft and the guide ring on the behavior of magnetic fluid grinding of ceramic balls (in Japanese). J. JSPE 1995, 61, 4, 585-590.

[5] B. Zhang, A. Nakajima. Dynamics of magnetic fluid support grinding of Si_3N_4 ceramic balls for ultraprecision bearings and its importance in spherical surface generation. Precision Engineering 2003, 27, 1-8.

[6] N. Umehara, K. Kato. A study on magnetic fluid grinding: 1st report, the effect of the floating pad on removal rate of Si_3N_4 balls (in Japanese). Trans. JSME 1988, 54, 1599-1604.

[7] T. H. C. Childs, S. Mahmood, H. J. Yoon. The material removal mechanism in magnetic fluid grinding of ceramic ball bearings. Proceedings of the Institution of Mechanical Engineers, Part B, 1994, 208, 47-60.

T. H. C. Childs, D. A. Jones, S. Mahmood, B. Zhang, K. Kato, N. Umehara. Magnetic fluid grinding mechanics. Wear 1994, 175, 189-198.

Chapter 3
Fundamental study of ELID

3.1 Introduction

As introduced in the chapter 1, the Electrolytic In-process Dressing technique (ELID), developed by Ohmori [1], has been found be widely used in industry. A lot of researches were carried out to investigate the grinding characteristic of ELID and the influence of grinding condition. Different abrasive size [2-4], bond material and grinding fluid [4], current duty factor [5] were tested. Experimental results [4] showed that bronze bond wheel achieves the lowest normal grinding force among cast iron bond, cobalt bond and bronze bond wheels. ELID with the cast iron-bronze hybrid bond wheel was reported succeeding in the centerless grinding for ZrO_2 optical fiber ferrules [6]. Bifano et al. [7] published a paper on both fundamental experiment and real grinding with bronze bond wheel in 1999. It was found that ELID improved the material removal rate of bronze bond grinding wheel. In 2007, Klocke et al. [8] analyzed the surfaces of iron-bronze, cobalt-bronze and normal bronze materials after electrolysis in CG-7. It was found that an increase in thickness of the oxide layer of iron and cobalt bronze alloy occurred while bronze showed no layer growth. Later in 2009, they reported that a pure anodic dissolution took place on bronze bond grinding wheel without oxide layer formation [9].

Although Ohmori proposed an explanation of the mechanism of ELID, the real understanding is far from sufficient. This chapter presents a basic research on the mechanism of electrolytic dressing by using a ball-on-disk friction test

machine in which electrolysis can be implemented simultaneously. The ball mimics the work piece, while the disk mimics the grinding wheel, especially the bond material, in grinding.

3.2 Experimental procedure

Figure 3-1 is the schematic of the ball-on-disk electrolysis-friction machine used in this study, on which friction test can be conducted together with electrolysis. The disk is rotated by a spindle in test. A ball is loaded down to the disk. Both the contact load and the friction force are monitored in test. To implement electrolysis to the disk, an electrode plate is located over the disk with a small clearance on the opposite side of the ball about the spindle. Electrical power is applied between the electrode plate and the disk, so that the electrode plate is cathode and the disk is anode.

The experimental conditions are listed in Table 3-1. Two different materials, 99.99% copper and 99.5% iron were used for disk since copper is one of the most widely used metal bond materials of super abrasive wheels, while iron is the special bond material for ELID. HIPed Si_3N_4 was used for ball. The hardness of copper and iron was 86 Hv0.1 and 127 Hv0.1, respectively, while that of Si_3N_4 was 1438 Hv1, a much higher value than that of copper and iron. Three different types of electrolyte; tap water, electrolyzed water and solution of CG-7 to tap water were investigated. CG-7 is a chemical solution type grinding fluid specially developed for ELID grinding. It consists of diethanolamine (22~25 wt%), inorganic salt (4~7 wt%), antirust additive (~0.5 wt%) and water (rest). The conductivities of tap water, electrolyzed water and CG-7 solution were 100 μS/cm, 110 μS/cm and 1050 μS/cm, respectively. Tap water had a lower pH value (pH 7.4) than both electrolyzed water (pH 9.1) and CG-7 solution (pH 9.5). The other experimental conditions were V=4V, n= 400 rpm, and W=1 N for all the test. The clearance between the disk and the electrode plate was set at 1 mm. Test was interrupted every 4 hours for the measurement and observation of the specimen surface.

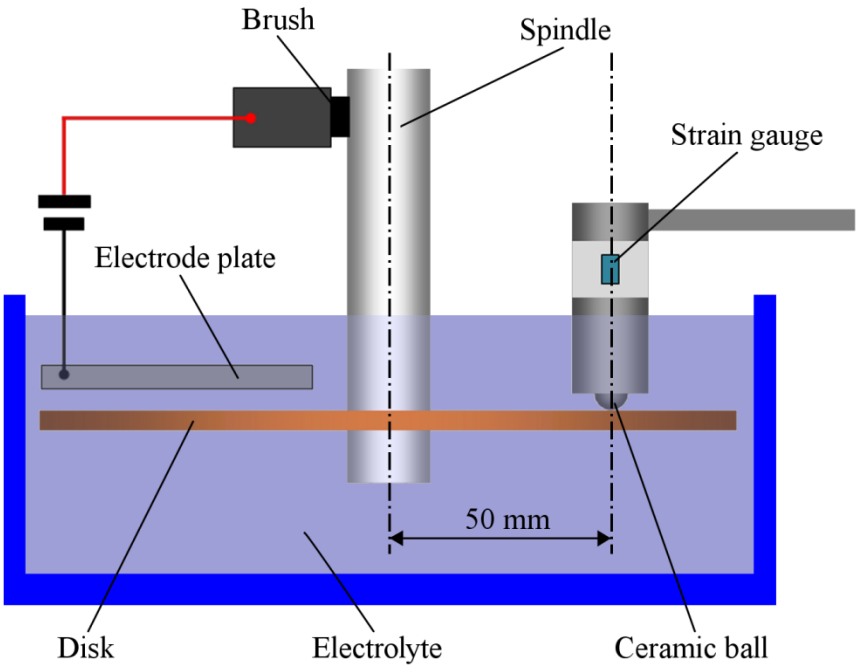

Fig.3-1 Schematic of ball-on-disk electrolysis-friction machine

Table 3-1 Dynamic experimental condition

Disk (ϕ150 mm)	Cu (99.99%, 86HV0.1, Ra0.133 μm) Fe (99.5%, 127HV0.1, Ra0.143 μm)
Ball	Si_3N_4 (HIP ϕ11, 1438HV1, Ra0.015 μm)
Electrode plate (mm × mm)	Stainless Steel (50 × 30)
Clearance (mm)	1
Electrolyte	Tap Water (pH7.4, 100 μS/cm) Electrolyzed Water (pH9.1, 110 μS/cm) CIMIRON CG-7(×50, pH9.5, 1050 μS/cm)
Rotation Speed (rpm)	400
Load (N)	1
Supply voltage (V)	4 (DC)

3.3 Experimental results

§3.3.1 Friction coefficient

Figure 3-2 and Figure 3-3 show the time dependence of friction coefficient of Si_3N_4 against copper disk (Fig.3-2) and against iron disk (Fig.3-3), respectively. From Fig.3-2, it is known that the friction coefficient of Si_3N_4 against copper was high in both tap water and electrolyzed water when electrolysis was conducted. And the initial friction coefficient was high in tap water without depending on whether electrolysis was on or off, but constant decrease in friction coefficient was observed for non-electrolysis in tap water. The friction coefficient was in range of 0.05~0.25. On the other hand, the friction coefficient in CG-7 solution was low, about 0.03~0.04, and stable for both non electrolysis and electrolysis.

As for the friction coefficients of Si_3N_4 against iron disk in Fig.3-3, they were all as low as about 0.01~0.04. The only exception was the experiment of electrolyzing in electrolyzed water, in which the friction coefficient showed a sudden increase, up to about 0.25, around 4 hours and then it declined again.

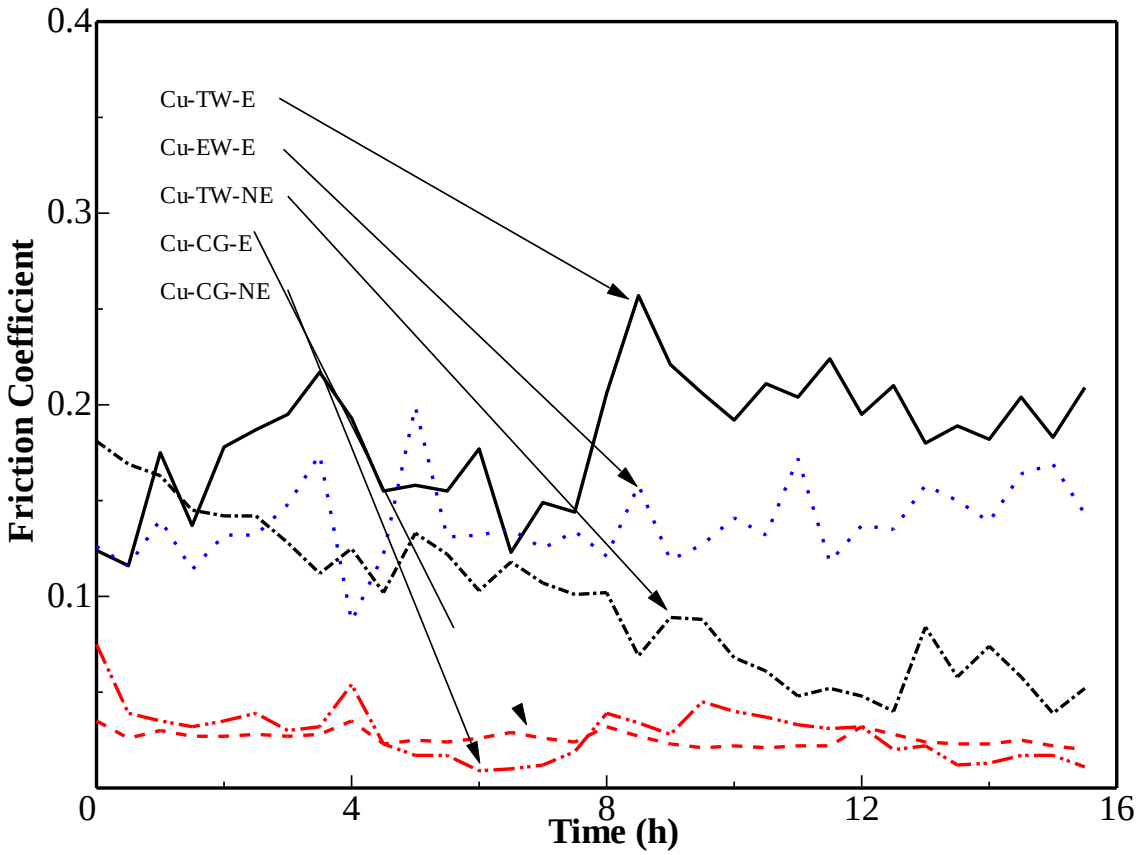

Cu-TW-E: Electrolyzed in taper water.

Cu-EW-E: Electrolyzed in electrolyzed water.

Cu-TW-NE: Tested in tap water without electrolysis.

Cu-CG-E: Electrolyzed in CG-7.

Cu-CG-NE: Test in CG-7 without electrolysis.

Fig.3-2 Time dependence of friction coefficient of Cu

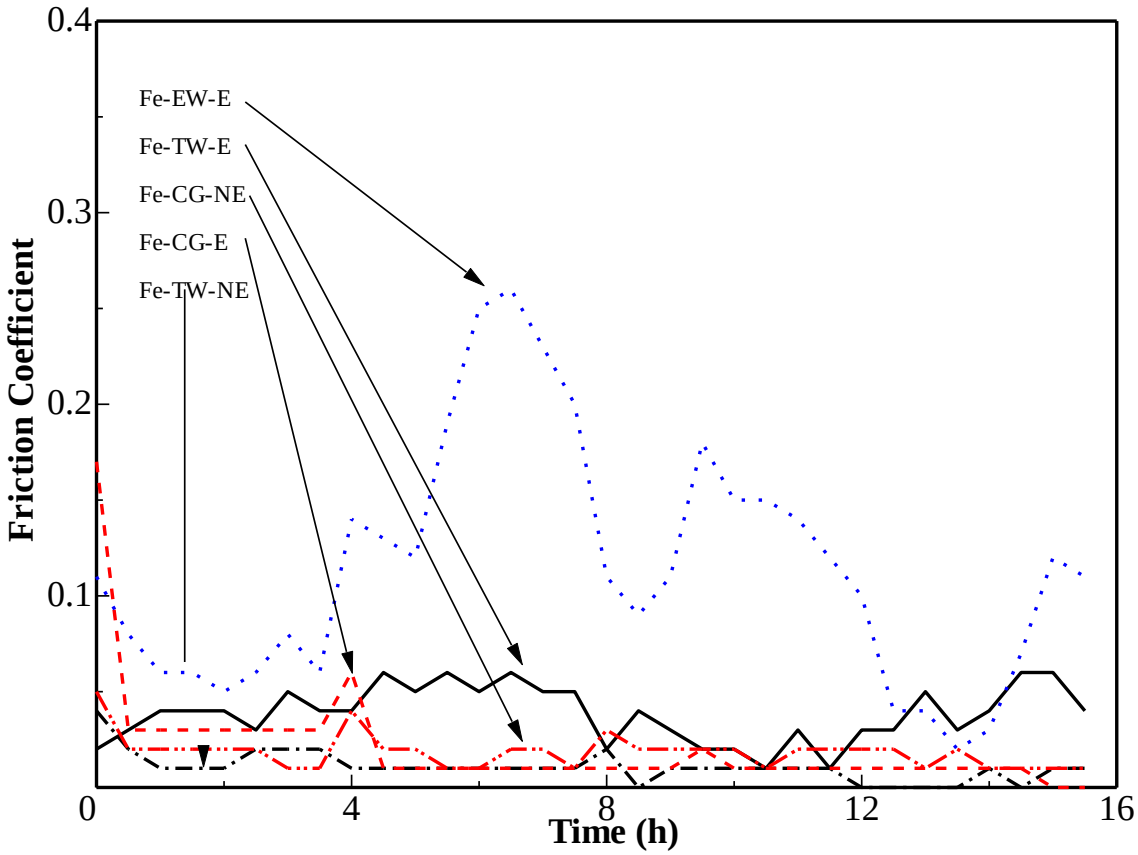

Fe-TW-E: Electrolyzed in taper water.

Fe-EW-E: Electrolyzed in electrolyzed water.

Fe-TW-NE: Tested in tap water without electrolysis.

Fe-CG-E: Electrolyzed in CG-7.

Fe-CG-NE: Test in CG-7 without electrolysis.

Fig.3-3 Time dependence of friction coefficient of Fe

§3.3.2 Wear of disks

Figure 3-4 and Figure 3-5 show the surfaces of wear tracks of copper disk and iron disk, respectively. From Fig.3-4, it is found that the wear tracks both in tap water and in electrolyzed water (Fig.3-4a) and b)) were rough and deep. The average roughnesses were 0.60 μm in tap water and 0.36 μm in electrolyzed water, and the depths were 4 μm and 8 μm, respectively. The wear track in CG-7 solution was much smaller and much shallower than that in tap water and in electrolyzed water. Sliding scratch was clearly observed, which did not appear on the wear tracks either in tap water or in electrolyzed water. The depth of the wear track was almost undetectable from the section profile (Fig.3-4c)). As a representative for non-electrolysis, Fig.3-4d) shows the wear track tested in tap water without electrolysis. The black color was observed in the track, but the surface profile almost did not change during the sliding and the depth of wear track was immeasurable.

As for iron disk, from Fig.3-5, the depths of wear tracks electrolyzed in tap water (Fig.3-5a)), in electrolyzed water (Fig.3-5b)), and in CG-7 solution (Fig.3-5c)) were ~0.2 μm, ~0.8 μm and 1.2 μm, respectively. In spite of the fact that the wear track in CG-7 solution was deepest among the three electrolytes, it was very smooth, Ra=0.057 μm, compared to Ra=0.269 μm in tap water and Ra=0.423 μm in electrolyzed water. In both tap water and electrolyzed water the wear track depths of iron disks were almost 10~20 times as shallow as copper disks. The only exception was the case of electrolysis in CG-7 solution where the wear track depth of iron disk was greater than that of copper disk. There was some rust in wear tracks when electrolyzed in both tap water and electrolyzed water, but not for that in CG-7 solution. Again as copper disk, the wear track depth of iron disk (Fig.3-5d))

was almost undetectable in tap water when electrolysis was not implemented.

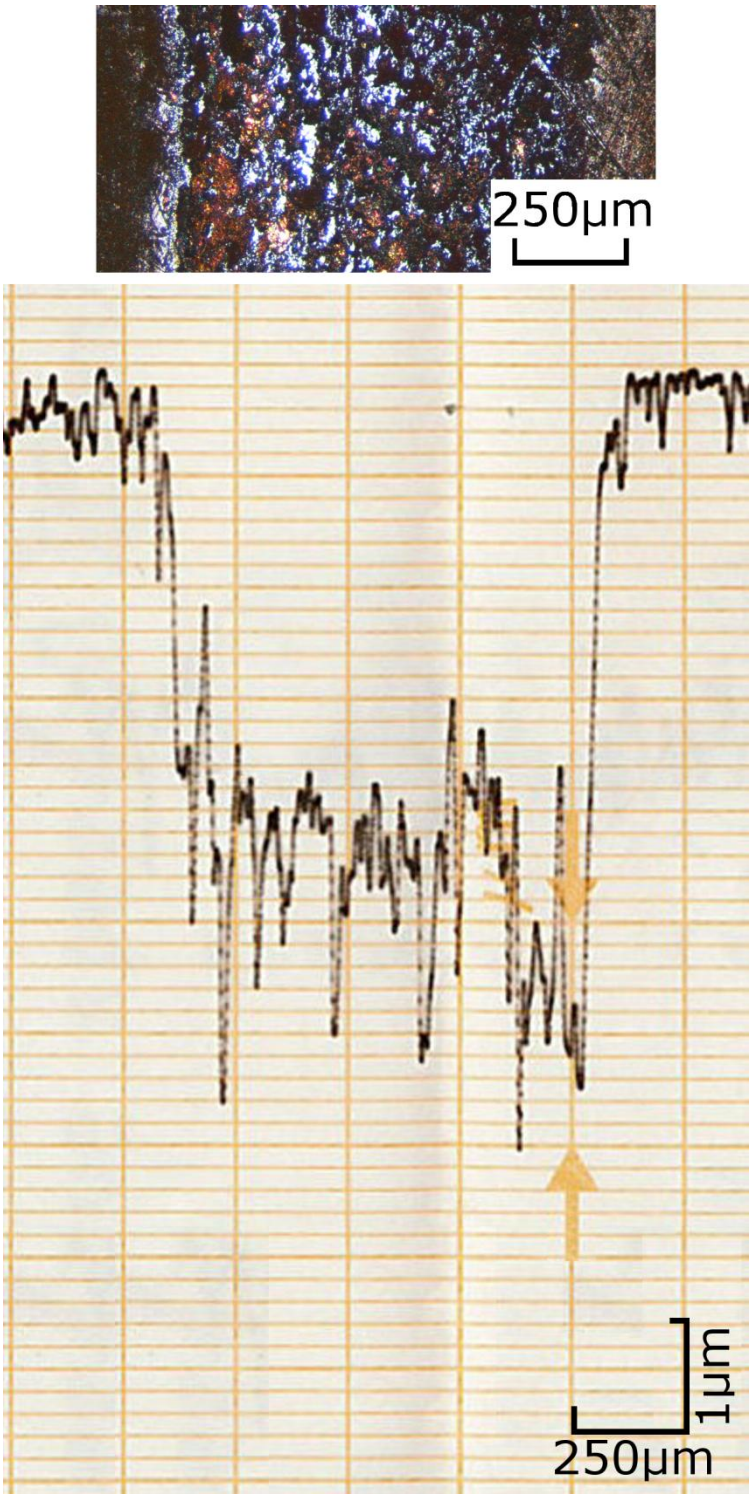

a) Cu-TW-E

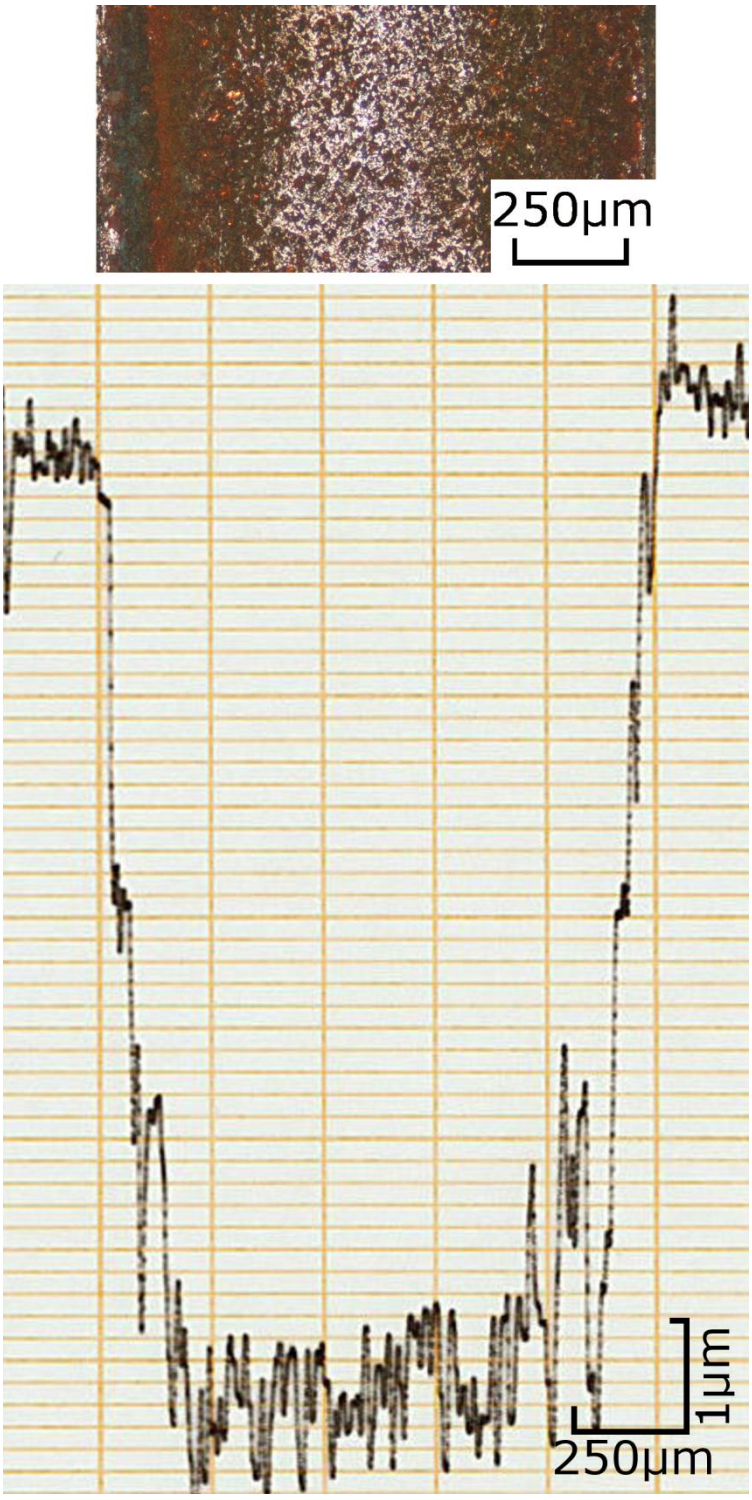

b) Cu-EW-E

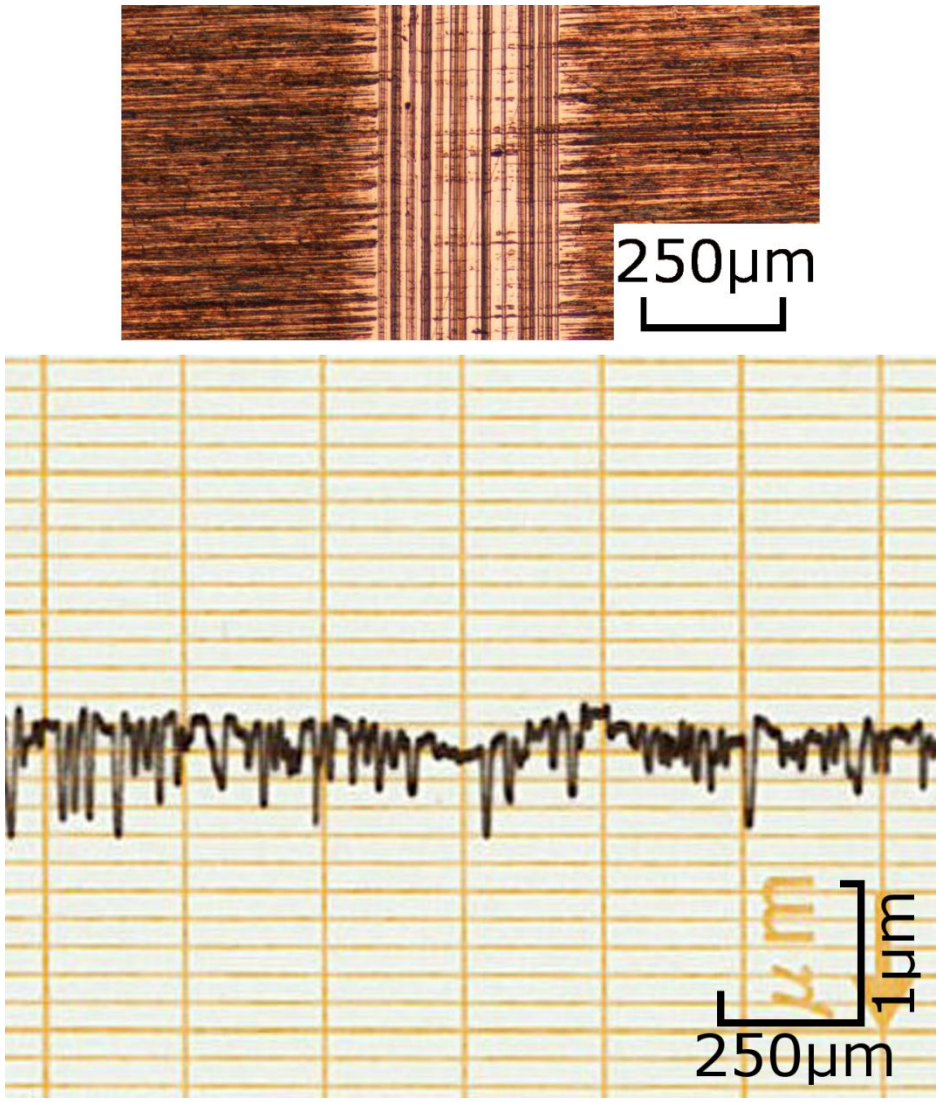

c) Cu-CG-E

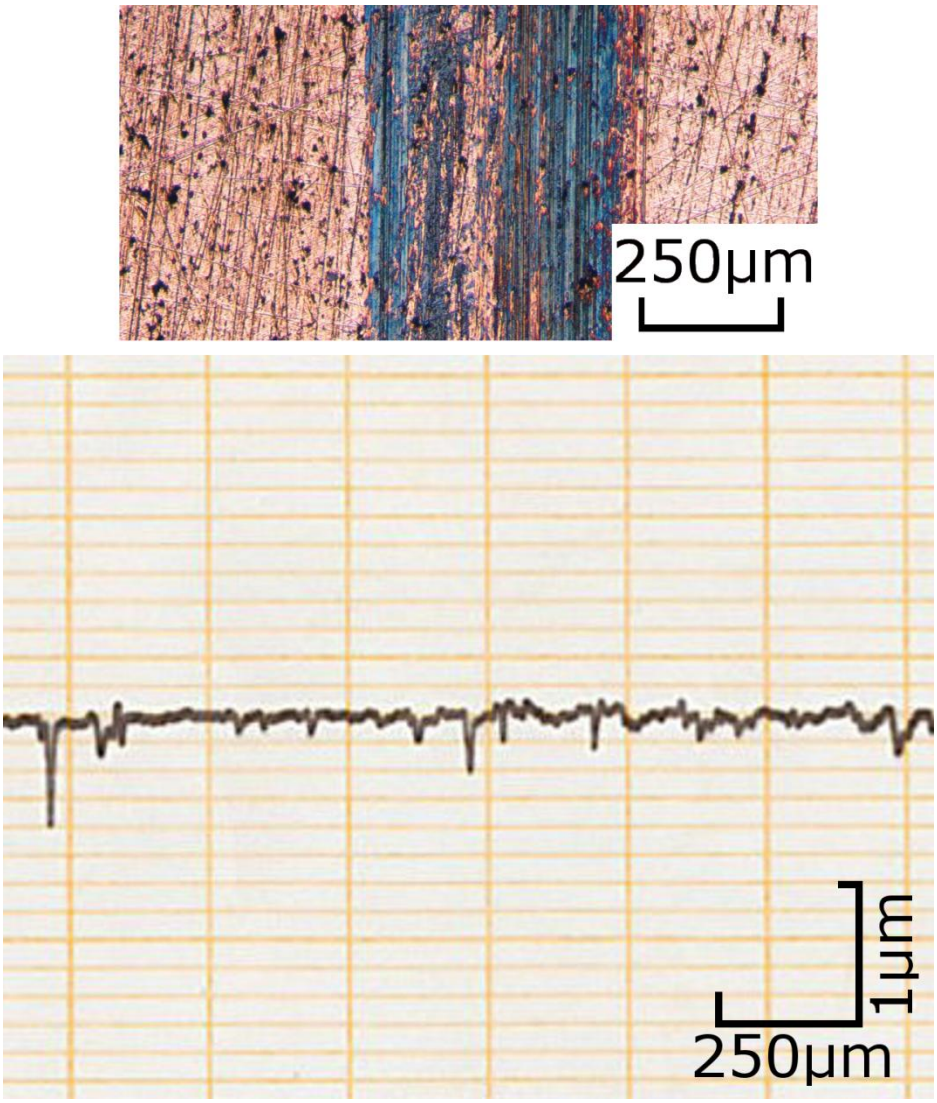

d) Cu-TW-NE

Fig.3-4 Wear track on copper disk after 16 hours

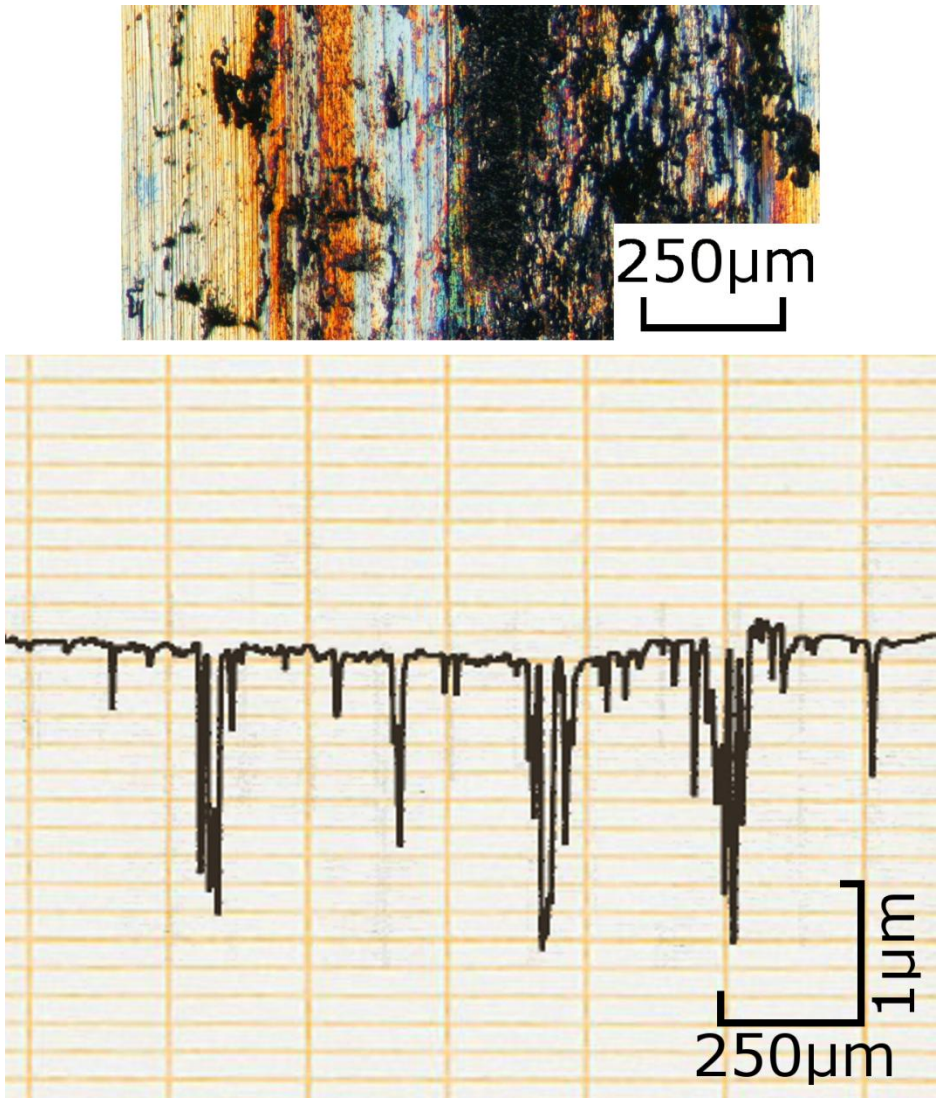

a) Fe-TW-E

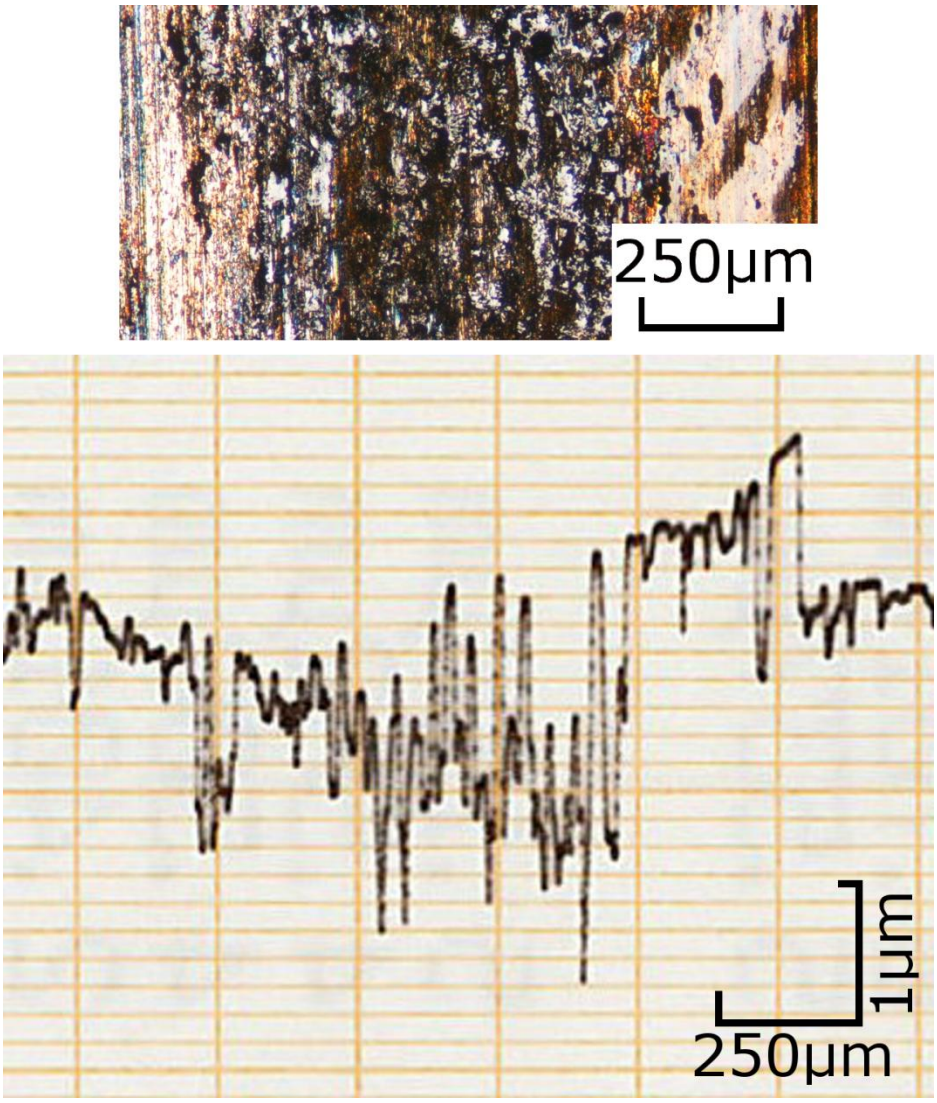

b) Fe-EW-E

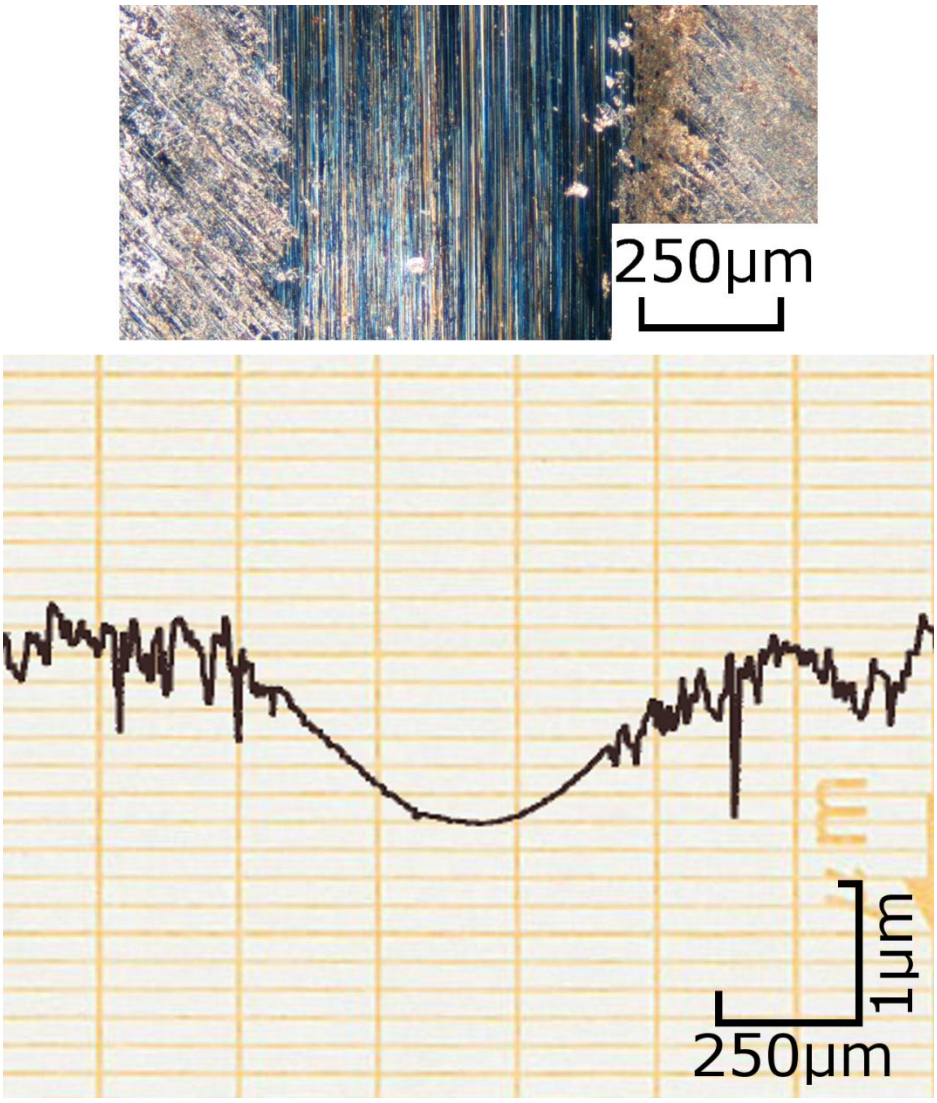

c) Fe-CG-E

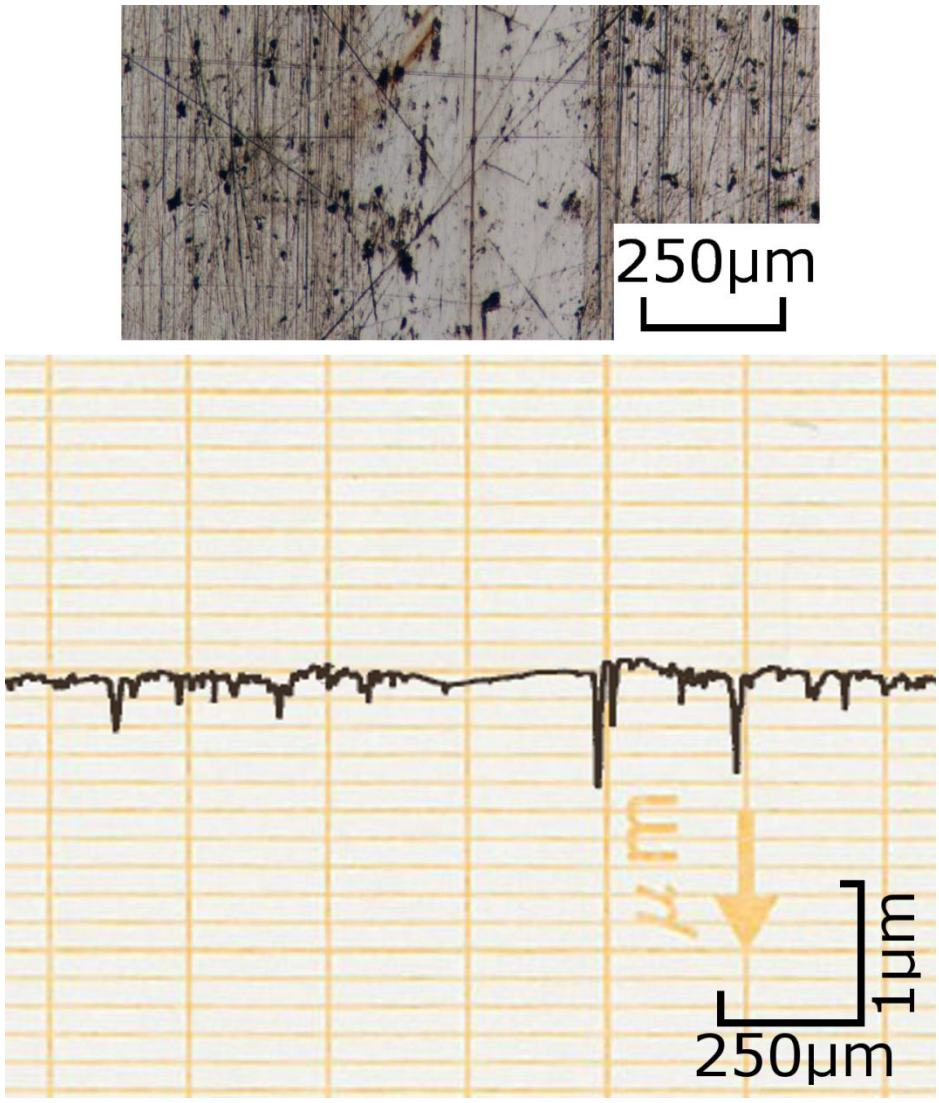

d) Fe-TW-NE

Fig.3-5 Wear track on iron disk after 16 hours

§3.3.3 Wear of Si_3N_4 balls

Figure 3-6 and Figure 3-7 show the wear marks on the Si_3N_4 balls sliding against copper and iron disk under each condition, respectively. The wear marks were extremely smooth in all the tested conditions, but the size of wear mark was different for different conditions. In spite of the fact that the testing time was 32 hours in Fig.3-6 with an exception of Fig.3-6e), of which the time was 16 hours, and the testing time was 16 hours in Fig.3-7, it can still be found that the wear mark of Si_3N_4 ball sliding against copper disk is generally smaller than that against iron disk under the same condition. Implementing electrolysis in both tap water and electrolyzed water tends to increase the wear mark size of Si_3N_4 balls for both copper disk and iron disk, but the effect for iron disk is greater than that for copper disk (See Fig.3-6a), b) and Fig.3-7a), b)). It is found that the minimal wear mark is on the ball sliding against the copper disk in CG-7 while the largest one on the ball sliding against the iron disk electrolyzed in electrolyzed water.

The wear volume of ball can be estimated from the wear mark diameter d_w and ball diameter d by the following equation.

$$V = \pi d_w^4 / 32d \qquad (3\text{-}1)$$

The calculated wear rates for all the conditions are summarized in Table 3-2. Under the same conditions sliding against iron disk always gave wear rate 6~60 times as high as copper disk, except for the condition of non-electrolysis in tap water where the wear rate for iron disk was lower than that for copper disk. In tap water, implementing electrolysis increased the wear rate from 1.58×10^5 $\mu m^3/h$ to 4.59×10^5 $\mu m^3/h$ for copper disk and from 0.72×10^5 $\mu m^3/h$ to 33.6×10^5 $\mu m^3/h$ for iron disk, but, in CG-7 solution, it decreased the wear rate a little for both copper and iron disks. The increase in the wear rate for

iron disk in tap water was notably high, about 50 times. Changing the electrolyte from tap water to electrolyzed water also increased the wear rate from 4.59×10^5 $\mu m^3/h$ to 9.19×10^5 $\mu m^3/h$ for copper disk and from 33.6×10^5 $\mu m^3/h$ to 54.4×10^5 $\mu m^3/h$ for iron disk.

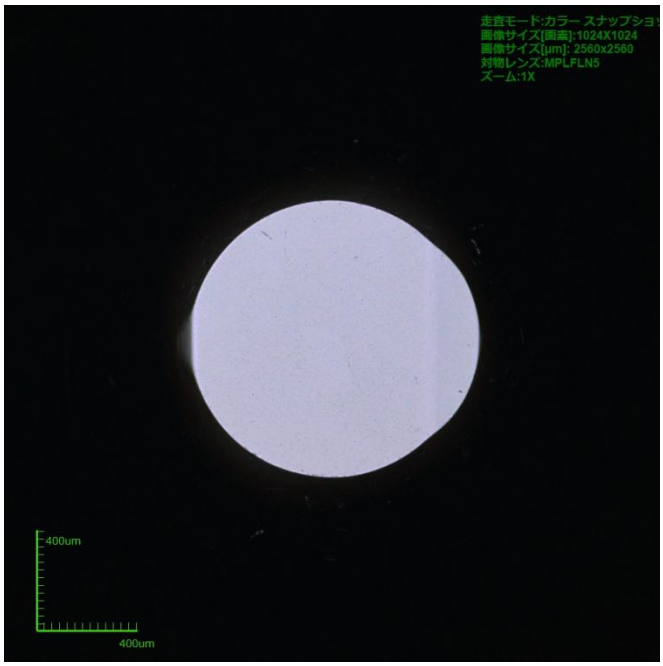

a) In tap water with electrolysis after 32 hours

Ra3 nm, d_w=1.13 mm.

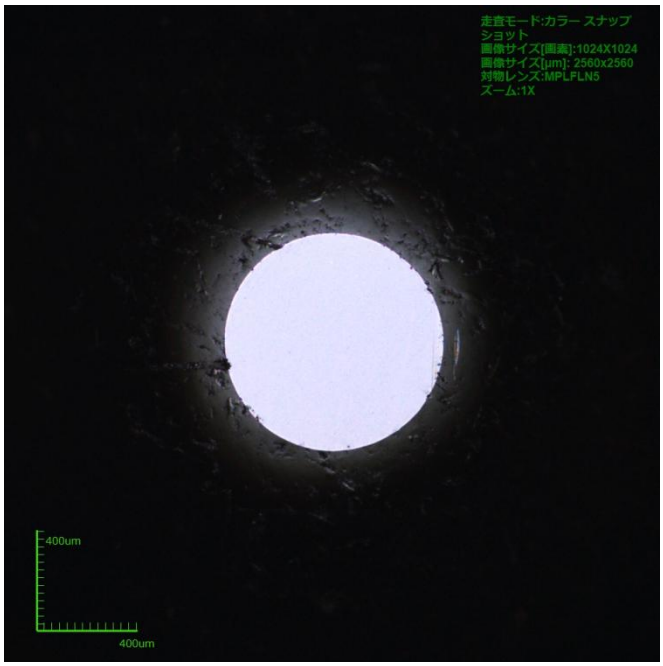

b) In tap water without electrolysis after 32 hours

Ra2 nm, d_w=0.87 mm.

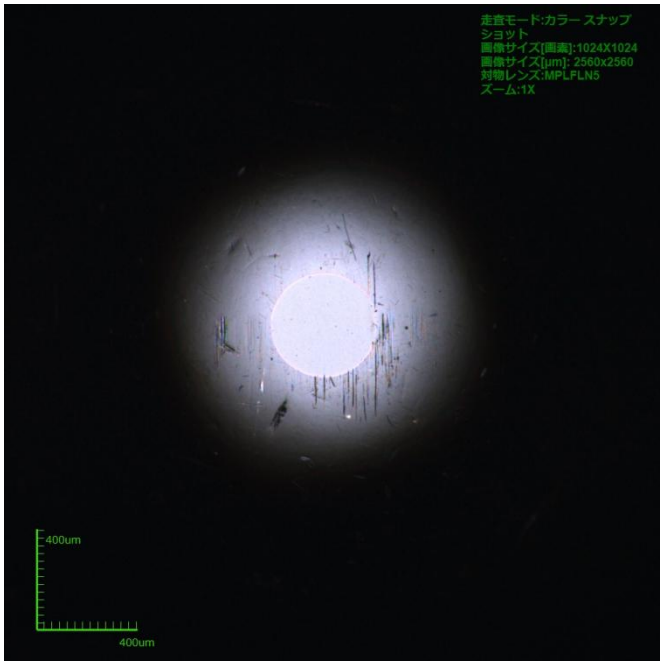

c) In CG-7 with electrolysis after 32 hours

Ra2 nm, d_w=0.40 mm.

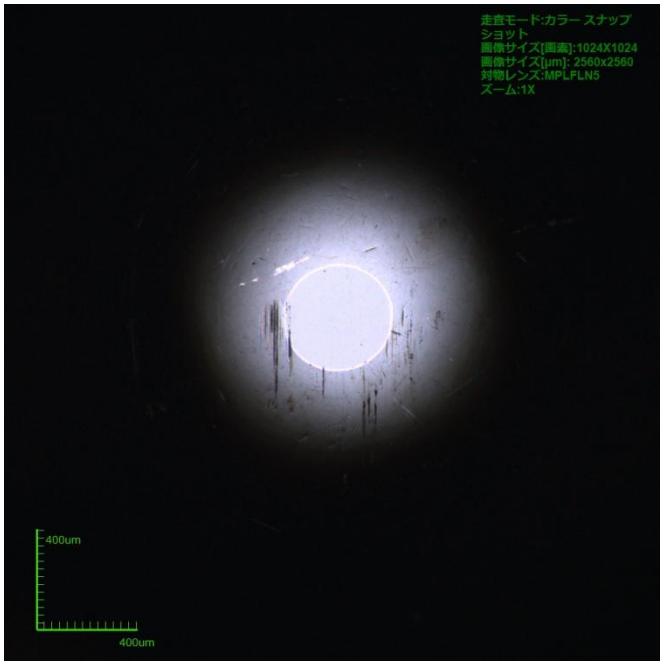

d) In CG-7 without electrolysis after 32 hours

Ra2 nm, d_w=0.43 mm.

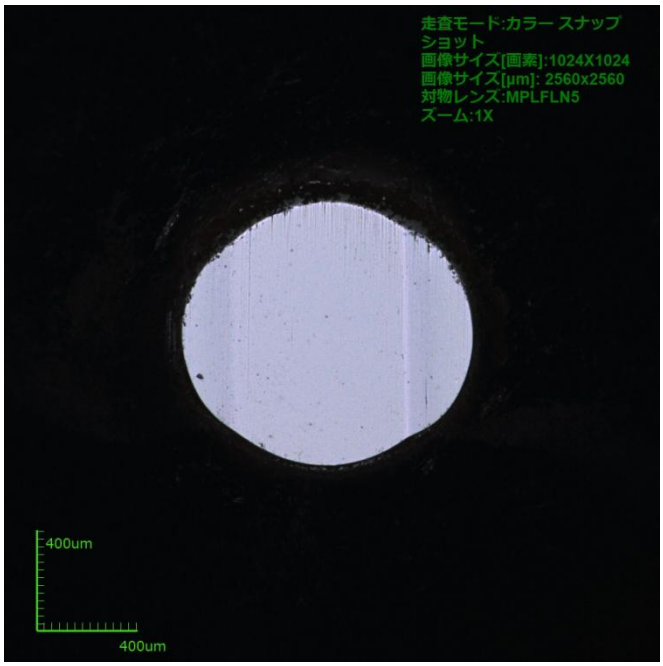

e) In electrolyzed water with electrolysis after 16 hours

Ra4 nm, d_w=1.13 mm.

Fig.3-6 Wear marks of Si_3N_4 ball sliding against copper disk

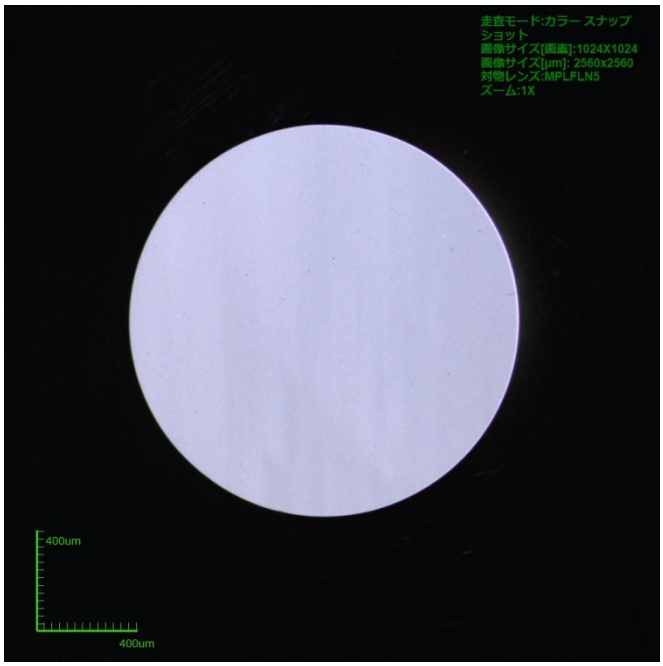

a) In tap water with electrolysis after 16 hours

Ra3 nm, d_w=1.57 mm.

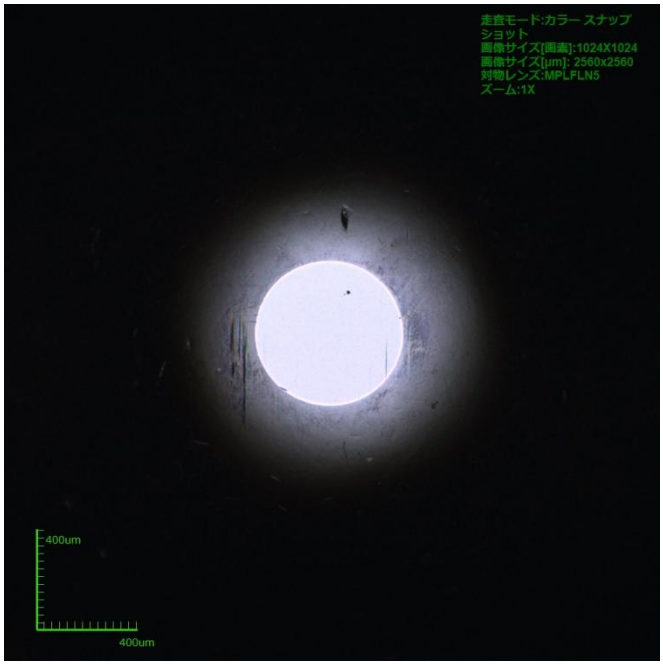

b) In tap water without electrolysis after 16 hours

Ra3 nm, d_w=0.60 mm.

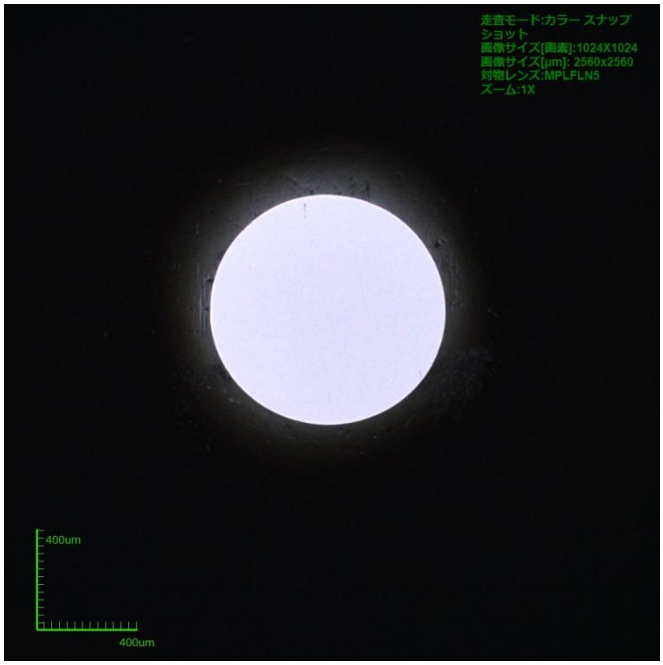

c) In CG-7 with electrolysis after 16 hours

Ra2 nm, d_w=1.57 mm.

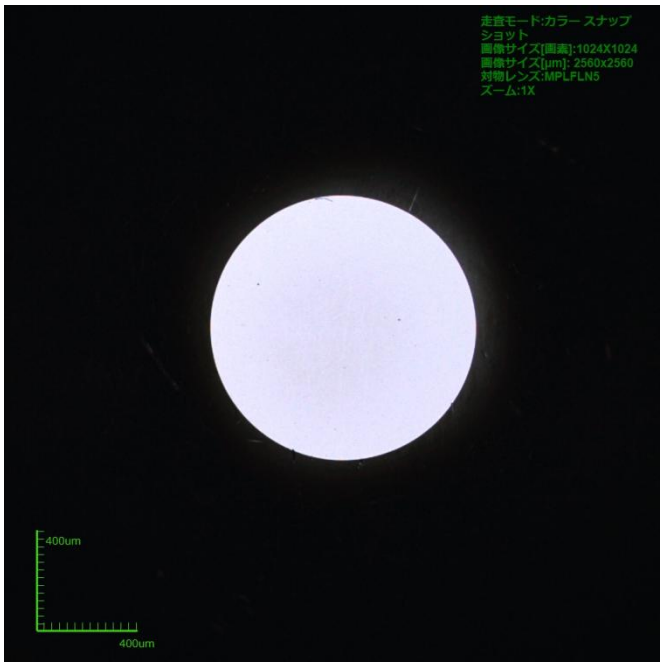

d) In CG-7 without electrolysis after 16 hours

Ra3 nm, d_w=1.54 mm.

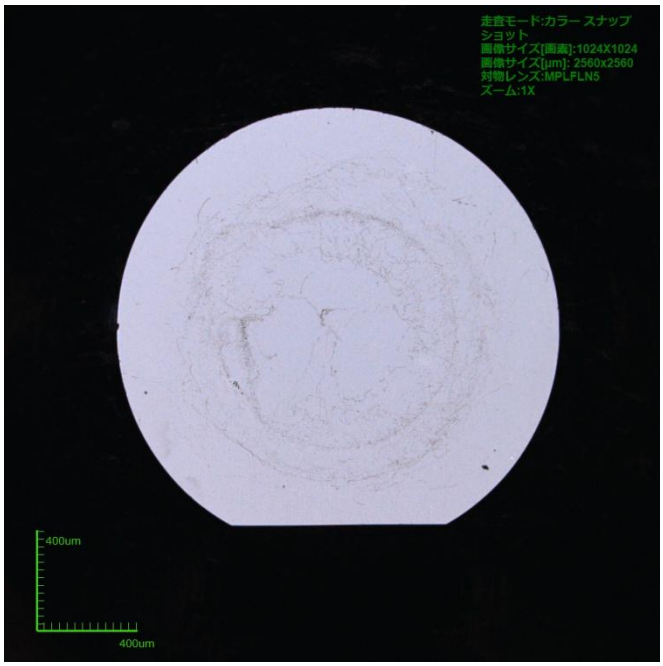

e) In electrolyzed water with electrolysis after 16 hours

Ra8 nm, d_w=1.77 mm.

Fig.3-7 Wear marks of Si_3N_4 ball sliding against iron disk

Table.3-2 Wear rate of Si_3N_4 ball under different experimental conditions (10^5 $\mu m^3/h$)

Electrolyte \ Disk		Copper	Iron
Tap water	Electrolysis	4.59	33.6
	Non-electrolysis	1.58	0.72
Electrolyzed water	Electrolysis	9.19	54.4
	Non-electrolysis		
CG-7 solution	Electrolysis	0.07	4.22
	Non-electrolysis	0.10	7.23

3.4 Discussions

§3.4.1 Friction coefficients

The decrement in friction coefficient with test time for the case of sliding against copper disk in tap water without electrolysis (Fig.3-2) may be due to run-in of the disk surface and the wear of Si_3N_4 ball, which led to increasing in hydrodynamic effect.

CG-7 gave lowest friction coefficient among the three types of electrolyte, since CG-7 contains the oiliness agent of diethanolamine.

The low friction coefficient of Si_3N_4 ball against iron disk both in tap water and in electrolyzed water may be due to both the good boundary lubrication property of the material combination under water lubrication condition and/or the smooth wear track surface. Experiments by Kondo et al. [10] showed that both iron and Fe_2O_3 have lower friction coefficient than Fe_3O_4. Our XPS analysis of iron surface electrolyzed in CG-7 also showed the existence of Fe_2O_3 (Figure 3-8). The increased friction coefficient of Si_3N_4 against iron disk electrolyzed in electrolyzed water arose from the rough surface of the wear track.

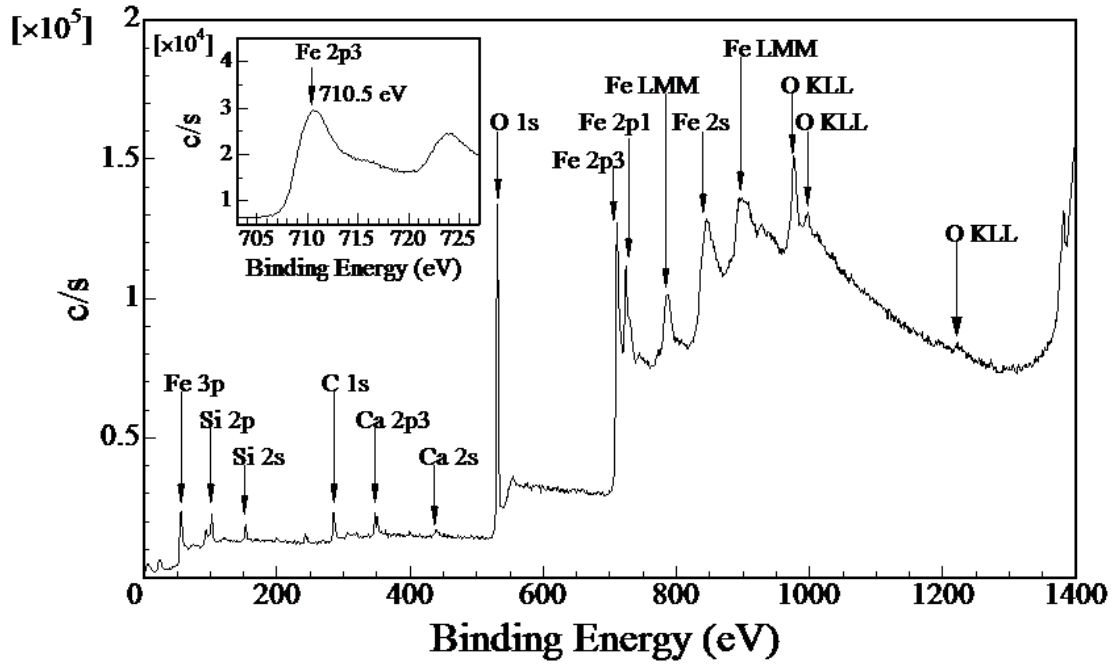

Fig.3-8 The XPS spectrum of iron surface electrolyzed in CG-7 solution.

§3.4.2 Wear of disk

It is known that copper is a noble metal, and the oxide film on the surface has a high protective effect from corrosion. However the corrosion resistance of copper comes from the thick oxide film (passivation). It is said that the necessary oxide film thickness is about 10 μm. this is the main reason why copper showed deeper wear track than iron, which is a passive metal and very thin film (about 10 nm) is sufficient to protect the bulk from corrosion. The sliding wear may break the oxide film and/or inhibits its growth, and therefore promote the electrolysis. This is the synergistic effect between wear and electrolysis.

However the synergistic effect was not observed for copper in CG-7 solution. This may be due to oiliness agent and antirust additive in CG-7 solution, which reduced the wear so greatly that sufficient protective film still remained at the surface, and therefore the electrolysis was prohibited. From the Pourbaix diagram of copper [11], it is known that copper shifts from corrosion to passivation when pH value of electrolyte is in the range from 8 to 12. It is expected that high pH value of CG-7 may also contribute to the reduction in the synergetic effect besides oiliness agent and antirust additive. The experimental results of wear of copper disk under electrolysis in electrolyzed water of which the pH value was 9.1, almost the same value as CG-7 solution, disproved the expectation. It is known that, from Fig.3a) and 3b), the synergetic effect in electrolyzed water was even stronger than that in tap water.

§3.4.3 Wear of Si_3N_4 ball

Because Si_3N_4 is much harder than both copper and iron, the wear of ball

must be chemically dominant. In the presence of water and oxygen, the following reactions occur [12, 14]:

$$Si_3N_4 + 6H_2O = 3SiO_2 + 4NH_3 \quad (4)$$

$$Si_3N_4 + 3O_2 = 3SiO_2 + 2N_2 \quad (5)$$

and SiO_2 will dissolute in water:

$$n SiO_2 + (2-x) n H_2O = [SiO_x(OH)_{4-2x}] \quad (6)$$

$[SiO_x(OH)_{4-2x}]_n$ is the general formula of silicic acid, such as metasilicic acid (H_2SiO_3), orthosilicic acid (H_4SiO_4) [15, 16]. The dissolution rate is higher when the water is basic [16].

Iron disk always produced higher wear rate of Si_3N_4 ball than copper disk, in spite of the fact that the friction coefficient of Si_3N_4 against iron disk was lower than that against copper disk. This is because that Fe_2O_3 known as Bengala is a traditional polish powder for glasses and experiments by Vora et al. [17] showed that Fe_2O_3 is also an effective abrasive for Si_3N_4. The XPS analysis confirmed the existence of Fe_2O_3 (Fig.3-8) at the iron disk surface.

It is considered that the increase in the wear rate in tap water by electrolyzing is mainly due to the roughening of wear track surfaces for copper disk, while it is for the chemical change in addition for iron disk. The roughening resulted in decreasing in hydrodynamic lubrication and increasing in the direct contact between ball and disk, and therefore increasing in wear rate. For iron disk, in addition to the roughening, electrolyzing promotes the generation of Fe_2O_3, and therefore an extra increment in the wear rate. However, in CG-7 solution, the electrolysis was so weak and the surfaces of both copper and iron disks were so smooth that the wear was not affected. The real reason for the decrease in the wear rate by implementing electrolysis in CG-7 solution is not clear yet.

The wear rate in electrolyzed water was higher than that in tap water for both copper and iron disks since the pH value of electrolyzed water was higher than that of tap water, and alkaline solution promotes the dissolution of the products of wear of Si_3N_4 [16].

3.5 Conclusions

Simulation experiments of electrolytic in-process dressing were conducted by using an electrolytic-friction test machine. The following conclusions are obtained:

1. Strong synergistic effect between the electrolysis and sliding wear was observed for copper in both tap water and electrolyzed water, and for iron in electrolyzed water and CG-7. Without electrolysis the wear of both copper disk and iron disk was almost undetectably small.
2. The wear tracks of copper disks electrolyzed in tap water and electrolyzed water were very rough, and the material removal mechanism is electrolytically dominant.
3. The friction coefficient of Si_3N_4 ball against iron disk is lower than that of Si_3N_4 ball against copper disk.

3.6 Reference

[1] H. Ohmori, T. Nakagawa. Mirror surface grinding of silicon wafers with electrolytic in-process dressing. Annals of the CIRP 1990, 39, 329-332.

[2] H. Ohmori, T. Nakagawa. Analysis of mirror surface generation of hard and brittle materials by ELID (Electrolytic In-Process Dressing) grinding with superfine grain metallic bond wheels. Annals of the CIRP 1995, 44, 287-290.

[3] H. Ohmori, I. Takahashi, B. P. Bandyopadhyay. Grinding characteristics of hard and brittle materials by fine grain lapping wheels with ELID. Journal of Material Processing Technology 1996, 57, 272-277.

[4] H. Ohmori, T. Nakagawa. Utilization of nonlinear conditions in precision grinding with ELID(Electrolytic In-Process Dressing) for fabrication of hard material components. Annals of the CIRP 1997, 46, 261-264.

[5] H. S. Lim, K. Fathima, A. S. Kumar, M. Rahman. A fundamental study on the mechanism of electrolytic in-process dressing (ELID) grinding. International Journal of Machine Tools and Manufacture 2002, 42, 935-943.

[6] H. Ohmori, W. Li, A. Makinouchi, B. P. Bandyopadhyay. Efficient and precision grinding of small hard and brittle cylindrical parts by the centerless grinding process combined with electro-discharge truing and electrolytic in-process dressing. Journal of Materials Processing Technology 2000, 98, 322-327.

[7] T. G. Bifano, R. Krishnaoorthy, H. Fawcett, E. Welch. Fixed-load electrolytic dressing with bronze bonded grinding wheels. Transaction of the ASME. J Manuf Sci Eng 1999, 121, 1, 20-27.

[8] F. Klocke, A. Klink, U. Schneider. Electrochemical oxidation analysis

for dressing bronze-bonded diamond grinding wheels. Production Engineering 2007, 1, 141-148.

[9] F. Klocke, A. Klink, M. Henerichs. ELID dressing behavior of fine grained bronze bonded diamond grinding wheels. International Journal of Abrasive Technology 2009, 2, 4, 358-367.

[10] Y. Kondo, K. Miyachika, F. Obata, Y. Yamamoto, T. Fukuda. Friction and wear characteristics of iron oxide coating. JSME annual meeting 2003, 4, 133-134.

[11] M. Pourbaix. Atlas of Electrochemical Equilibria in Aqueous Solutions. NACE, Houston 1966, 388.

[12] S. Sasaki. The effects of the surrounding atmosphere on the friction and wear of alumina, zirconia, silicon carbide, and silicon nitride. Wear 1989, 134, 185-200.

[13] X. Dong, S. Jahanmir. Wear transition diagram for silicon nitride. Wear, 1993, 165, 168-180.

[14] M. Akazawa, K. Kato, K. Umeya. Wear properties of silicon nitride in rolling contact. Proc. Wear 1986, 110, 285-293.

[15] N. N. Greenwood, A. Earnshaw. Chemistry of the Elements, 2nd ed. Butterworth-Heinemann, Oxford, UK, 1997.

[16] R, K, Iler. The Chemistry of Silica. Wiley, New York, 1979.

[17] H. Vora, T. W. Orent, R. J. Stokes. Mechanochemical polishing of silicon nitride. Journal of the American Ceramic Society 1982, 65(9), C140-C141.

Chapter 4
Electrolytic In-Process Dressing Grinding of Ceramic Balls

4.1 Introduction

As claimed by Pavel [1], the traditional off-line dressing techniques need to interrupt the workflow and the additional dressing time may cancel out the dressing advantage. Several new dressing techniques have been developed in the past two decades. The electro-discharge dressing (EDD) was probably first proposed by Suzuki et al. [2], and a variant of the technology, electro contact discharge dressing (ECDD) which uses two electrodes in contact with the grinding wheel was devised by Tonshoff and Friemuth [3]. In addition, laser assisting grinding was first proposed by Westkamper for dressing and truing of CBN grinding wheels [4]. However, both discharge and laser dressing would pose the risk of thermal damage to the diamond abrasive.

The Electrolytic In-process Dressing technique, known as ELID, has been successfully used in industry, which was developed by Ohmori [5]. ELID is efficient in mirror grinding of advanced ceramics and other hard and brittle materials. A lot of researches were carried out to investigate the grinding characteristic of ELID and the influence of grinding condition. The effect of different abrasive sizes from SD4,000 to SD120,000 was investigated by Ohmori and Nakagawa [5]. Later, the investigation of ELID was expanded to SD325 [6] and SD3,000,000 [7]. The effect of bond material, current type and grinding fluid were also investigated by Ohmori and Nakagawa [8], and it was

found that iron bonded wheel with DC-Pulse power showed the best grinding performance among four kinds of grinding fluid and three kinds of metal bonded grinding wheel: cast iron bond, cobalt bond and bronze bond. Other conditions such as current duty factor [9] and gap between the electrodes [10] were also investigated.

Ohmori [6] proposed an explanation of the mechanism of ELID. Generally, ELID is composed of two stages: pre-dressing stage and in-process dressing stage. In the pre-dressing stage, the bond material of iron is electrolyzed into Fe^{2+} firstly. The ionized Fe then forms $Fe(OH)_2$ and/or $Fe(OH)_3$, and further changes into oxides such as Fe_2O_3. The electro-conductivity of the grinding wheel surface reduces due to the growth of these insulating oxides at the surface, and the current decreases. The pre-dressing is completed when the current reaches a critical low value. Then the pre-dressed wheel is put into use in grinding with electrolysis. The oxide layer is much easier to wear than the original bond, making it possible to keep the protrusion appropriate even when the grain is worn. The electrolysis produces constantly the oxide layer. When the growth rate of the oxide layer is equal to the wear rate, the layer thickness will be almost constant during grinding and the dressing process is stable. According to the research on the grinding of brittle materials with ELID by Kumar et al. [11], it is claimed that the oxide layer has strength enough to hold the grits during grinding. However, in a later research on nano finish grinding, the same research team said that the grits in the oxide layer are loosely held, thus act like in lapping, resulting in a smoother surface [12].

To the best of our knowledge, all the researches of ELID was limited to the sliding grinding processes such as the plane and curved surface grinding. The research of ELID of the rolling grinding process such as grinding of balls has

not been reported.

Existing ball lapping process is what is called V-groove lapping which is very low in efficiency especially for ceramic balls since ceramics are hard and brittle. The grinding efficiency has been greatly increased by introducing the magnetic fluid grinding method [13]. The method has been modified by sealing magnetic fluid into a closed chamber, which makes possible to choose grinding fluid freely, and by using diamond wheel, which increases the grinding efficiency furthermore and saves the expensive diamond abrasive as well [14]. This method is called the magnetic fluid support grinding of ceramic balls since at this time the magnetic fluid is used only for support of ceramic balls. Grinding experiments by changing the grinding load, speed of wheel and the abrasive grit size have been conducted to investigate their effects on both the sphericity and grinding efficiency. Other types of supports different from the magnetic fluid support have also been investigated with respect to their effect on the spherical surface generation [15].

In this chapter the ELID was applied to the grinding of ceramic balls by using a magnetic fluid support grinding machine. The effects of dressing current, the type of bond material and the type of electrolyte on both the grinding efficiency and ground surface roughness were investigated.

4.2 Experimental procedure

The schematic of the electrolytic dressing grinding system used in this study is shown in Fig 1. Ceramic balls (1) to be ground are placed within a circular space formed by a grinding wheel (2), the inner surface of a guide ring (3) and the upper surface of a taper thrust (4). The taper thrust is fixed on a float (5) through a thrust bearing (6) which enables the taper thrust to rotate freely. The chamber beneath the float is filled with magnetic fluid (7) which produces magnetic buoyancy to the float due to the divergent magnetic field generated by magnets (8). The buoyancy increases as the gap between the float and the magnets decreases, thus provides a flexible support. For more details of the magnetic fluid support grinding system is referred to [14]. The grinding load is monitored by a load cell (9). To implement the electrolytic dressing grinding, a power supply (10) is attached to the system. The metal bonded grinding wheel is connected to the positive pole through a brush (11) while the guide ring is connected to the negative pole.

Table 1 lists the experimental condition. To investigate the dressing effect on the superfine grinding wheel, both bronze bonded and cast iron bonded grinding wheels of SD16000I75 were used, both of which had outer diameter 150 mm. The thickness of diamond layer was 5 mm for the bronze bonded wheel while it was 3 mm for the cast iron bonded wheel. The concentration of both wheels was 75 and the grade of hardness was I. The ceramic balls were HIPed Si_3N_4 of density 3.2 g/cm^3 and about 11 mm in diameter. The grinding load was set at 25 N in all the experiments. The current was increased by steps from 40, 80, 160 to 320 mA, and in later investigation of bond material and electrolyte, two types of electrolyte were used: tap water and CG-7 to water of 1:50.

The diameter of the ceramic balls was measured by a digital micrometer for every 4 grinding hours to evaluate the grinding efficiency. The duration of every 4 hours was set to ensure that the reduction in diameter before grinding is larger than 1 μm which is the division of the micrometer. The grinding experiments were repeated for 36 hours until the reduction rate was stable even though there still were some exceptions depending on the grinding conditions. The surfaces of the ground balls and grinding wheels were observed with a microscope.

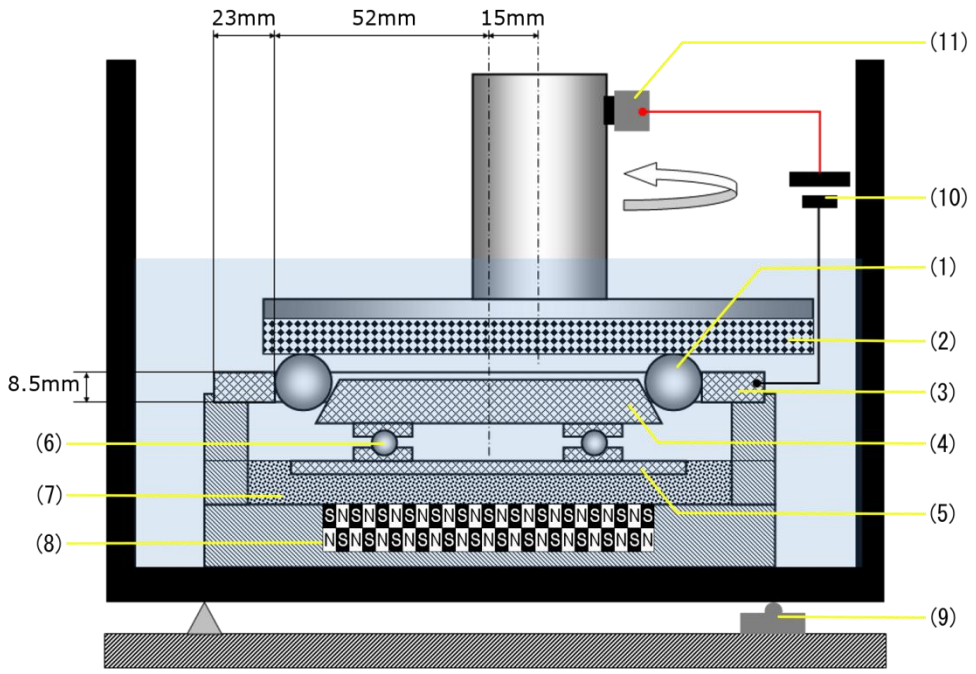

(1) Ceramic balls; (2) Grinding wheel; (3) Guide ring; (4) Taper thrust; (5) Float; (6) Thrust bearing; (7) Magnetic fluid; (8) Magnets; (9) Load cell; (10) Power supply; (11) Brush.

Fig. 4-1 Schematic of the electrolytic dressing grinding machines

Table 4-1 Experimental condition

Grinding Wheel	SD16000I75M40 (Bronze bond, ϕ150t5) SD16000I75M3.0 (Cast iron bond, ϕ150t3)
Ceramic Ball	Si_3N_4 (HIP ϕ11×25, 1438HV1)
Electrolyte	Tap water (pH7.4, 100 μS/cm) CG-7(×50, pH9.5, 1050 μS/cm)
Total Grinding Load (N)	25
Rotation Speed (rpm)	440
Current (mA)	40, 80, 160, 320
Area of electrode (mm^2)	9200

4.3 Experimental results

§4.3.1 Effect of dressing current

Figure 4-2 shows the dependence of the diameter reduction rate on the dressing current. The diameter reduction rate was about 0.25 μm/h for non-electrolytic dressing. It increased steadily with the dressing current up to 160 mA, and then jumped up between 160 mA and 320 mA. The diameter reduction rate at 320 mA was 1.6 μm/h, which is about 8 times as much as that without dressing.

Figure 4-3 shows the ground surface of ceramic balls under different dressing current. The surfaces were smooth when the dressing current was less than 80 mA (Fig. 4-3(a), Fig. 4-3(b) and Fig. 4-3(c)). Some scratches were observed when the dressing current increased to 160 mA and the scratch became larger when the dressing current increased further. It is clear that the dressing was excessive at the current of 320 mA. In the following experiments the dressing current was fixed at 40 mA.

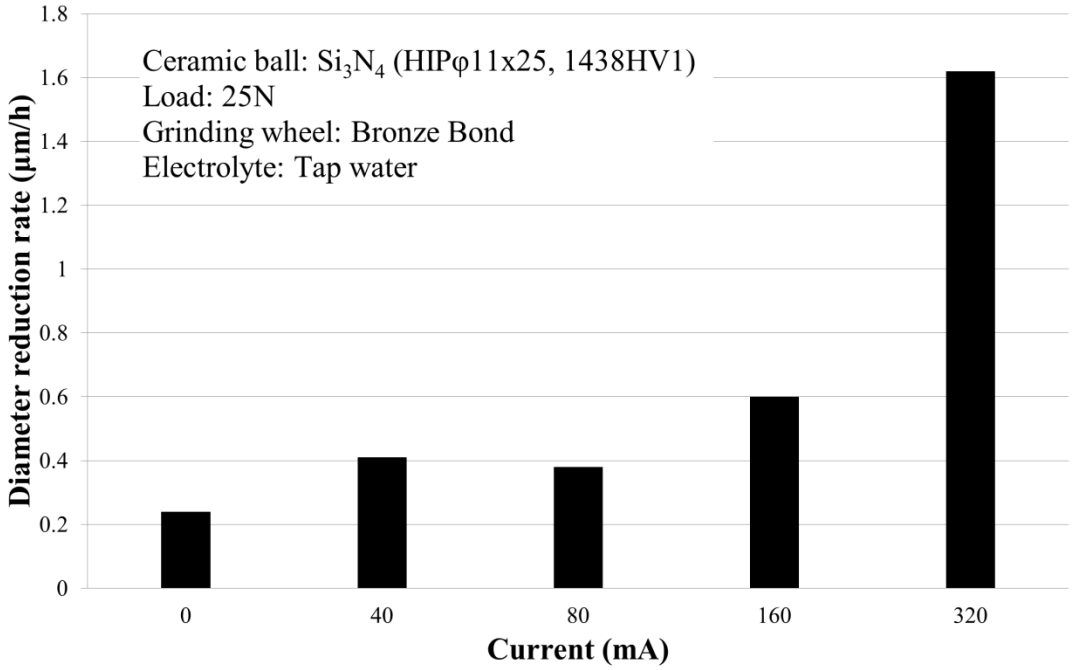

Fig. 4-2 Dependence of the diameter reduction rate on dressing current

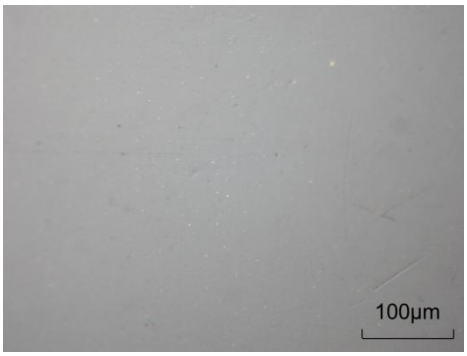

a) I = 0

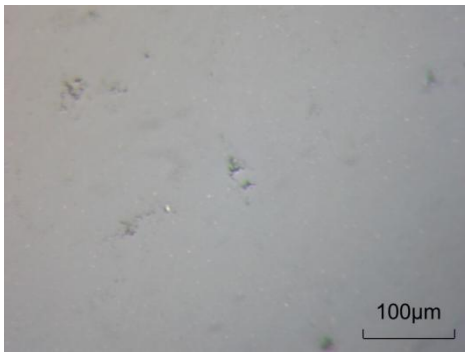

b) I = 40 mA

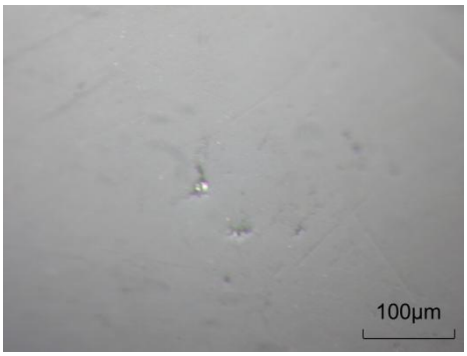

c) I = 80 mA

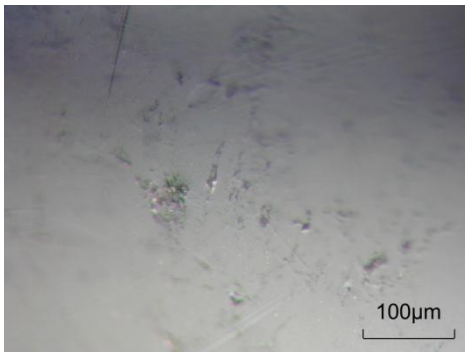

d) I = 160 mA

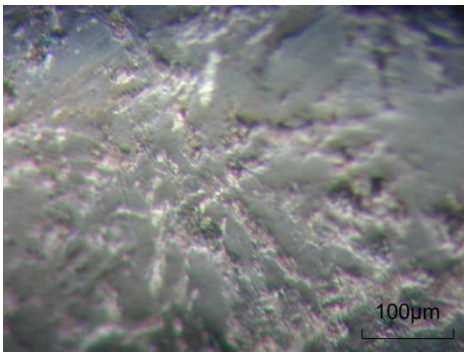

e) I = 320 mA

Fig. 4-3 Surface of Si_3N_4 ball ground under different dressing current

§4.3.2 Effect of bond material and grinding fluid

Figure 4-4 shows the dependence of the diameter reduction rate on grinding time for both the bronze bonded wheel and the cast iron bonded wheel in tap water and CG-7 solution. All the grindings started with non-electrolytic dressing for 8 hours. For all the experimental conditions in non-electrolytic dressing, the diameter reduction rates were almost the same, about 0.2 μm/h. This suggests that, diameter reduction rate in non-dressing grinding was affected neither by bond materials of grinding wheel nor by types of the grinding fluid used in this study. On the contrary, in electrolytic dressing grinding, the diameter reduction rate was very different depending on the grinding conditions. For the bronze bonded wheel, when dressed in tap water, the diameter reduction rate firstly stayed at 0.35 μm/h, and then increased to 1.1 μm/h rapidly, and the average diameter reduction rate was about 4 times as high as that without dressing. However when dressed in CG-7, the diameter reduction rate decreased gradually, to a minimum value of 0.1 μm/h, and then returned to 0.35 μm/h once again. The total average diameter reduction rate was 0.2 μm/h, almost as same as that without dressing.

For the cast iron bonded wheel, when dressed in tap water, the diameter reduction rate increased from 0.18 μm/h to 0.8 μm/h, but decreased later. The total average diameter reduction rate was 0.29 μm/h, which is about a 50% increase from that without dressing. However, when dressed in CG-7, the diameter reduction rate decreased to almost immeasurably low value after 8 hours' dressing. Although the diameter reduction rate returned to the normal level after 20 hours' dressing, the total average diameter reduction rate was 0.19 μm/h, which was very close to that of non-dressing grinding.

In summary, the bronze bonded grinding wheel shows higher increase in the

diameter reduction rate than the cast iron bonded wheel by electrolytic dressing in tap water, and, against to expectations, electrolytic dressing in CG-7 solution did not improve the grinding efficiency for both the bronze bonded wheel and the cast iron bonded wheel.

The ground ball surfaces were showed in Fig. 4-5. It is known from the observations that, without electrolytic dressing, no matter which grinding wheel and grinding fluid was used, the ground surfaces were extremely smooth after 8 hours' grinding. The surface roughness was about 4 nm Ra. For electrolytic dressing, only grinding with bronze bonded wheel in tap water generated a scratched surface, while the rest produced very smooth surface. This observation coincided with the results of the diameter reduction rate, in which electrolytic dressing grinding with bronze bonded wheel in tap water shows the highest improvement in grinding efficiency among all the grinding conditions in this study.

Figure 4-6 shows the surfaces of both bronze bonded and cast iron bonded grinding wheels in tap water and CG-7 solutions, respectively. The surface was homogeneous in all the conditions for bronze bonded wheel, but there appeared sliding track in non-dressing condition for cast iron bonded grinding wheel. It is known that, for electrolytic dressing grinding in all the conditions, the wheel surfaces consisted mainly of two parts: metallic-color area and the dark gray area. The light metallic-color area was convex.

The metallic-color area decreased as the electrolytic dressing proceeded, and this trend was the strongest for the bronze bonded wheel dressed in tap water in this study. This change in the surface of grinding wheels was an indication of dressing effect, and the results agreed with that of the diameter reduction rate. The increase in the diameter reduction rate in Fig.2 was

contributed to the electrolytic dressing, while the following decrease in the diameter reduction rate with grinding time may be due to the decrease in the metallic-color area, which is considered to be the active area in grinding for it is convex.

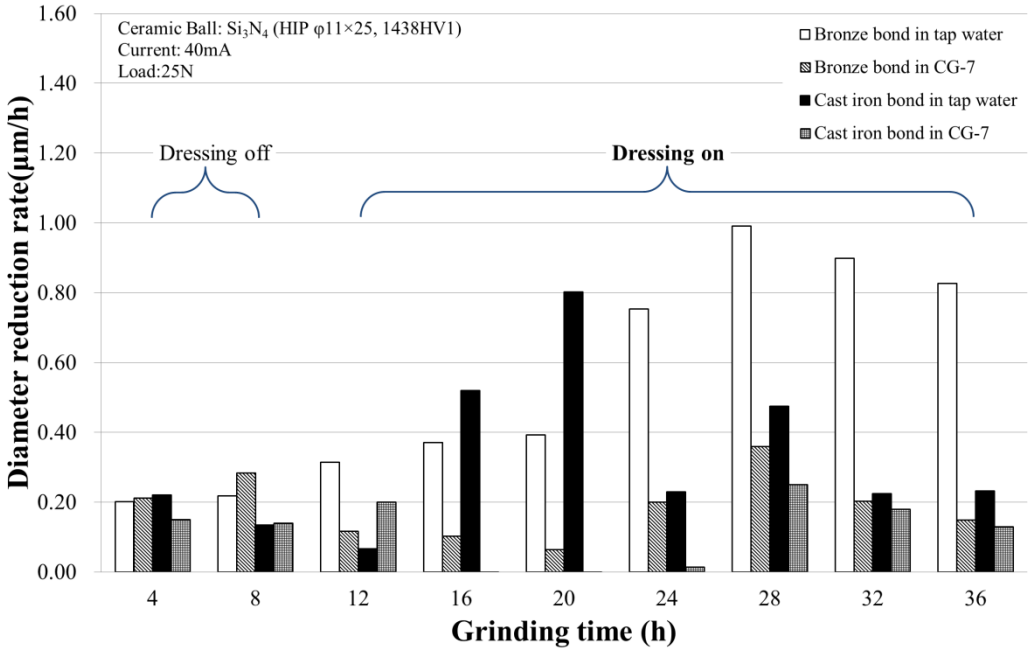

Fig. 4-4 Dependence of the diameter reduction rate on grinding time for both bronze and cast iron bonded wheels in tap water and CG-7 solution

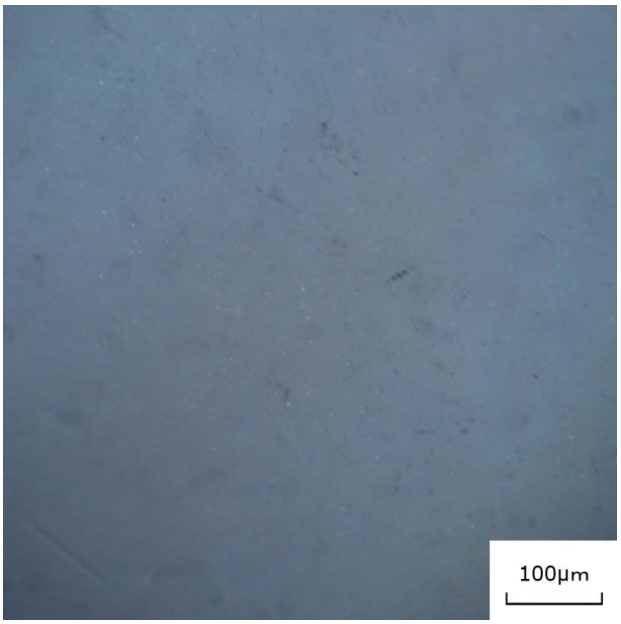

a) Ball surface ground by bronze bond wheel in tap water without dressing

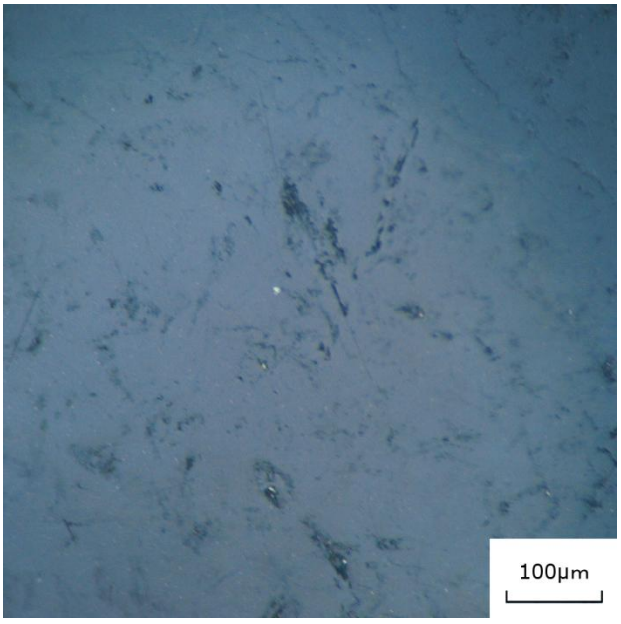

b) Ball surface ground by bronze bond wheel in tap water with dressing for 28H

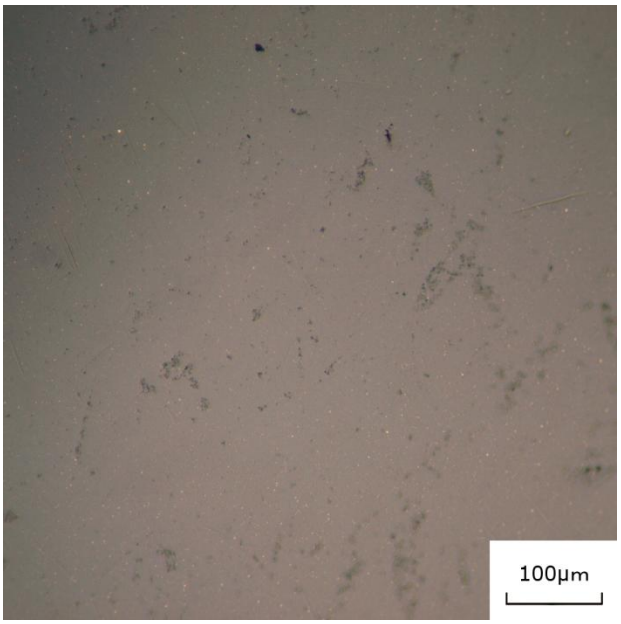

c) Ball surface ground by bronze bond wheel in CG-7 without dressing

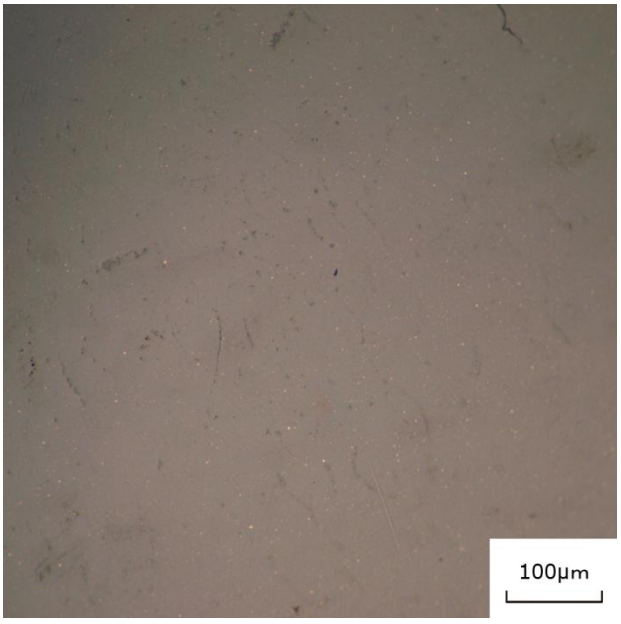

d) Ball surface ground by bronze bond wheel in CG-7 with dressing for 28H

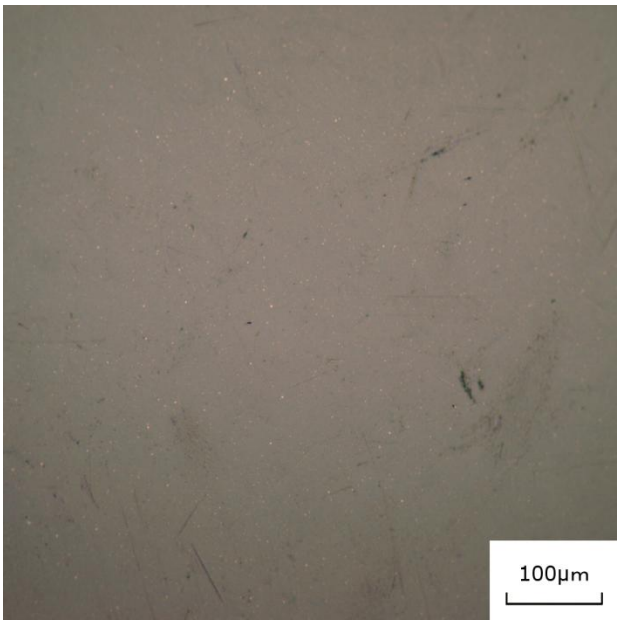

e) Ball surface ground by cast iron bond wheel in tap water without dressing

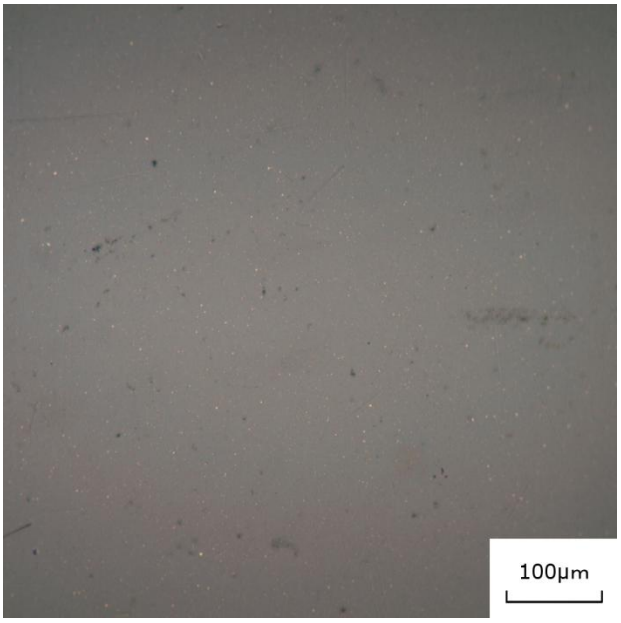

f) Ball surface ground by cast iron wheel in tap water with dressing for 28H

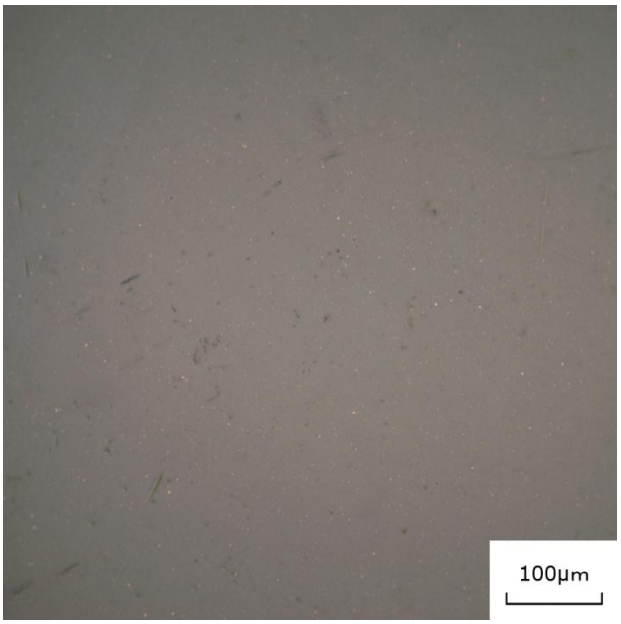

g) Ball surface ground by cast iron bond wheel in CG-7 without dressing

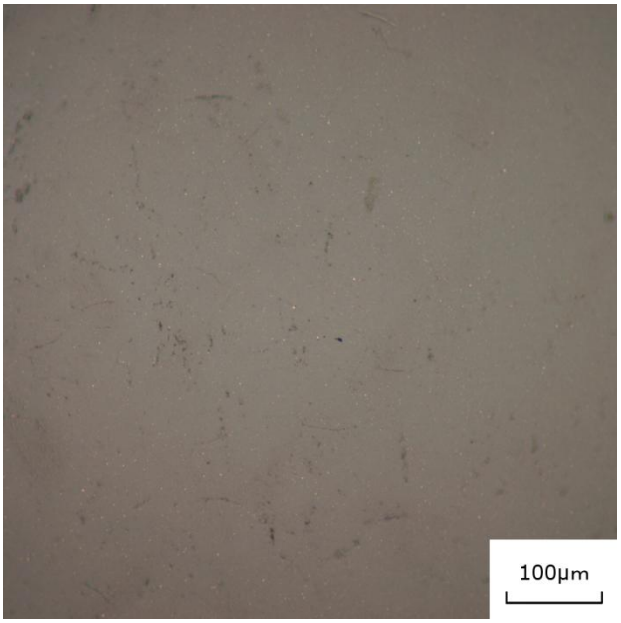

h) Ball surface ground by cast iron wheel in CG-7 with dressing for 28H

Fig. 4-5 Ground Surfaces of Si_3N_4 balls

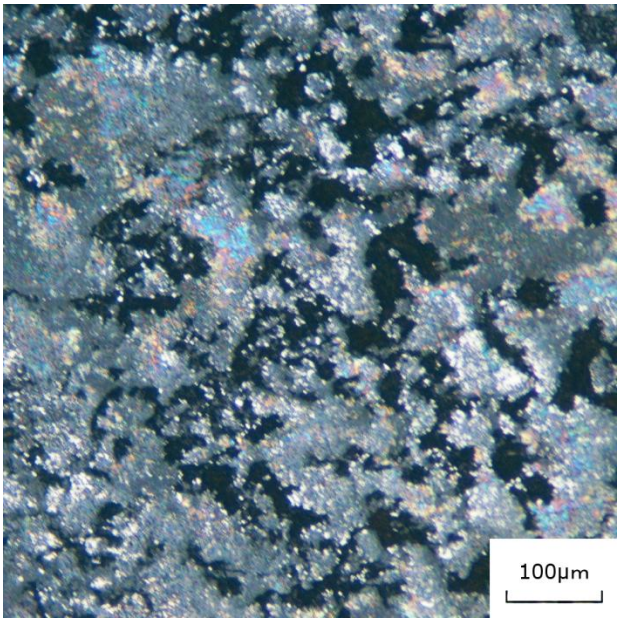

a) Surface of the bronze bond wheel used in tap water without dressing

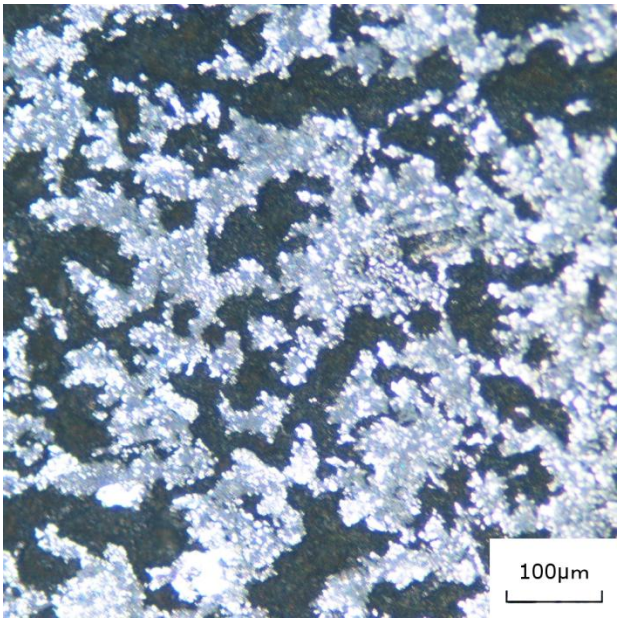

b) Surface of the bronze bond wheel used in tap water with dressing for 28H

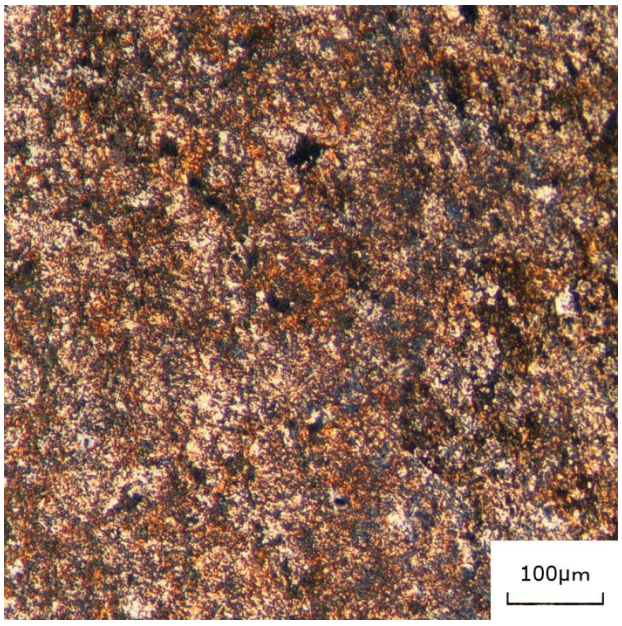

c) Surface of the bronze bond wheel used in CG-7 without dressing

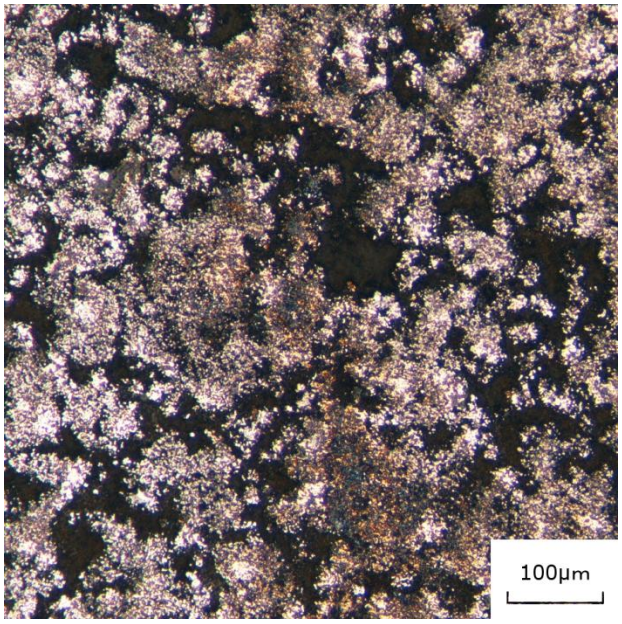

d) Surface of the bronze bond wheel used in CG-7 with dressing for 28H

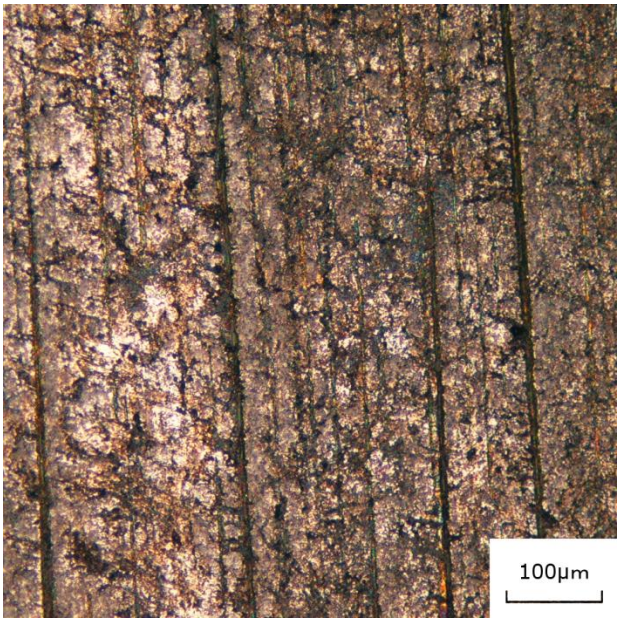

e) Surface of the cast iron bond wheel used in tap water without dressing

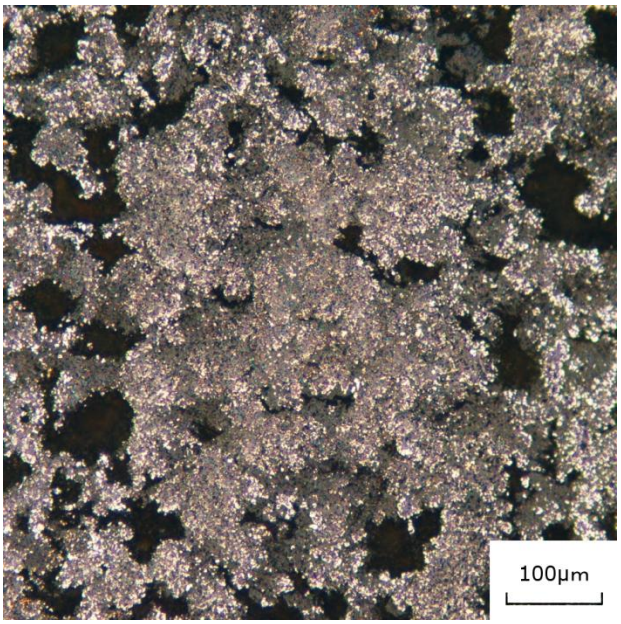

f) Surface of the cast iron bond wheel used in tap water with dressing for 28H

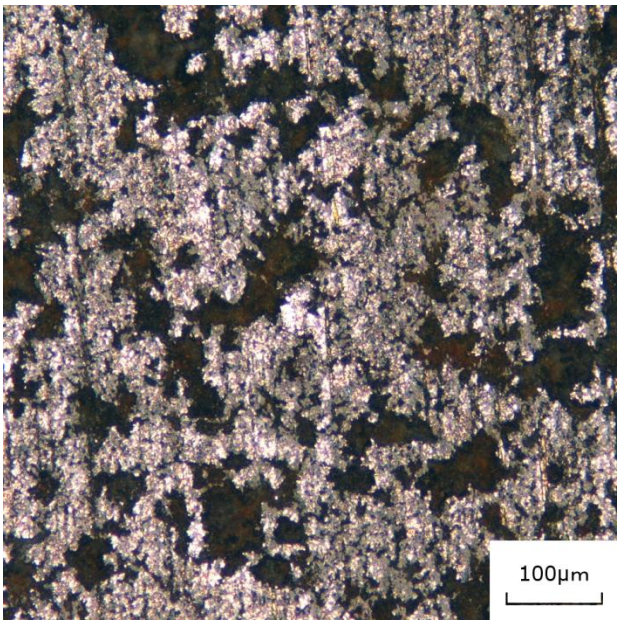

g) Surface of the cast iron bond wheel used in CG-7 without dressing

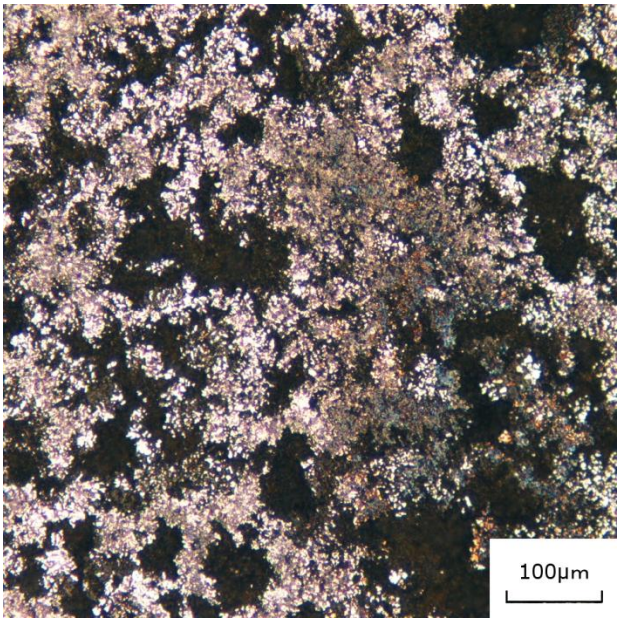

h) Surface of the cast iron bond wheel used in CG-7with dressing for 28H

Fig. 4-6 Surfaces of the grinding wheels

4.4 Discussions

The change in diameter reduction rate with grinding time for both bronze and cast iron bonded wheels electrolyzed in tap water may be related to the change in morphology of grinding wheel. The first increase in diameter reduction rate with grinding time was due to the electrolytic dressing effect which protruded the buried grit and therefore increased the number of active grit at the grinding wheel surface. In this study pre-dressing was not implemented and instead non-dressing grinding was conducted to get the same grinding wheel surface before the dressing grinding for all experiments. Therefore it was expected that the active grit was fewest at the beginning. The increase in the number of active grit was eventually saturated as the dressing proceeded and the reduction rate became constant at an increased value. On the contrary, the reduction rate turned to decreasing after reaching a maximum. This decrement in the reduction rate is considered to be attributed to the change in the morphology of the grinding wheel surface during dressing process. The grinding surface was uneven and there were convex and concave areas. The convex area decreased as the dressing proceeded. It is known that the grinding is implemented only when the grinding wheel surface, precisely the grit, contact directly with the workpiece. The decrease in the convex area means that the decrease in the direct contact and therefore the decrease in the reduction rate.

The homogenous surface was typical for rolling wear and electrolysis. When electrolysis was superimposed the concave area increased for both bronze and cast iron bonded wheels, and the sliding wear track disappeared for cast iron bonded wheel. The increase in the concave area by superimposing electrolysis was limited to the grinding area of the grinding

wheel, out of the grinding area no such increase was observed. This suggests that the electrolysis is more open to concave area than to convex area for both bronze and cast iron bonded wheels. This mechanism is schematically shown in Fig. 4-7. The convex area was smoothened by wear, and the surface area was reduced (Fig.4-7 (b)). This reduction in surface area led to a decrement in electrolytic rate γ_{ep} at the convex area. Because the wear rate γ_{wp} was much less than the electrolytic rate (otherwise electrolytic dressing is not necessary) the change in electrolytic rate at the convex area broke the balance in the material removal rates between the convex and concave areas, and, as a result, the concave area was deepened as the electrolytic dressing grinding proceeded (Fig.4-7 (c)). The disappearance of sliding wear track of cast iron bonded wheel was the evidence that wear rate was much less than electrolysis rate.

The experimental results showed that the bronze bonded grinding wheel was easier to be dressed than the cast iron bonded grinding wheel. The difference between the two grinding wheel can be explained by the differences in anode reactions and in the chemical equivalent. The pH values of the tap water and the CG-7 solution were 7.4 and 9.5 respectively, and the voltage in these experiments was over 4V. According to the Pourbaix diagram of copper [16], the anode reactions for the bronze bonded grinding wheel are:

$$Cu + 2OH^- \rightarrow CuO + H_2O + 2e^- \quad (1)$$

$$4OH^- \rightarrow O_2 + 2H_2O + 4e^- \quad (2)$$

The reaction (1) is directly related to the dressing, while the reaction (2) is not.

For cast iron bond, the reaction (2) is the same, and the oxidation reaction of iron [17] is:

$$Fe + 8OH^- \rightarrow FeO_4^{2-} + 4H_2O + 6e^- \quad (3)$$

The electrolytic current is the sum of the currents of the metal oxidation and the water decomposition. Assuming that the current of the metal oxidation for the two bond materials is the same under the same condition, the oxidation speed is proportional to the chemical equivalent of metal. From reactions (1) and (3), it is known that the valence of copper is 2, while it is 6 for iron. The atomic weight and the density are 63.546 and 8.920 g/cm^3 for copper while they are 55.842 and 7.874 g/cm^3 for iron. Therefore the equivalent volume is about 7.12 cm^3 for copper and 2.36 cm^3 for iron, respectively. The equivalent volume of iron is only one-third of that of copper. In other words, to achieve the same dressing effect, the current for the cast iron bonded grinding wheel may be three times as high as that for the copper bonded grinding wheel. The difference in chemical equivalent between copper and iron is considered to be the dominant cause why the bronze bonded grinding wheel has better dressing effect than cast iron bonded grinding wheel, under the same current.

As the effect of different electrolyte on dressing, it may be considered that the change in ratio of metal oxidation current to water decomposition current occurs. According to the Pourbaix diagram, increasing the pH value of electrolyte will accelerate the decomposition of water. CG-7 solution had a higher pH value than the tap water, and therefore the decomposition rate of water of CG-7 solution was higher than that of the tap water. Since the electrolytic current was the same, increments in the water decomposition current in CG-7 solution lead to the same magnitude of reduction in the metal oxidation current, and therefore a reduction in the dressing effectiveness.

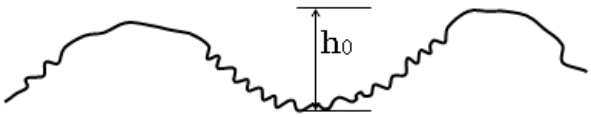

(a) Initial surface generated after grinding without electrolysis

$\gamma_{wp} << \gamma_{ev}$, $\gamma_{ep} < \gamma_{ev}$

(b) Developing surface in electrolytic dressing grinding

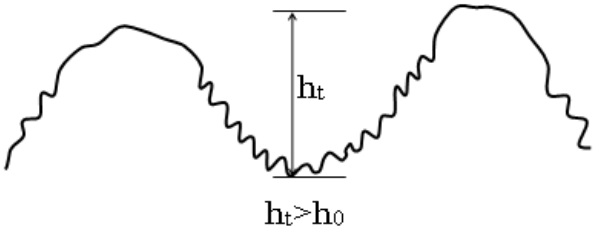

(c) Developed surface in electrolytic dressing grinding

Fig. 4-7 Mechanism of grinding wheel surface generation in electrolytic dressing

4.5 Conclusions

A series of electrolytic in-process dressing grindings of ceramic balls were carried out by using fine diamond grinding wheels of SD16000. The effects on dressing of electrolytic current, bond material and electrolyte were investigated in terms of material removal rate and ground surface finish. The following conclusions were obtained:

1. Grinding efficiency increases with electrolytic current.
2. Bronze bonded grinding wheel shows higher electrolytic dressing effectiveness than cast iron bonded grinding wheel in both tap water and CG-7 solution.
3. Tap water is more effective than CG-7 solution as an electrolyte for both bronze and cast iron bonded grinding wheels.
4. The diameter reduction rate of bronze bonded grinding wheel increased 4 times by electrolytic dressing in tap water.

4.6 Reference

[1] R. Pavel, M. Pavel, I. Marinescu. Investigation of pre-dressing time for ELID grinding technique. Journal of Materials Processing Technology 2004, 149, 591-596.

[2] K. Suzuki, T. Uematsu, T. Nakagawa. On-machine trueing/dressing of metal bond grinding wheels by electro-discharge machining. Annals of the CIRP 1987, 33, 115-118.

[3] H. K. Tonshoff, T. Friemuth. In-process dressing of fine diamond wheels for tool grinding. Precision Engineering 2000, 24, 58-61.

[4] E. Westkamper. Grinding assisted by Nd:YAG lasers. Annals of the CIRP 1995, 44, 317-320.

[5] H. Ohmori, T. Nakagawa Mirror surface grinding of silicon wafers with electrolytic in-process dressing. Annals of the CIRP 1990, 39, 329-332.

[6] H. Ohmori, I. Takahashi, B. P. Bandyopadhyay. Ultra-precision grinding of structural ceramics by electrolytic in-process dressing (ELID) grinding. Journal of Material Processing Technology 1996, 57, 272-277.

[7] H. Ohmori, T. Nakagawa. Analysis of mirror surface generation of hard and brittle materials by ELID (Electrolytic In-Process Dressing) grinding with superfine grain metallic bond wheels. Annals of the CIRP 1995, 44, 287-290.

[8] H. Ohmori, T. Nakagawa. Utilization of nonlinear conditions in precision grinding with ELID (Electrolytic In-Process Dressing) for fabrication of hard material components. Annals of the CIRP 1997, 46, 261-264.

[9] H. S. Lim, K. Fathima, A. S. Kumar, M. Rahman. A fundamental study on the mechanism of electrolytic in-process dressing (ELID) grinding. International Journal of Machine Tools and Manufacture 2002, 42, 935-

943.

[10] J. Kim, E. Lee. A study of mirror-like grinding of fine ceramics with in-process electrolytic dressing. International Journal of Advanced Manufacturing Technology 1996, 12, 246-254.

[11] A. S. Kumar, H. S. Lim, M. Rahman, K. Fathima. A study on the grinding of glass using electrolytic in-process dressing. Journal of electronic materials 2002, 31, 10, 1039-1046.

[12] M. Rahman, A. S. Kumar, H. S. Lim, K. Fathima. Nano finish grinding of brittle materials using electrolytic in-process. Sadhana 2003, 28, 5, 957-974.

[13] N. Umehara, and K. Kato. A study on magnetic fluid grinding – 1st report. Jpn. Soc. Mech. Eng. (in Japanese) 1988, 54, 503, 1599-1604.

[14] B. Zhang, T. Uematsu and A. Nakajima. High efficiency and precision grinding of Si_3N_4 ceramic balls aided by magnetic fluid support using diamond wheels. JSME Intl Journal Series C 1998, 41, 3, 499-505.

[15] B. Zhang, and A. Nakajima. Dynamics of magnetic fluid support grinding of Si_3N_4 ceramic balls for ultraprecision bearings and its importance in spherical surface generation. Precision Engineering 2003 27, 1-8.

[16] M. Pourbaix. Atlas d'Equifibres Electrochimiques (ed. M. Pourbaix). Gauthier-Villars and Cie, Paris 1963, 380

[17] B. Beverskog, I. Puigdomenech. Revised pourbaix diagrams for iron at 25–300 °C. Corrosion Science 1996, 38, 12, 2121–2135.

Chapter 5
Conclusions

The electrolytic in-process dressing was first introduced into the superfine grinding of ceramic balls. The mechanism of the material removal was made clear and the effect of some parameters is investigated.

The main conclusions obtained in the chapters are as follows:

1) Simulation experiments of electrolytic in-process dressing were conducted by using an electrolytic-friction test machine. Strong synergistic effect between the electrolysis and sliding wear was observed for copper in both tap water and electrolyzed water, and for Fe in electrolyzed water and CG-7. Without electrolysis the wear was almost undetectably small. The wear tracks of copper electrolyzed in tap water and electrolyzed water were very rough. Wear track was very smooth only for iron in CG-7 among the cases where the synergistic effect was observed.

2) A series of electrolytic in-process dressing grindings of ceramic balls were carried out by using fine diamond grinding wheels of SD16000. The effects on dressing of electrolytic current, bond material and electrolyte were investigated in terms of material removal rate and ground surface finish. Grinding efficiency increases with electrolytic current. Bronze bonded grinding wheel shows higher electrolytic dressing effectiveness than cast iron bonded grinding wheel in both tap water and CG-7 solution. Tap water is more effective than CG-7 solution as an electrolyte for both bronze and cast iron bonded grinding wheels. The diameter reduction rate of bronze bonded grinding wheel increased 4 times by electrolytic dressing in tap water.

The result of the simulation experiment and the grinding test matches for bronze bond but does not match for the cast iron bond material. The grinding efficiency for the cast iron bond grinding wheel dressed in tap water increased, but the wear track of the iron disk was immeasurable small in the simulation experiment. The results of the iron in CG-7 are reverse, where no dressing effect was observed but deep wear track was generated in the simulation experiment.

Acknowledgments

This work has been carried out at the Department of Mechanical Engineering, Saga University in Japan.

First of all, I would like to sincerely thank my supervisor, Professor Bo Zhang, of Saga University. It is him who has given me the precious opportunity to study at Saga University. Under his guidance, I learned a lot about mechanics, especially knowledge of tribology which I have never learned at the undergraduate school. He also taught me how to work with others and independent thinking. It was in his teachings; I was able to finish this thesis. His guidance will benefit me all my life. Without his valuable advice and discussions, none of this research would be achieved.

I wish to express my sincere gratitude to Professor Akira Nakajima at Saga University for his encouragement and helpful suggestions during the study.

I would like to thank Assistant Professor Toshifumi Mawatari for his great help in experiments and discussions about the study.

I would like to thank Noritake Super Abrasive Co., Ltd. for providing the diamond wheels. Furthermore, I sincerely thank the Japanese Monbukagakusho for this work is supported by Japanese Government (Monbukagakusho) Scholarship.

I am also indebted to Mr. Yousuke Aonuma, Mr. Muneharu Matsuoka, Mr. Tetsuo Matsumoto, Mr. Satoshi Morizono, and Mr. Akio Muraoka at the factory attached to Saga University.

Last but no least I wish to thank my parents for their warm encouragement and support.